UNIVERSITY OF SOUTHERN CALIFORNIA

Department of Civil Engineering

ROTATIONS IN THE TRANSIENT RESPONSE OF NONLINEAR SHEAR BEAM

by

Vlado Gicev and Mihailo D. Trifunac

Report CE 06-02

November, 2006

http://www.usc.edu/dept/civil_eng/Earthquake_emg/

ABSTRACT

We present analysis of linear and nonlinear strains (rotations and drifts) in a uniform shear beam subjected to a strong-motion pulse at its base. We describe the dependence of the computed strains on the amplitude and duration of the wave pulse and on the material properties of the shear beam. Our results should provide a useful elementary background that can serve to help further understanding of the advantages of the displacement-based design and of the power design method.

1. INTRODUCTION

The traditional earthquake resistant design has evolved from the linear concepts of the relative-response spectrum, using vibrational theory, and the mode superposition method (Biot, 1942). However, this approach has a low-pass filtering effect on the end result, because in practical engineering applications the higher modes are usually neglected. Furthermore, the traditional response spectrum method is not suitable for representation of the early transient response, particularly for excitations by high-frequency pulses, which have durations shorter than the travel time for an incident wave to reach the top of a building.

Recent summaries of the known concepts in seismic design through "performance-based" objectives, and proposals that it may be more rational to develop some displacement-based design procedures as a replacement for the traditional force-based approach, have emphasized the need to understand and to quantify the inter-story drift (Fajfar and Krawinkler, 1992). At the Bled workshop in 1997 (Fajfar and Krawinkler, 1997) it was concluded that (Fajfar, 1998) "The most suitable approach for seismic design practice appears to be deformation-controlled design. This approach uses deformation rather than forces as the starting point for seismic design, with the presumption that control of global displacement, drift, or strain is the key to controlling the performance of the structure…the inter-story drift is a very useful performance indicator. The important component(s) of drift will depend on the evaluation objective, considering that inter-story drift may be caused by shear distortion within the story, cumulative flexural rotations (e.g., in walls), and rotation at the bottom of the structure due to foundation flexibility."

Inter-story drifts are the point rotations averaged over a story height, and thus they are directly related to the space derivatives of the waves propagating through the structure (Trifunac, 2006). Because this relationship holds for both linear and nonlinear wave motion, extension of the use of the average story drifts (rotations) to the drifts at a point (point rotations) offers advantages and can become a valuable new tool in the design of structures. The creation of plastic hinges in beams, columns, and walls corresponds to strain localization associated with nonlinear waves in a continuum, and therefore quantifying point rotations (i.e., strains and drifts) and understanding the circumstances and conditions that lead to large point rotations are essential for the development of new rational methods in earthquake-resistant design.

Since the modes of vibration are standing waves that result from constructive interference of the incoming wave and the wave reflected from the top of the building, the building starts vibrating in the first mode only long after time $t = 2H/\beta$ has elapsed (H and β are the height and vertical shear wave velocity of the building, respectively). While in principle the representation of the response as a linear combination of the modal responses is mathematically complete, analyses of response to short "impulsive" representation would require considering many modes (infinitely many for a continuous model), which is impractical. The wave

propagation methods are therefore more *natural* for representation of the *early* transient response and should be explored further and used to solve the problems where the modal approach is limited.

Wave-propagation models for analyses of the response of buildings have been used since the 1930s (Sezawa and Kanai, 1935, 1936; Kanai, 1965), but they are only recently beginning to be verified against actual observations (Todorovska et al., 2001 a, b). Continuous 2-D wave-propagation models (homogeneous, horizontally layered, and vertically layered shear plates) were employed to study the effects of traveling waves on the response of long buildings (Todorovska et al., 1988; Todorovska and Trifunac, 1989, 1990a,b; Todorovska and Lee, 1989), and discrete-time 1-D wave-propagation models were proposed to study the seismic response of tall buildings (Safak, 1998; Gicev and Trifunac, 2006).

In the following, we use the elementary principles of wave propagation through a homogeneous shear beam model to study the relationships between the amplitude of an incident pulse of strong ground motion and the building response in terms of the computed transient and permanent drifts (rotations).

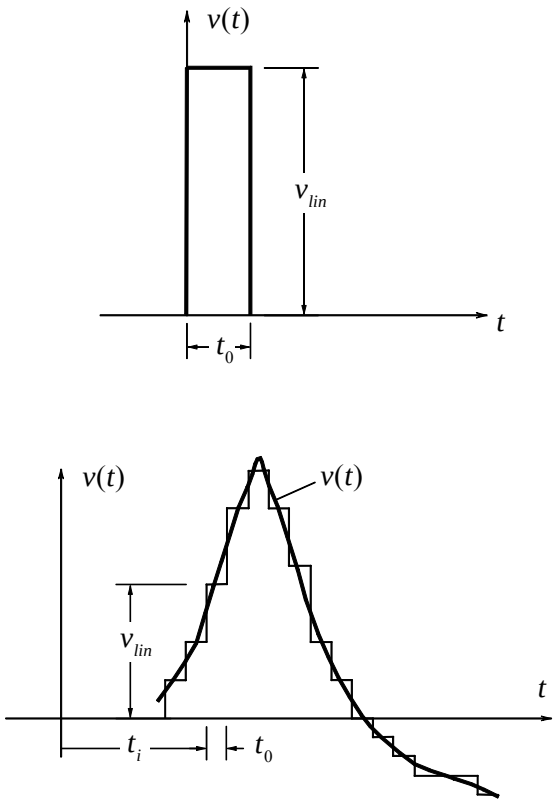

Fig. 1 A velocity pulse with amplitude v_{lin} and duration t_0 (top), and a general velocity pulse v(t) bottom).

1.1 Strong-Motion Pulses

Strong ground motion can be viewed as resulting from a sequence of pulses emitted from failing asperities on the fault surface (Trifunac, 1972a,b; 1998). Through multiple arrivals with different source-to-station paths and scattering, the strong motion observed at a site assumes the

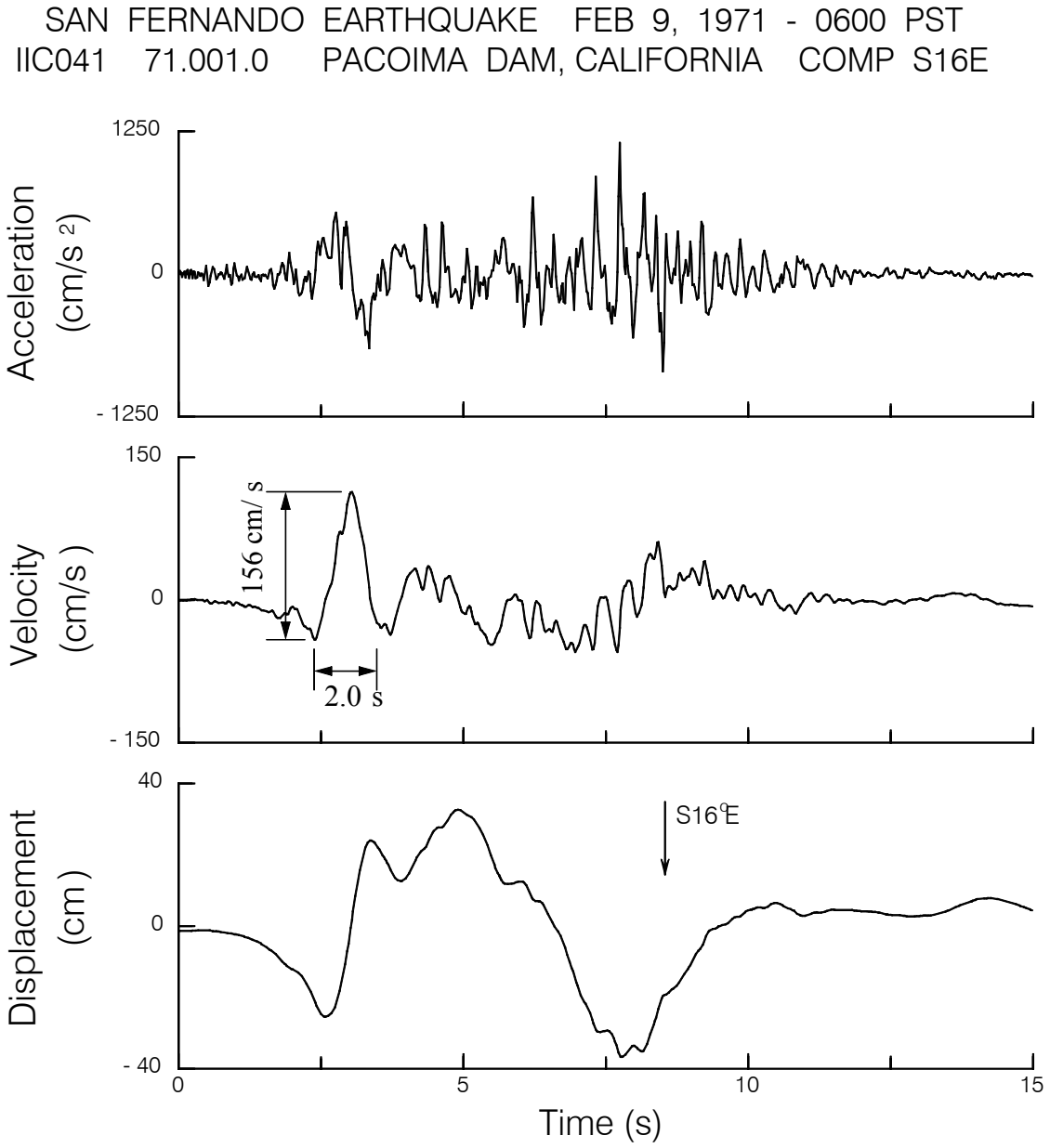

Fig. 2 S16° E component of strong motion acceleration, velocity and displacement, recorded at Pacoima dam during the San Fernando, California, earthquake of 1971 [Trifunac and Hudson, 1971].

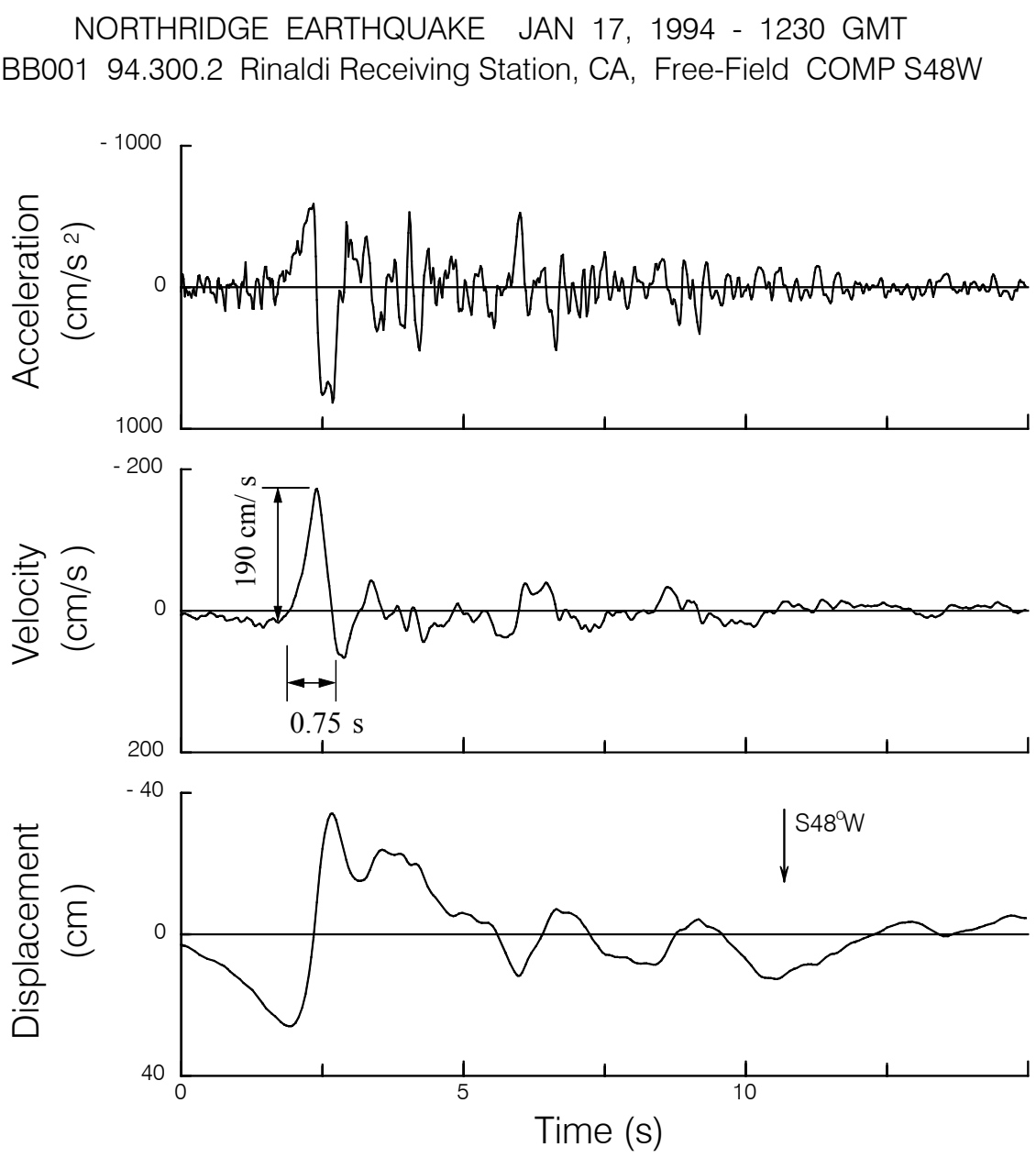

Fig. 3 S48° W component of strong motion acceleration, velocity and displacement recorded at Rinaldi Receiving Station, during the Northridge, California, earthquake of 1994 [Trifunac et al, 1998].

appearance of irregular oscillations in time, but it usually preserves one or several large and long displacement and velocity "pulses." These pulses are "spread out" in time due to multiple arrival paths and dispersion, but they do appear systematically in recordings at adjacent stations, at epicentral distances approaching 100 km (Todorovska and Trifunac 1997a,b; Trifunac et al., 1998).

To illustrate the response in terms of propagating waves, we consider the foundation motion transmitting a velocity pulse with amplitude v_{lin} and duration t_0 (Fig. 1a). For small t_0, this pulse approximates a delta function and can be used as a building block to represent more general velocity pulses in input motion (Fig. 1b). Figures 2 and 3 illustrate large-velocity pulses in the near field recorded during the 1971 San Fernando (Fig. 2) and 1994 Northridge (Fig. 3) earthquakes in California.

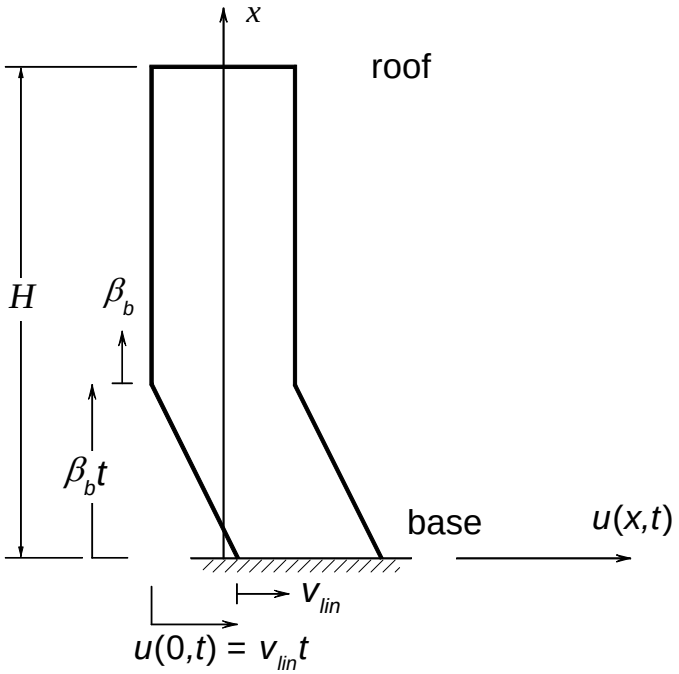

Fig. 4 A wave caused by sudden movement at the base of the shear building, for constant velocity pulse with amplitude V_{lin}, for time $t<t_0$ (= pulse duration).

For an elastic building on rigid soil (i.e., no soil-structure interaction), a velocity pulse with amplitude v_{lin} will create a wave propagating up the building with velocity β_b (see Fig. 4). For times shorter than H/β_b and for elastic strain γ ($\gamma = \partial u/\partial x = v_{lin}/\beta_b$)—i.e., displacement $u(x,t)$ smaller than the elastic limit u_y (Fig. 5)—the wave propagating up into the building will be defined by a straight line:

$$u(x,t)=\begin{cases} 0 & \text{, for } t \le \dfrac{x}{\beta_b} \quad \text{or} \quad x \ge \beta_b t \\ v_{lin}\left(t-\dfrac{x}{\beta_b}\right) & \text{, for } \dfrac{x}{\beta_b} \le t \le \dfrac{x}{\beta_b}+t_0 \quad \text{or} \quad \beta_b(t-t_0) \le x \le \beta_b t \\ v_{lin}\cdot t_0 & \text{, for } t \ge \dfrac{x}{\beta_b}+t_0 \quad \text{or} \quad x \le \beta_b\cdot(t-t_0) \end{cases} \tag{1.1}$$

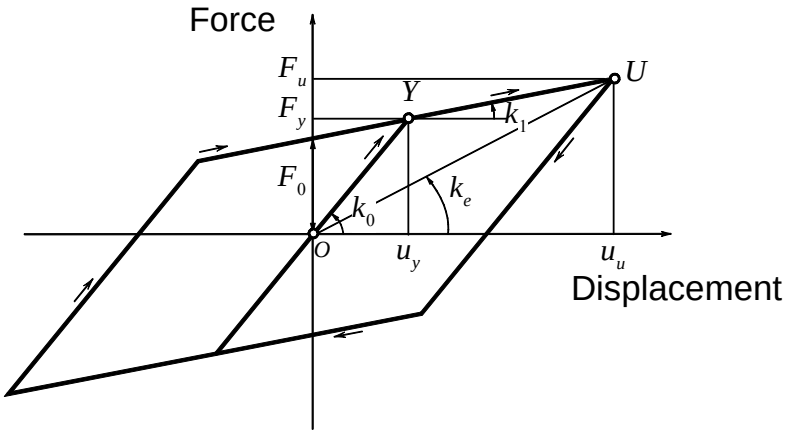

Fig. 5 Bilinear force-deformation representation of a shear-beam model experiencing nonlinear response.

During reflection from the stress-free top of the building, the incident wave from below and the reflected wave from above will interfere with each other, leading to double amplitude at the roof. The propagation of the energy of the pulse will continue downward as a linear wave as long as the incident wave amplitude is smaller than $u_y/2$.

Figure 6 illustrates the peak drift amplitudes (v_{lin}/β_b) in a linear shear beam model of a building, assuming that β_b = 100 m/s, short transient pulses, and linear response. For twelve earthquakes recorded in the VN7SH building (Trifunac et al., 2003), the maximum drift at the base of a structure is plotted versus v_{lin} (solid points). For the Landers, San Fernando, and Northridge earthquakes, the maximum drift at the roof is also shown ($2v_{lin}/\beta_b$). It can be seen that the maximum drift at the base occurs during the Northridge earthquake and is approximately 0.5%, while at roof it is equal to about 1%.

For a building supported by flexible soil, the soil-structure interaction will lead to horizontal and rocking deformations of the soil, and in general, this will reduce the amplitude v_{lin} of the strong-motion pulse entering the structure. Partitioning of the incident wave energy into horizontal and rocking motions of the building-foundation-soil system and scattering of the

incident wave from the foundation will thus reduce the energy available to cause relative deformation of the structure.

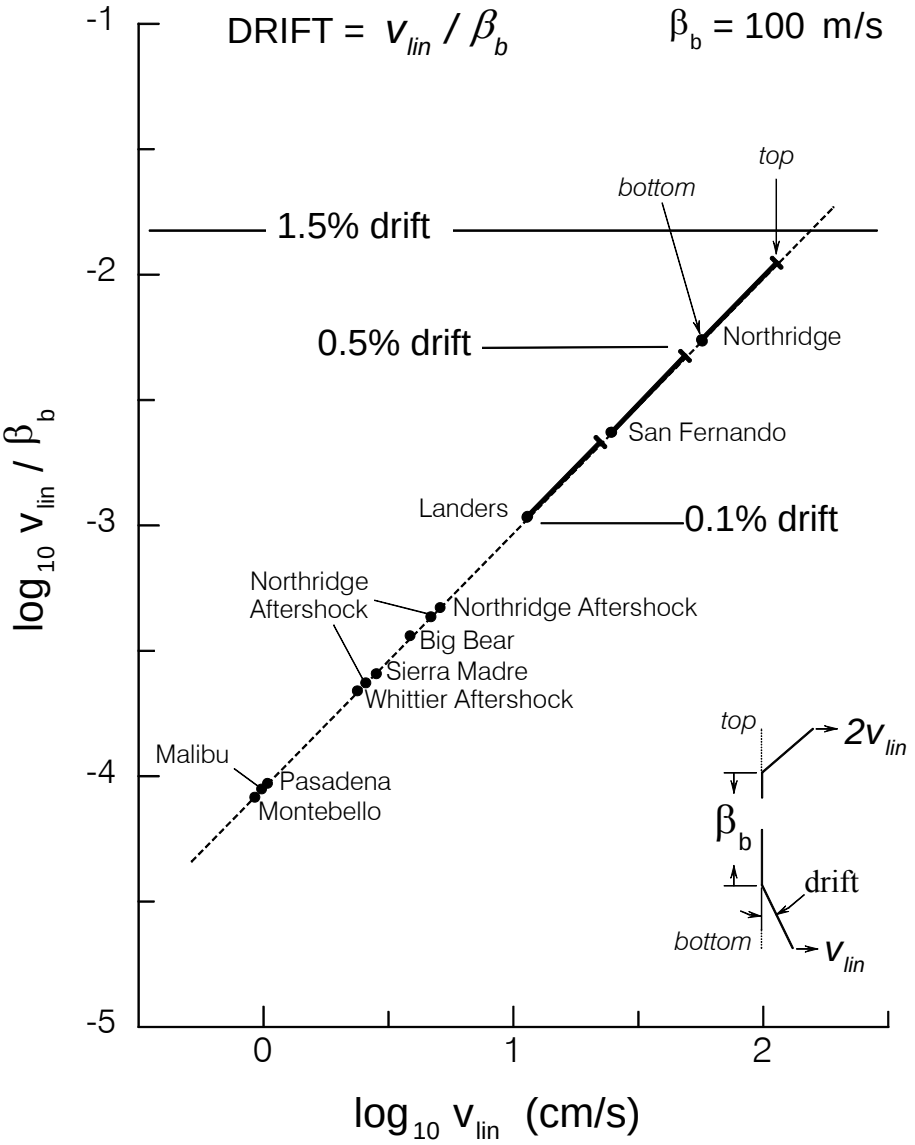

Fig. 6 Drift amplitudes in a shear-beam building with linear shear wave velocity $\beta_b = 100 m/s.$

The presence of the foundation within the soil creates an impedance jump for incident wave motion, and this causes scattering of the incident waves (Trifunac 1972c; Lee et al., 1982; Moslem and Trifunac, 1987; Todorovska and Trifunac 1990 a, b, c; 1991, 1992, 1993; Todorovska et al.). For the simple model employed in this work, this scattering is not strong because the strong motion excitation is described by one-dimensional incident wave motion.

In the above examples, we considered linear waves in the simple shear beam (when the incident wave amplitude is smaller than $u_y/2$), which led to the maximum shear strain (drift) equal to v_{lin}/β_b. For larger incident waves, nonlinear deformations in the beam will lead to more complicated relationships between the maximum strain (drift) and the governing variables of the problem. The purpose of what follows is to illustrate these relationships through a series of numerically simulated examples and to show where and how large the local strains (drifts) can be.

2. MODEL

We consider horizontal deformations, u, in a one-dimensional model of a building supported by one-dimensional half space and excited by a vertically propagating shear wave described by a half-sine-pulse (Fig. 7). For simplicity, the incident displacement in the soil is chosen to be a sinusoidal pulse with characteristics shown in Fig. 7. The constitutive law of the building material is assumed to be bilinear with the first slope, μ_0, representing the linear (initial) shear modulus, and the second slope, $\mu_1 = \gamma\mu_0$, representing the material during yielding (Fig. 8). The yielding strain in the building is ε_{yb}. To maintain the continuity of the stresses at the interface, the yielding strain at contact point 3 is obtained from $\mu_b\varepsilon_{yb} = \mu_3\varepsilon_{y3}$, as follows:

$$\varepsilon_{y3} = \frac{\mu_b}{\mu_3}\cdot\varepsilon_{yb}\,, \tag{2.1}$$

where μ_b is the shear modulus in the building and μ_3 is the equivalent shear modulus at point 3. The initial equivalent shear modulus for this point is obtained from the condition of continuity of the displacements and of the stresses at the interface as:

$$\mu_3 = \frac{\mu_s\mu_b\left(\Delta x_s + \Delta x_b\right)}{\mu_s\Delta x_b + \mu_b\Delta x_s}\quad . \tag{2.2}$$

The equation of motion is:

$$v_t = \frac{1}{\rho}(\sigma)_x\quad , \tag{2.3a}$$

and the relation between the derivative of the strain and the velocity is:

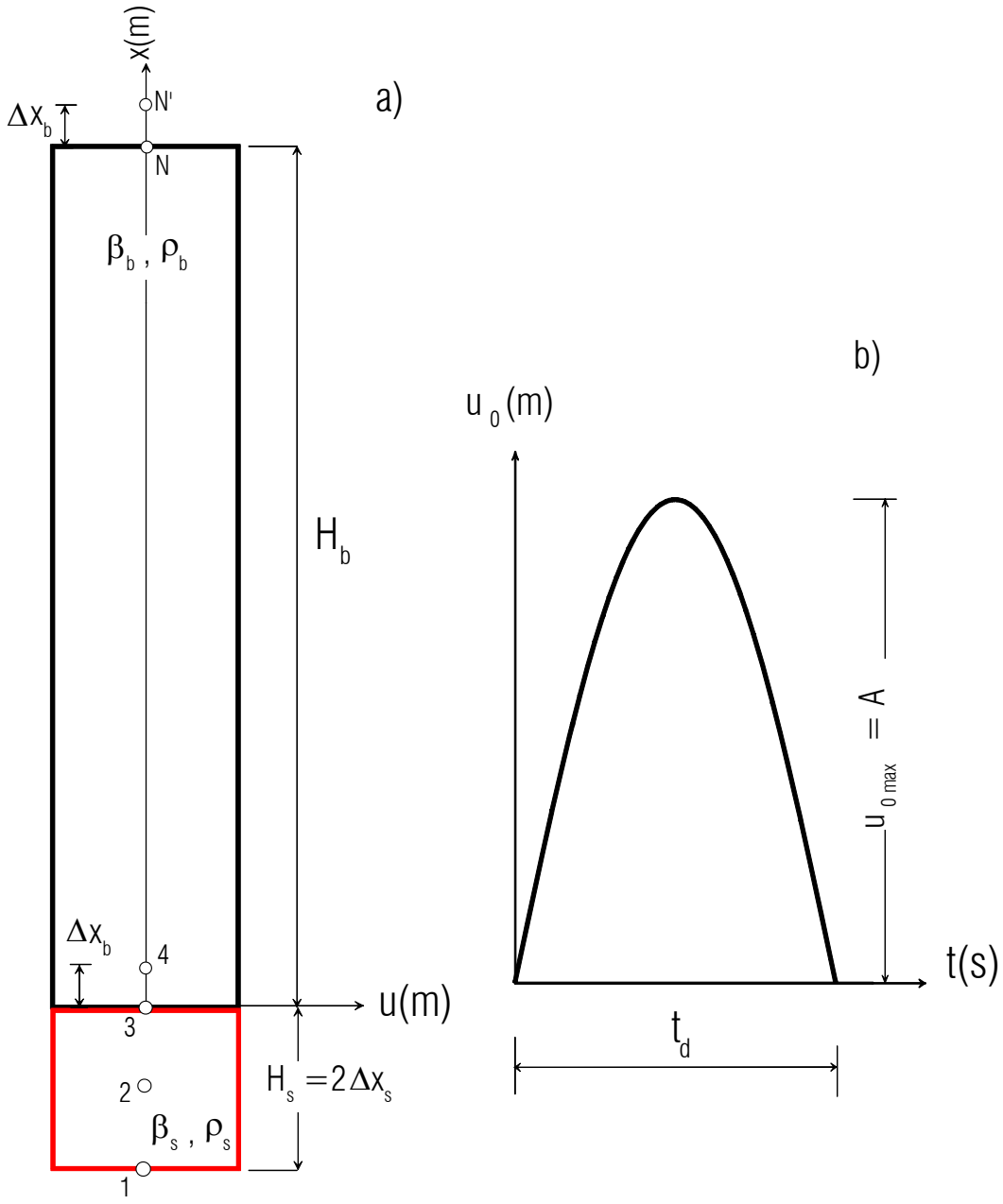

Fig. 7 Shear beam and incoming strong motion displacement pulse: (a) model of the beam, and (b) the pulse in the soil.

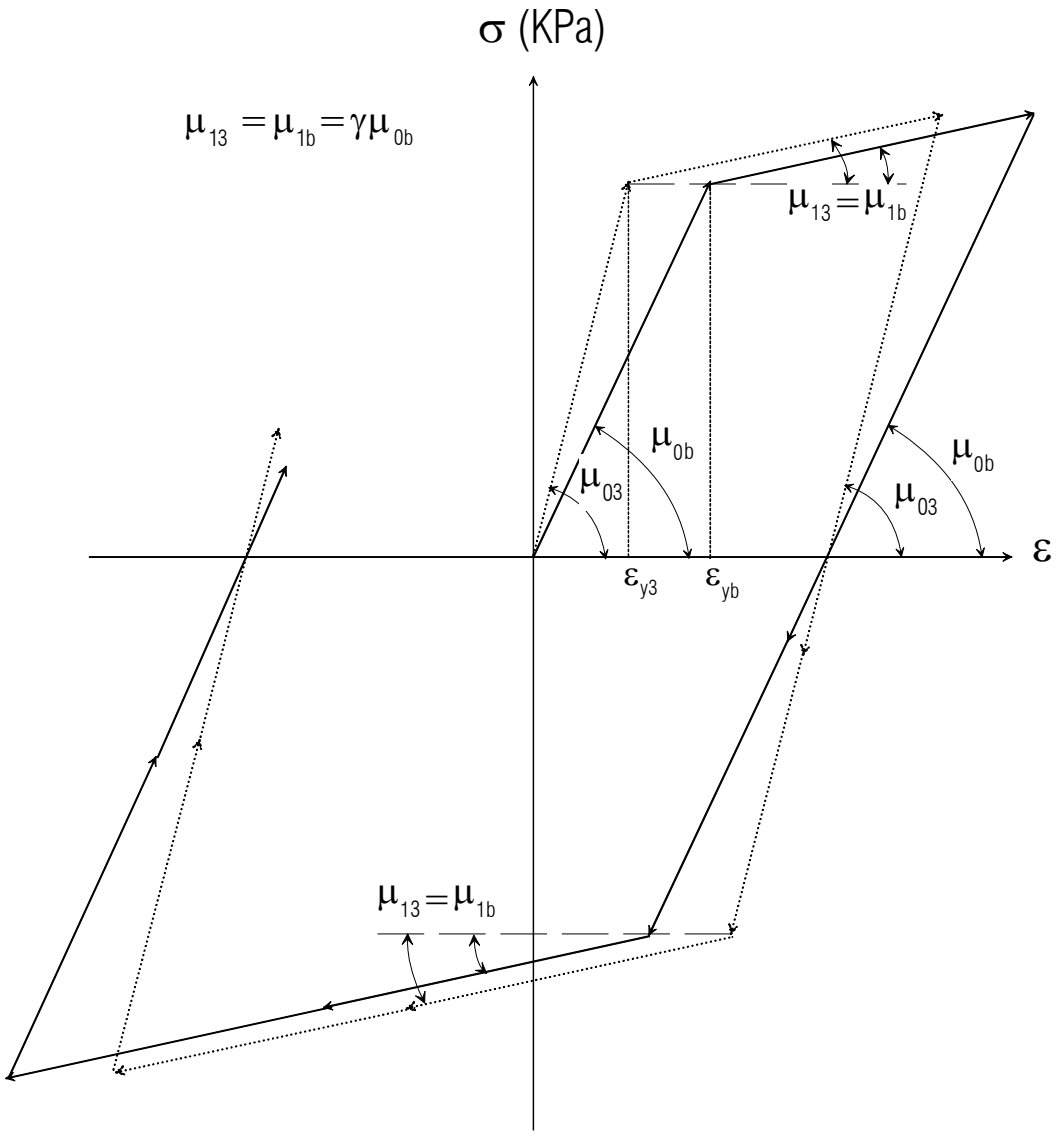

Fig. 8 The constitutive laws, σ - ε, for the building (solid line) and for the interface (dotted line).

$$\varepsilon_t = v_x \quad , \tag{2.3b}$$

where v, ρ, σ, and ε are particle velocity, density, shear stress, and shear strain, respectively, and the subscripts t and x represent derivatives with respect to time and space.

The domain consists of two materials (see Fig. 7): (1) soil with physical properties ρ_s and μ_s, and (2) a building with physical properties ρ_b and μ_b, where ρ_i is the density and μ_i is the

initial shear modulus in the soil (i = s) or in the building (i = b). $v = \frac{\partial u}{\partial t}$ and $\varepsilon = \frac{\partial u}{\partial x}$ are the velocity and the strain of a particle, respectively, and u is the out-of-plane displacement of a particle perpendicular to the velocity along the propagation ray.

It is assumed that the incoming wave is known and that its displacement as a function of t is prescribed at the soil point 1 ($x = -2\Delta x_s$). For analysis, in this paper it is assumed that the soil is always in the linear elastic state. To model the radiation of the wave from the building, we provide an artificial boundary at the bottom of the model.

The transparent boundary adopted for this study is described in Fujino and Hakuno (1978) (Fig. 9). This is a perfect transparent boundary for one-dimensional waves, when $\frac{\beta \Delta t}{\Delta x} = 1$. In Fig. 9, the horizontal axis is time and the vertical axis is space. The first coordinate represents discrete space while the second coordinate represents discrete time.

Point 1 is where the prescribed displacement is applied. We assume that this displacement travels upward in each time step. Point 2 is the boundary point of the model, where the quantities of motion are updated in each time step. Point 3 is the first spatial point, where the motion is computed using finite differences.

The motion at each point results from two components of motion, one from a wave going up, and the other from a wave going down. To update the motion at boundary point 2, in time step k, we proceed as follows. The total motion at 2 is

$$u(2,k) = \uparrow u(2,k) + \downarrow u(2,k), \tag{2.4}$$

where the arrows denote direction of the wave propagation ($\uparrow$ for up and $\downarrow$ for down). The motion at point 1 results from up-going wave $u(1,t/\Delta t) = \uparrow u(1,t/\Delta t) = u_0(t/\Delta t)$. Then,

$$\uparrow u(2,k) = u(1,k-1) = u_0(k-1). \tag{2.5}$$

The component of motion from the wave traveling down is

$$\downarrow u(2,k) = \downarrow u(3,k-1). \tag{2.6}$$

From $u(3,k-1) = \uparrow u(3,k-1) + \downarrow u(3,k-1)$, it follows that

$$\downarrow u(3,k-1) = u(3,k-1) - \uparrow u(3,k-1). \tag{2.7}$$

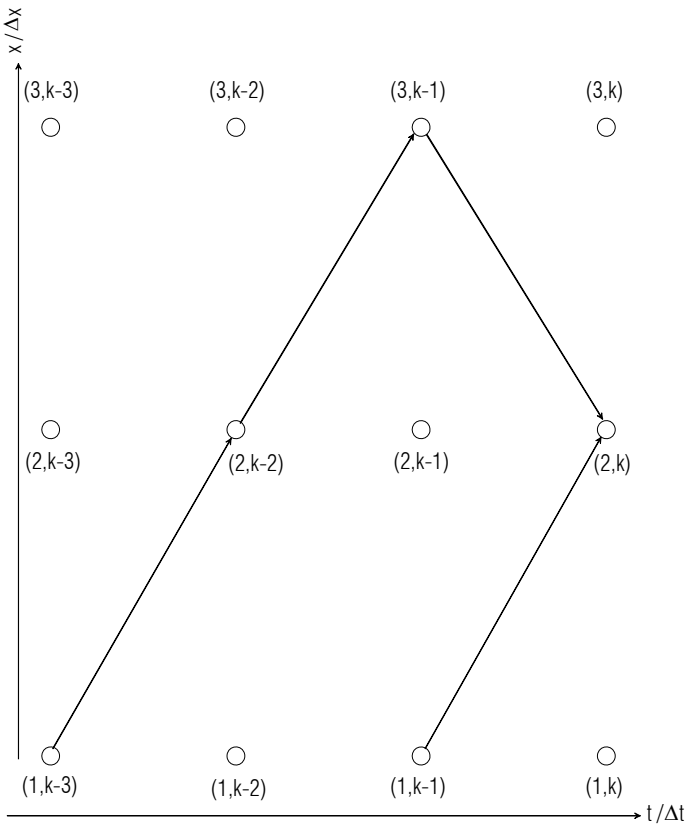

Fig. 9 The model of the absorbing boundary.

The motion at 3 at time step (k-1) from the wave traveling upward is the motion at 2 from the wave traveling upward in the previous time step (k-2). The motion at 2 from the wave traveling upward in time step (k-2) is the given motion at time step (k-3), so that with $\uparrow u(3,k-1) = \uparrow u(2,k-2) = u_0(k-3)$ equations (2.6) and (2.7) become

$$\downarrow u(2,k) = \downarrow u(3,k-1) = u(3,k-1) - u_0(k-3). \tag{2.8}$$

Substituting Eq.(2.5) and Eq.(2.8) into Eq.(2.4), the motion at point 2 is

$$u(2,k) = u_0(k-1) + u(3,k-1) - u_0(k-3) \qquad \forall k\ . \tag{2.9}$$

Equation (2.9) is the boundary condition at the transparent boundary point 2, where u stands for velocity, strain, or stress.

3. NUMERICAL SCHEME

As noted by Dablain (1986), for the solution of 1-D wave propagation a finite difference scheme with accuracy $O(\Delta t^2, \Delta x^2)$, where Δx and Δt are the space and time increments, leads to the exact solution for $\frac{\beta \Delta t}{\Delta x} = 1$, where β is the velocity of shear waves. With a ratio of the spatial intervals $\frac{\Delta x_b}{\Delta x_s} = \frac{\beta_b}{\beta_s}$, we can meet this requirement.

The Lax-Wendroff $O(\Delta t^2, \Delta x^2)$ finite difference method (Lax and Wendroff, 1964) for a set of simultaneous equations is used to solve the problem. A mesh with different spatial intervals in the soil and in the building is used. The spatial intervals are defined by $\Delta x_i = \beta_i \cdot \Delta t$, where β_i is the velocity of shear waves in the soil (i = s) or in the building (i = b) and Δt is the time step.

The height of the building is divided into 197 spatial intervals and the soil into 2 spatial intervals, so the properties of the mesh are:

$$\Delta x_b = \frac{H_b}{197}, \quad \text{and} \quad \Delta x_s = \frac{\beta_s}{\beta_b} \Delta x_b \qquad . \tag{3.1a}$$

The cell length at interface point 3 (x = 0) is:

$$\Delta x_3 = \frac{\left(\Delta x_b + \Delta x_s\right)}{2} \qquad . \tag{3.1b}$$

The time step is constant during the analysis:

$$\Delta t = \frac{\Delta x_b}{\beta_b} = \frac{\Delta x_s}{\beta_s} . \tag{3.2}$$

Above the top point, N, additional dummy point N' is introduced at distance Δx_b. For a stress-free point N, for all time, the velocities and the stress at point N' are updated as:

$$v_{N'} = v_{N-1} \tag{3.3a}$$

$$\sigma_{N'} = -\sigma_{N-1} \qquad . \tag{3.3b}$$

Equations (2.3) can be written in vector form as:

$$\frac{\partial \mathbf{U}}{\partial t} = \frac{\partial \mathbf{F}}{\partial x} \quad , \tag{3.4}$$

where

$$\mathbf{U} = \begin{Bmatrix} \mathrm{v} \\ \varepsilon \end{Bmatrix} \quad \text{and} \quad \mathbf{F} = \begin{Bmatrix} \sigma \\ \rho \\ \mathrm{v} \end{Bmatrix} \quad . \tag{3.5}$$

The vector **U** at point i in time (j+1) Δt expanded in Taylor series is:

$$\mathbf{U}_{i,j+1} = \mathbf{U}_{i,j} + \Delta t \left(\frac{\partial \mathbf{U}}{\partial t} \right)_{i,j} + \frac{\Delta t^2}{2} \left(\frac{\partial^2 \mathbf{U}}{\partial t^2} \right)_{i,j} + O(\Delta t^3) \, ,$$

and from Eq.(3.4):

$$\mathbf{U}_{i,j+1} = \mathbf{U}_{i,j} + \Delta t \left(\frac{\partial \mathbf{F}}{\partial x} \right)_{i,j} + \frac{\Delta t^2}{2} \frac{\partial}{\partial t} \left(\frac{\partial \mathbf{F}}{\partial x} \right)_{i,j} + O(\Delta t^3)$$

$$\mathbf{U}_{i,j+1} = \mathbf{U}_{i,j} + \Delta t \left(\frac{\partial \mathbf{F}}{\partial x} \right)_{i,j} + \frac{\Delta t^2}{2} \frac{\partial}{\partial x} \left(\mathbf{A}(\mathbf{U}) \frac{\partial \mathbf{F}}{\partial x} \right)_{i,j} + O(\Delta t^3) \quad . \tag{3.6}$$

A(U) is the Jacobian matrix:

$$\mathbf{A}(\mathbf{U}) = \frac{\partial \mathbf{F}}{\partial \mathbf{U}} = \begin{bmatrix} \dfrac{\partial \sigma}{\rho \partial v} & \dfrac{\partial \sigma}{\rho \partial \varepsilon} \\ \dfrac{\partial v}{\partial v} & \dfrac{\partial v}{\partial \varepsilon} \end{bmatrix} = \begin{bmatrix} 0 & \dfrac{1}{\rho} \dfrac{d\sigma}{d\varepsilon} \\ 1 & 0 \end{bmatrix} \quad . \tag{3.7}$$

4. RESULTS

For the numerical examples in this paper, we consider a shear beam supported by elastic soil, as shown in Fig. 7. The densities of the soil and of the beam are assumed to be the same $\rho_b = \rho_s = \rho = 2000$ kg/m^3. The velocity of the shear waves in the soil is taken as $\beta_s = 250 m/s$, and the velocity in the building as $\beta_b = 100\, m/s$. The height of the building is $H_B = 10m$.

To study nonlinear response and the development of transient and permanent strains in the beam, we introduce two dimensionless parameters:

dimensionless amplitude $\alpha = \dfrac{A}{H_b \cdot \varepsilon_{yb}}$, (4.1)

where A is the amplitude of the pulse (see Fig. 7), H_b is the height of the building, and ε_{yb} is the yielding strain in the building; and

dimensionless frequency $\eta = \dfrac{H_b}{\dfrac{\lambda_b}{2}} = \dfrac{H_b}{\dfrac{\beta_b \cdot 2t_d}{2}} = \dfrac{H_b}{\beta_b t_d}$, (4.2)

where: λ_b is the wavelength of the wave in the building, β_b is the shear wave velocity in the building, and t_d is the duration of the half-sine pulse.

In our previous paper (Gicev and Trifunac, 2006), we derived the conditions for the first occurrence of permanent strain in the building. For our example in this work, $C_B = 0.2228$. These conditions relate the amplitude and the frequency of the pulse, the physical properties of the building, and the soil stiffness:

$$\alpha\eta > \frac{1}{\pi k_t} = \frac{\beta_b + \beta_s}{2\pi\beta_s} = C_B = 0.2228 \tag{4.3}$$

$$\alpha\eta > \frac{1}{2\pi k_t} = \frac{\beta_b + \beta_s}{4\pi\beta_s} = C_T = \frac{C_B}{2} = 0.1114 \tag{4.4}$$

$$\alpha\eta > \frac{1}{\pi k_t (2 + |k_r|)} = \frac{\beta_b + \beta_s}{2\pi\beta_s (2 + |k_r|)} = \frac{C_B}{2 + |k_r|} = 0.09174 \quad . \tag{4.5}$$

The condition (4.3) requires the biggest product $\alpha\eta$, and if it is satisfied, it describes the occurrence of the first permanent strain, which is always located at the bottom of the building. If this condition (4.3) is not satisfied, the condition (4.4) becomes relevant and, if it is satisfied, the first permanent strain occurs at some point (T) between the base and top of the building. Finally, if both conditions (4.3) and (4.4) are not satisfied, and $\eta \le 0.5$, the condition (4.5) describes the occurrence of the first permanent strain.

For the shear wave velocities in our example ($\beta_s = 250 m/s$ and $\beta_b = 100 m/s$), the coefficient of transmission of the wave from the soil to the building is $k_t = \dfrac{10}{7}$, and the coefficient of reflection of the incident wave from the building, back to the building, is $k_r = -\dfrac{3}{7}$.

We will consider the range of the dimensionless frequencies $0.06 \le \eta \le 5$. In this frequency range, the response of the beam for the five dimensionless amplitudes $\alpha = 0.01, 0.05, 0.10, 0.20,$ and 0.30, and the four ratios between the moduli $\gamma = \frac{\mu_1}{\mu_0} = 0.0, 0.1, 0.2, \text{and } 0.3$, will be considered (see Fig. 8). The analysis will last two seconds, during which time the wave will have ten reflections from the interface. After this time, we assume that the portion of the wave energy remaining in the beam is negligible.

In Fig.10, the maximum strain in the building, $\varepsilon_{\max}$, versus the dimensionless frequency, η, is shown for five different dimensionless amplitudes. This strain is the absolute maximum of the strain occurring in the beam at any time of its response. Together with the curves $\varepsilon_{\max}(\eta)$, the curve v_{lin} / β_b versus η for $\alpha = 0.3$ is shown. The quantity $v_{lin} = v_{entr}^{lin}$ is the maximum velocity entering the beam, supposing that the beam is linear, for the considered frequency of the pulse. As can be seen from the plot, this relation is linear in η, which follows from the linear relation:

$$v_{lin} = \frac{\pi A}{t_d} \cdot k_t = \pi \alpha \eta \varepsilon_{yb} \beta_b k_t . \tag{4.6}$$

Instead of studying the absolute maximum of the strain, we will consider:

- the normalized maximum strain, which we define by the ratio

$$\varepsilon_{norm}^{\max} = \frac{\varepsilon_{\max}}{\frac{v_{lin}}{\beta_b}} = \frac{\varepsilon_{\max}}{\varepsilon_{lin}} \quad . \tag{4.7}$$

This quantity will show the degree of nonlinearity in the building response and the effects of the interference on the amplification of the linear entry strain. This strain is always larger than one.

- the normalized strain at the end of the analysis, which is the ratio

$$\varepsilon_{norm}^{end} = \frac{\varepsilon_{end}}{\frac{v_{lin}}{\beta_b}} = \frac{\varepsilon_{end}}{\varepsilon_{lin}} \quad . \tag{4.8}$$

This quantity will show us the ratio of the permanent strain (after all of the wave energy exits the building) and of the linear entry strain. This strain can be larger or smaller than one, and for linear waves (when neither condition 4.4 nor condition 4.5 are satisfied) it is zero.

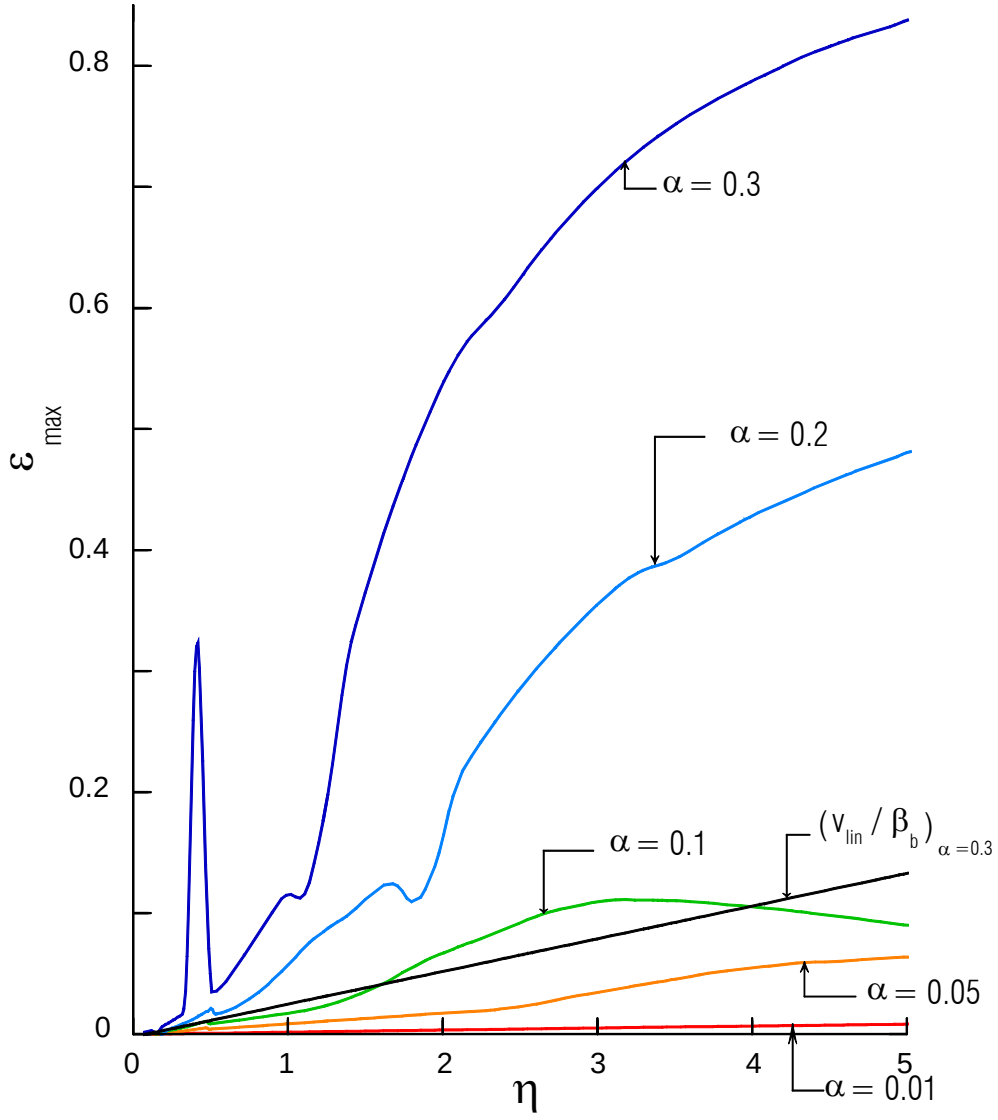

Fig. 10 Maximum strain versus dimensionless frequency for five dimensionless amplitudes α .

the maximum strain normalized by the yielding strain

$$\varepsilon_{norm}^{y} = \frac{\varepsilon_{\max}}{\varepsilon_{yb}}, \tag{4.9}$$

which is useful for design purposes. If this quantity at some point of the building is larger than the maximum allowed ductility $\mu = \frac{\varepsilon_{fail}}{\varepsilon_{yb}}$, where ε_{fail} is the largest strain that can occur in the material, the building may collapse. For linear waves, this normalized strain is smaller than one.

In Fig. 11a, the normalized strain $\varepsilon_{norm}^{\max}$ versus dimensionless frequency η is shown for the five dimensionless amplitudes $\alpha = 0.01, 0.05, 0.1, 0.2, 0.3$ and for elasto-plastic material ($\gamma = 0$). In the further discussions, the region (η, x) will be divided into three sub-regions (zones):

Zone 1: $Z_1 = \{(\eta, x) | \eta < 0.5, \forall x\}$ **Zone 2:** $Z_2 = \{(\eta, x) | 0.5 \le \eta \le 5, x \le 1\}$

Zone 3: $Z_3 = \{(\eta, x) | 0.5 \le \eta \le 5, x > 1\}$.

The boundary between zones 2 and 3 is taken close to the soil-building contact. For convenience, we put this boundary at one tenth of the height of the building, at x = 1.

For $\alpha = 0.01$, the condition (4.5) is not satisfied in the zone Z_1, ($\eta \le 0.5$), because $\eta > \frac{C_B}{(17/7)\cdot\alpha} = \frac{0.2228 \cdot 7}{17 \cdot 0.01} = 9.174 > 0.5$, and so there in no permanent strain in this region. The condition (4.4) gives $\eta > \frac{C_B}{2\alpha} = \frac{0.2228}{2 \cdot 0.01} = 11.14 > 5$, which means that in the range $0.06 \le \eta \le 5$ the response of the beam for $\alpha = 0.01$ is always linear. The absolute maximum occurs in zone Z_1, for η close to 0.5 ($\eta = 0.45$), at the bottom of the beam. Its value is 2.5363 (see Table 1). For $\eta > 0.5$, this normalized strain is constant and equal to 2. In zone Z_2 the largest normalized strain occurs at the beginning of the second wave passage, and its theoretical value is $1 + |k_r| = \frac{10}{7} = 1.4286$. The numerical calculation gives 1.4266. In Fig. 12, which shows the normalized strain at the end of the analysis, when there is no wave energy remaining in the building, this case is illustrated by the zero-ordinates line.

For $\alpha = 0.05$, the response in Z_1 is linear, and the ordinates in Fig. 11a are equal to those for $\alpha = 0.01$. The condition (4.4) gives $\eta > \frac{C_B}{2\alpha} = \frac{0.2228}{2 \cdot 0.05} = 2.228$, indicating that for these frequencies the permanent strain occurs at the top of the beam, in zone Z_3. The maximum

Table 1. Maximum $\varepsilon_{n,\max}$ and minimum $\varepsilon_{n,\min}$ normalized strains at time when maximum occurs and their locations in the three zones.

$$\varepsilon_n = \left(\frac{\varepsilon \cdot \beta_b}{v_{entr}} \right)_{t=t(\varepsilon_{\max})}$$

Zone 1: $\eta < 0.5 \bigcup x \le 10m$

Zone 2: $0.5 \le \eta \le 5 \bigcup x \le 1m$

Zone 3: $0.5 \le \eta \le 5 \bigcup x > 1m$

Normalization with linear entry velocity $v_{entr} = v_{entr}^{lin} = \frac{A\pi}{t_d} \cdot k_t$

$\gamma = \frac{\mu_2}{\mu_1}$	Fig. No.	Zone #	α	$\eta_{\max}$	$x_{\max}$ (m)	$\varepsilon_{n\max}$	$\eta_{\min}$	$x_{\min}$ (m)	$\varepsilon_{n\min}$
0.0	15a	1	0.01	0.45	0.	2.5363	0.07	1.88	-1.0979
			0.05	0.46	0.	2.5669	0.10	0.	-1.0974
			0.1	0.46	0.	2.5621	0.11	2.13	-1.0774
			0.2	0.46	0.	2.6814	0.11	0.	-1.0774
			0.3	0.40	0.	29.7380	0.11	0.	-1.0774
		2	0.01	/	/	/	/	/	/
			0.05	5.00	0.	0.0344	4.49	0.05	-0.1926
			0.1	4.49	0.	1.4307	3.74	0.10	-0.4651
			0.2	1.70	0.	2.7906	2.99	0.	-6.6910
			0.3	1.07	0.	3.9902	2.03	0.	-10.038
		3	0.01	0.5	1.78	2.0192	/	/	/
			0.05	4.31	9.24	3.0956	/	/	/
			0.1	2.63	8.78	4.2464	/	/	/
			0.2	1.52	8.07	4.4169	1.97	1.02	-0.5657
			0.3	1.07	7.21	4.6230	1.28	1.02	-0.5804
0.1	16a	1	0.01	0.45	0.	2.5363	0.07	1.88	-1.0979
			0.05	0.46	0.	2.5669	0.10	0.	-1.0974
			0.1	0.46	0.	2.5621	0.11	2.13	-1.0774
			0.2	0.46	0.	2.7458	0.11	0.	-1.0774
			0.3	0.41	0.	5.3459	0.11	0.	-1.0774
		2	0.01	/	/	/	/	/	/
			0.05	5.00	0.	0.0812	4.49	0.05	-0.1354
			0.1	4.49	0.	1.4454	5.00	0.	-2.2442
			0.2	1.97	0.	1.4678	3.98	0.	-3.1995
			0.3	1.25	0.	1.4392	3.32	0.	-3.6930
		3	0.01	0.5	1.78	2.0192	/	/	/
			0.05	4.13	9.19	2.7873	/	/	/
			0.1	2.18	8.43	3.2201	/	/	/
			0.2	1.25	7.31	3.3316	/	/	/
			0.3	0.80	5.79	3.1367	/	/	/

Continued on the next page

Table 1. (continued)

$\gamma = \frac{\mu_2}{\mu_1}$	Fig. No.	Zone #	α	$\eta_{\max}$	$x_{\max}$ (m)	$\varepsilon_{n\max}$	$\eta_{\min}$	$x_{\min}$ (m)	$\varepsilon_{n\min}$
0.2	17a	1	0.01	0.45	0.	2.5363	0.07	1.88	-1.0979
			0.05	0.46	0.	2.5669	0.10	0.	-1.0974
			0.1	0.46	0.	2.5621	0.11	2.13	-1.0774
			0.2	0.46	0.	2.7745	0.11	0.	-1.0774
			0.3	0.41	0.	4.2735	0.11	0.	-1.0774
		2	0.01	/	/	/	/	/	/
			0.05	5.00	0.	0.0698	4.49	0.05	-0.0978
			0.1	4.37	0.	1.2049	5.00	0.	-1.8560
			0.2	5.00	0.	2.4277	3.98	0.	-2.4368
			0.3	4.79	0.	2.7357	2.96	0.	-2.7004
		3	0.01	0.5	1.78	2.0192	/	/	/
			0.05	4.22	9.19	2.5401	/	/	/
			0.1	2.24	8.43	2.8346	/	/	/
			0.2	1.13	6.80	2.8517	4.70	1.47	-0.2373
			0.3	0.71	4.97	2.7213	4.31	1.02	-0.3879
0.3	18a	1	0.01	0.45	0.	2.5363	0.07	1.88	-1.0979
			0.05	0.46	0.	2.5669	0.10	0.	-1.0974
			0.1	0.46	0.	2.5621	0.11	2.13	-1.0774
			0.2	0.46	0.	2.7267	0.11	0.	-1.0774
			0.3	0.41	0.	3.7739	0.11	0.	-1.0774
		2	0.01	/	/	/	/	/	/
			0.05	5.00	0.	0.0795	4.49	0.	-0.0753
			0.1	5.00	0.	1.4136	4.37	0.91	-0.0771
			0.2	5.00	0.	2.0413	2.45	0.	-1.9067
			0.3	5.00	0.	2.2563	1.82	0.	-2.1236
		3	0.01	0.5	1.78	2.0192	/	/	/
			0.05	4.31	9.19	2.3928	/	/	/
			0.1	2.12	8.22	2.6254	4.58	1.68	-0.4869
			0.2	1.10	6.55	2.5878	2.69	2.69	-0.4143
			0.3	0.68	4.52	2.4890	4.79	1.02	-0.6067

normalized strain reaches its maximum value 3.0956 at the point $(\eta, x) = (4.31, 9.24)$ (see Table 1). This is the largest amplification of the entering strains for $\alpha = 0.05$ in the considered frequency range. At this frequency, a small permanent strain starts to develop at Z_2 for $\eta > \frac{C_B}{\alpha} = \frac{0.2228}{0.05} = 4.46$, after condition (4.3) is satisfied (see Fig. 15a, and Fig. 15b).

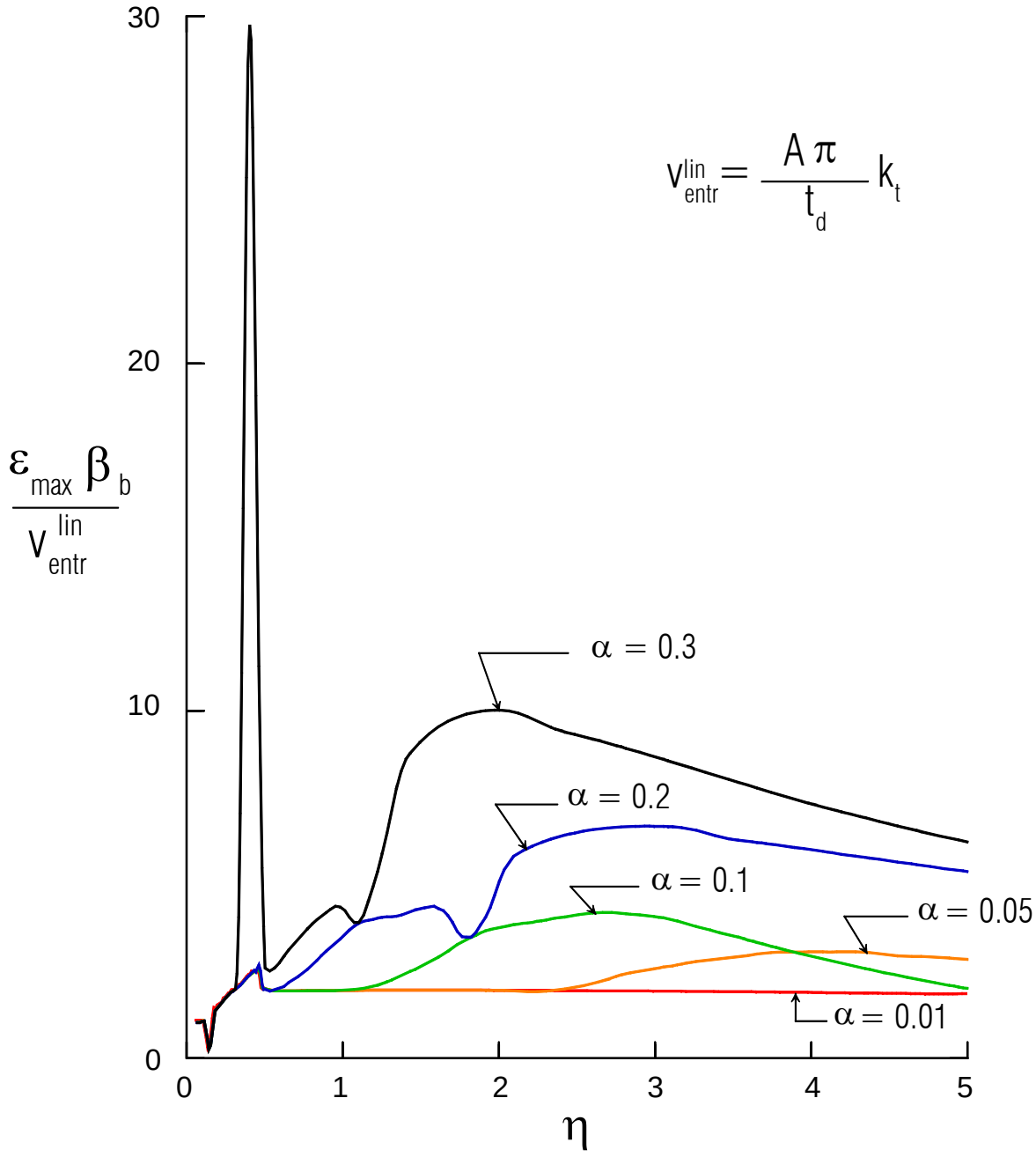

Fig. 11a Maximum normalized strain versus dimensionless frequency for five dimensionless amplitudes α.

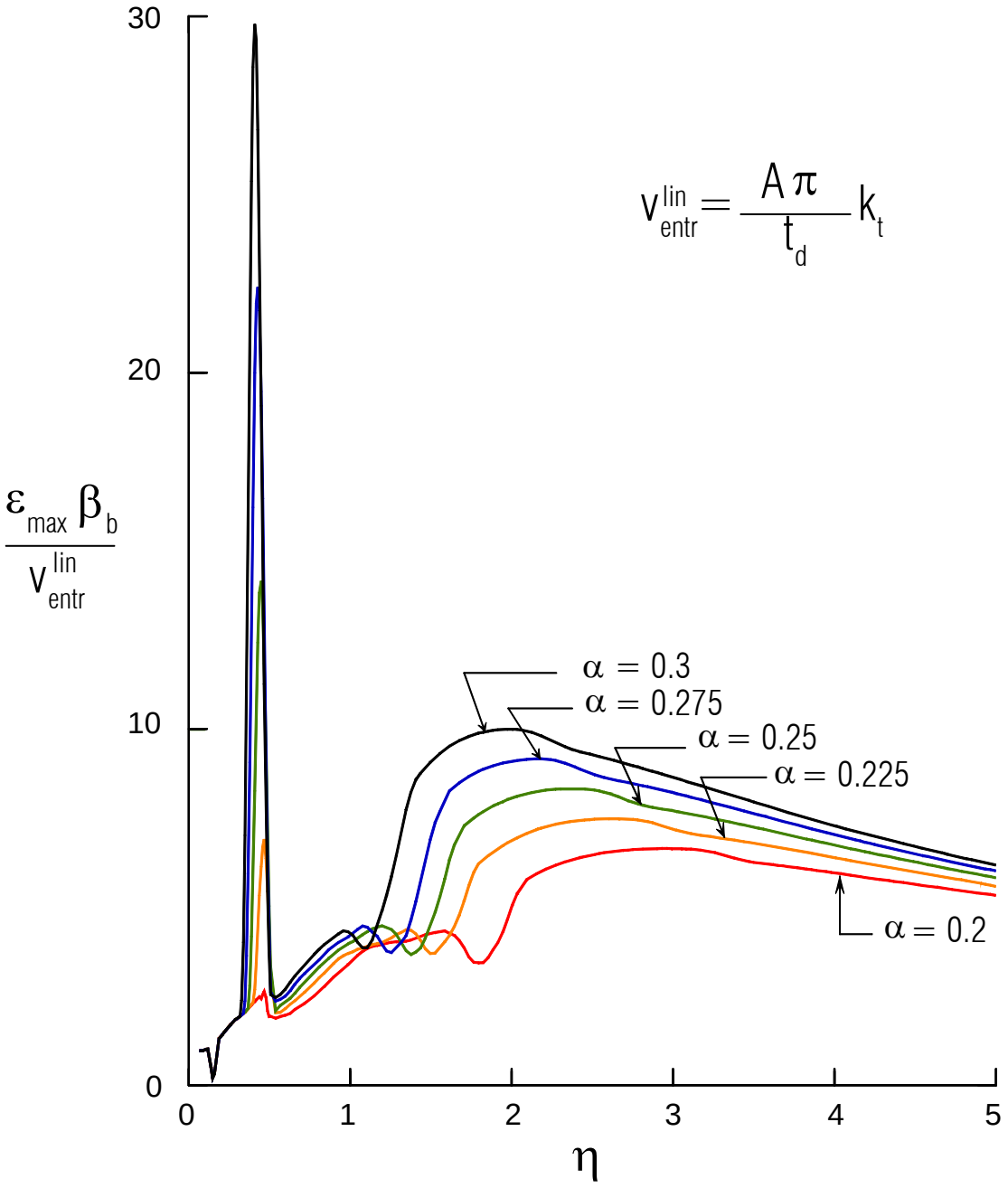

Fig. 11b Maximum normalized strain versus dimensionless frequency for dimensionless amplitudes α = 0.2, 0.225, 0.25, 0.257, and 0.3.

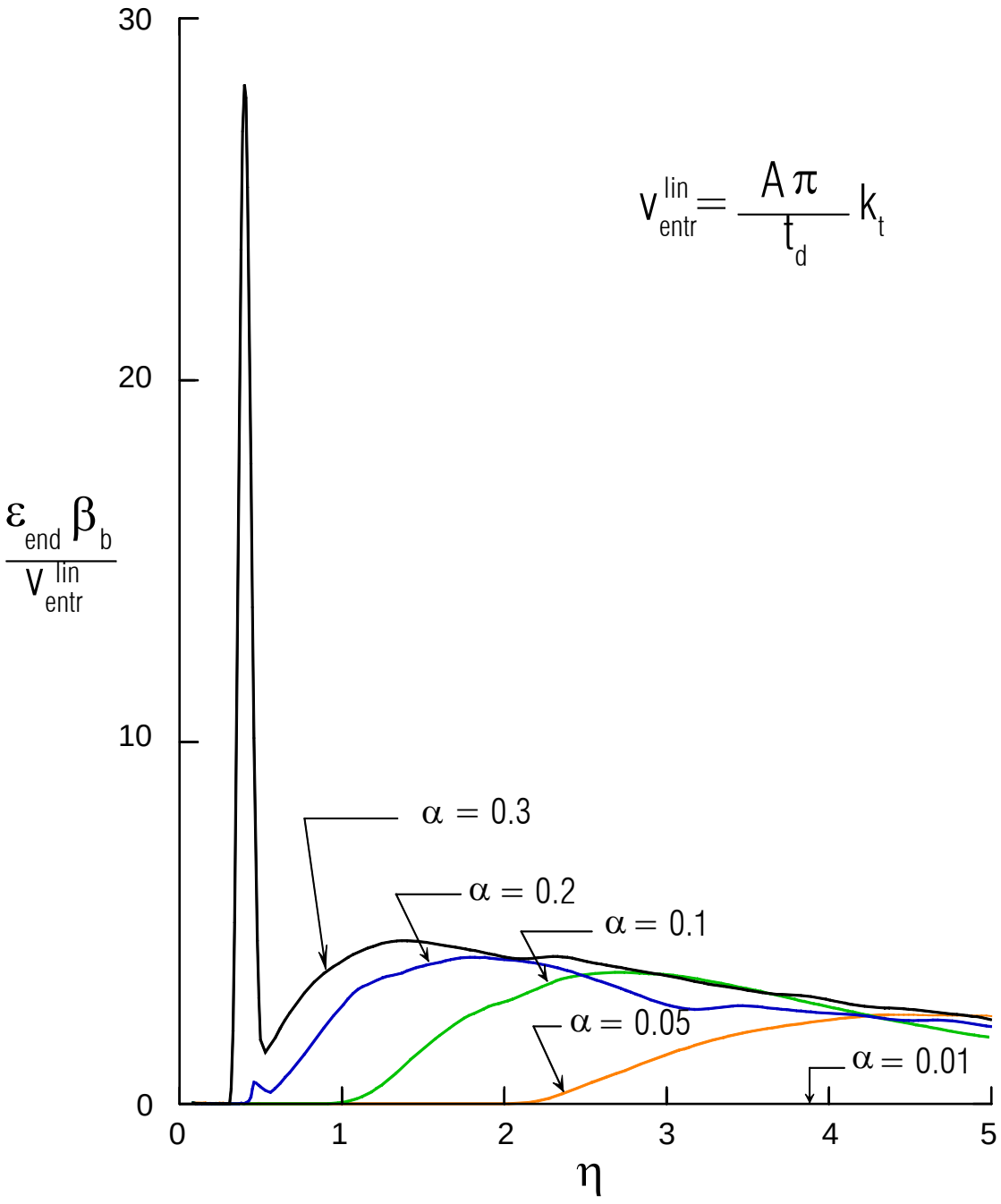

Fig. 12 Normalized remaining permanent strain versus dimensionless frequency, for five dimensionless amplitudes.

For development of this permanent strain at the bottom, a certain amount of the input wave energy is spent, so the wave traveling up is smaller, leading to smaller permanent strain at the top. In Fig. 12, while η is less than 2.228, the normalized strain at the end is zero, and for

$\eta > 2.228$ it has nonzero ordinates with maximum amplitude equal to 2.4746 at $(\eta, x) = (4.58, 9.24)$ (see Table 2).

The response is similar for $\alpha = 0.1$. Again, in Z_1 the response is linear and the first permanent strain occurs for $\eta > \frac{C_B}{2\alpha} = \frac{0.2228}{2 \cdot 0.1} = 1.114$ (see Fig. 12). The curve for $\alpha = 0.1$ and for $\eta \le 1.114$ coincides with the curves for $\alpha = 0.01$ and $\alpha = 0.05$. The maximum occurs in zone Z_3 for $(\eta, x) = (2.63, 8.78)$, and its value is 4.2464 (see Table 1).

For $\alpha = 0.2$ in zone Z_1, condition (4.5) gives $\eta > \frac{C_B}{\frac{17}{7} \cdot \alpha} = \frac{0.2228 \cdot 7}{17 \cdot 0.2} = 0.4587 < 0.5$, which indicates the appearance of a permanent strain at the beginning of the second passage of the wave through the beam. Condition (4.4) gives $\eta > \frac{C_B}{2\alpha} = \frac{0.2228}{2 \cdot 0.2} = 0.557$. This indicates that in the very narrow interval $0.5 < \eta \le 0.557$ the response of the beam is linear (equal to 2 in Fig. 11a). In zone Z_1 there is an appearance of a small permanent strain with a maximum value of the normalized maximum strain 2.6814 at $(\eta, x) = (0.46, 0)$ (for the linear case this value is $\frac{17}{7} = 2.4286$), and a maximum value of ε_{norm}^{end} equal to 0.5988 occurs at the same point $(\eta, x) = (0.46, 0)$. The maximum $\varepsilon_{norm}^{\max}$ in zone 3 is 4.4169, and it occurs at a smaller frequency, $(\eta, x) = (1.52, 8.07)$, than that for $\alpha = 0.1$. After this frequency, $\varepsilon_{norm}^{\max}(\eta)$ occurs in Z_2. In this zone is the absolute extremum for this dimensionless amplitude. It is the minimum strain in zone 2, which occurs at point (2.99,0), and its value is –6.691.

For the largest considered amplitude, $\alpha = 0.3$, large $\varepsilon_{norm}^{\max}$ occurs in zone 1, at (0.40, 0), and its value is 29.738. The condition (4.5) gives $\eta > \frac{C_B}{\frac{17}{7} \cdot \alpha} = \frac{0.2228 \cdot 7}{17 \cdot 0.3} = 0.3058 < 0.5$, while condition (4.4) gives $\eta > \frac{C_B}{2\alpha} = \frac{0.2228}{2 \cdot 0.3} = 0.37133$. The occurrence of this large peak can be explained as follows. Because for $\eta < 0.5$ point T is below the interface point (see Gicev and Trifunac, 2006), the two effects (interference from the top of the beam and the summation of three positive strains in the beginning of the second passage) add up, which leads to a large strain at the beginning of the second passage.

Table 2. Maximum $\varepsilon_{end}^{\max}$ and minimum $\varepsilon_{end}^{\min}$ strains at the end of the analysis and their locations in the three zones

$$\varepsilon_{end} = \left(\frac{\varepsilon \cdot \beta_b}{v_{entr}} \right)_{t=t_{end}}$$

Zone 1: $\eta < 0.5 \bigcup x \le 10m$

Zone 2: $0.5 \le \eta \le 5 \bigcup x \le 1m$

Zone 3: $0.5 \le \eta \le 5 \bigcup x > 1m$

$\gamma = \frac{\mu_2}{\mu_1}$	Fig. No.	Zone #	α	$\eta_{\max}$	$x_{\max}$ (m)	$\varepsilon_{n\max}$	$\eta_{\min}$	$x_{\min}$ (m)	$\varepsilon_{n\min}$
0.0	15b	1	0.01	/	/	/	/	/	/
			0.05	/	/	/	/	/	/
			0.1	/	/	/	/	/	/
			0.2	0.46	0.	0.5988	/	/	/
			0.3	0.40	0.	28.173	/	/	/
		2	0.01	/	/	/	/	/	/
			0.05	/	/	/	4.49	0.05	-0.1931
			0.1	4.49	0.	1.4307	3.74	0.10	-0.4651
			0.2	2.06	0.	2.9576	2.06	0.10	-0.8854
			0.3	1.37	0.	4.4974	1.34	0.10	-1.3070
		3	0.01	/	/	/	/	/	/
			0.05	4.58	9.24	2.4746	/	/	/
			0.1	2.66	8.78	3.6655	/	/	/
			0.2	1.79	8.38	4.1492	/	/	/
			0.3	1.43	8.02	4.5798	/	/	/
0.1	16b	1	0.01	/	/	/	/	/	/
			0.05	/	/	/	/	/	/
			0.1	/	/	/	/	/	/
			0.2	0.46	0.	0.4151	/	/	/
			0.3	0.43	0.	3.3194	/	/	/
		2	0.01	/	/	/	/	/	/
			0.05	5.00	0.	0.1254	4.49	0.05	-0.1198
			0.1	5.00	0.	1.5880	5.00	0.36	-0.2031
			0.2	2.30	0.	1.7401	2.93	0.61	-0.2393
			0.3	1.46	0.	1.7343	1.91	0.86	-0.2463
		3	0.01	/	/	/	/	/	/
			0.05	4.31	9.19	1.8281	/	/	/
			0.1	2.36	8.53	2.2566	/	/	/
			0.2	1.22	7.16	2.2807	/	/	/
			0.3	0.80	5.74	2.1065	1.40	1.02	-0.2028

Continued on the next page

Table 2. (continued)

$\gamma = \frac{\mu_2}{\mu_1}$	Fig. No.	Zone #	α	$\eta_{\max}$	$x_{\max}$ (m)	$\varepsilon_{n\max}$	$\eta_{\min}$	$x_{\min}$ (m)	$\varepsilon_{n\min}$
0.2	17b	1	0.01	/	/	/	/	/	/
			0.05	/	/	/	/	/	/
			0.1	/	/	/	/	/	/
			0.2	0.46	0.	0.3578	/	/	/
			0.3	0.45	0.	1.9184	/	/	/
		2	0.01	/	/	/	/	/	/
			0.05	5.00	0.	0.1819	4.49	0.05	-0.0704
			0.1	4.79	0.	1.1679	4.61	0.61	-0.1274
			0.2	2.18	0.	1.1673	4.07	0.86	-0.1197
			0.3	1.46	0.	1.1279	/	/	/
		3	0.01	/	/	/	/	/	/
			0.05	4.31	9.19	1.3291	/	/	/
			0.1	2.15	8.27	1.4490	/	/	/
			0.2	1.10	6.60	1.4101	/	/	/
			0.3	0.77	5.18	1.4109	2.42	1.37	-0.1099
0.3	18b	1	0.01	/	/	/	/	/	/
			0.05	/	/	/	/	/	/
			0.1	/	/	/	/	/	/
			0.2	0.46	0.	0.2934	/	/	/
			0.3	0.46	0.	1.2516	/	/	/
		2	0.01	/	/	/	/	/	/
			0.05	5.00	0.	0.2146	4.49	0.25	-0.0205
			0.1	5.00	0.	0.8554	4.49	0.91	-0.0804
			0.2	2.45	0.	0.9088	/	/	/
			0.3	1.67	0.	0.9204	/	/	/
		3	0.01	/	/	/	/	/	/
			0.05	3.83	9.04	0.8727	/	/	/
			0.1	1.91	7.92	0.9124	/	/	/
			0.2	0.98	5.89	0.8533	/	/	/
			0.3	0.74	4.92	0.9595	/	/	/

The maximum normalized strain in Z_3 is shifted to a smaller frequency than that for $\alpha = 0.2$. It occurs at (1.07, 7.21), and its value is 4.623. The largest peak of $\varepsilon_{norm}^{\max}(\eta)$ occurs in Z_2, with its maximum value being –10.038 at (2.03, 0) (see Table 1).

It can be seen in Fig. 11a that for $\eta > 0.5$, and for $\alpha = 0.2$ and $\alpha = 0.3$, local maxima occur in zone 3 (e.g., $\eta = 1.7$ for $\alpha = 0.2$ and $\eta = 1.07$ for $\alpha = 0.3$). This indicates that with increasing η the nonlinear strain entering the beam increases, causing loss of energy and decreasing the permanent strain, which is formed by reflection from the top. After the maximum normalized

strain is reached at the top, the normalized strain for the next frequency is smaller than the normalized strain at the top for the previous frequency. This indicates that the curve $\varepsilon_{\max}(\eta)$ grows more slowly than the straight line $\varepsilon_{\text{lin}}(\eta)$, because $\frac{\partial \varepsilon_{\max}}{\partial \eta} < \frac{\partial \varepsilon_{\text{lin}}}{\partial \eta}$, and so taking into account (4.6) and $\varepsilon_{\text{lin}} = \frac{\mathrm{v}_{\text{lin}}}{\beta_{\text{b}}}$ we have

$$\frac{\partial \varepsilon_{\max}}{\partial \eta} < \pi \alpha \varepsilon_{\text{yb}} \mathrm{k}_{\text{t}} . \tag{4.10}$$

After the local minimum is reached, the curve $\varepsilon_{\max}(\eta)$ grows faster than the straight line $\varepsilon_{\text{lin}}(\eta)$, and, after reaching the last local maximum, $\varepsilon_{\max}(\eta)$ again grows more slowly than the entry strain in the hypothetical linear beam, $\varepsilon_{\text{lin}}(\eta)$.

The trends for large strain amplitudes are further illustrated in Fig. 11b, where the plots of $\varepsilon_{norm}^{\max}(\eta)$ are shown for $\alpha = 0.2$, 0.225, 0.25, 0.275, and 0.3. The development of the peak in zone 1 with increasing amplitude of the pulse is shown in this figure. The frequency where this peak occurs decreases with increasing amplitude.

A feature of all of the curves shown is that they have three extreme points for frequencies $\eta > 0.5$. The first local maximum occurs at frequency $\eta_{03}(\alpha)$, followed by the local minimum at frequency $\eta_{23}(\alpha)$, and the last extreme is maximum at frequency $\eta_{02}(\alpha)$. Frequencies where all of these extrema occur, decrease with increasing α, and moreover the products $(\alpha \cdot \eta_{03})$; $(\alpha \cdot \eta_{23})$; and $(\alpha \cdot \eta_{02})$ are approximately equal for all α in the considered range, $0.2 \le \alpha \le 0.3$. The first maximum occurs in zone Z3. The strain $\varepsilon_{\max}(\eta)$ is the result of reflection from the top, ε_{T}, weakened by the occurrence of a small permanent strain, ε_{B}, at the bottom during the entrance of the wave into the beam. The slope of $\varepsilon_{\max}(\eta)$ overcomes the slope of the linear strain, $\varepsilon_{\text{lin}} = \frac{\mathrm{v}_{\text{lin}}(\eta)}{\beta_{\text{b}}}$, of the hypothetical linear beam. The product $\alpha \cdot \eta_{03}$ is approximately equal to 0.29, and the maxima are approximately equal, $\varepsilon_{\text{norm}}^{\max} \approx 4.5$, for all α.

For the next larger frequency, $\eta = \eta_{03} + \mathrm{d}\eta$, the strain in zone 2 (bottom), ε_{B}, is large enough to weaken the strain in zone 3 (top), ε_{T}, such that the slope of ε_{T} is smaller than the slope of the straight line ε_{lin}, and the normalized strain $\varepsilon_{\text{norm}}^{\max}$ decreases to the next extremum, which is a minimum occurring at frequency $\eta_{23}(\alpha)$. The product $\alpha \cdot \eta_{23}$ is approximately equal

to 0.34. The interval $\eta_{03} < \eta < \eta_{23}$ is a transition interval where the location of the maximum strain in the beam changes the zones, and the strain at the top is approximately equal with the strain at the bottom.

With increasing η, $\eta > \eta_{23}$, the strain ε_{B} becomes larger than the strain at the top and is the main contributor to the strain $\varepsilon_{\max}(\eta)$. The slope of this curve is larger than the slope of the straight line $\varepsilon_{\mathrm{lin}}$, and the normalized strain $\varepsilon_{\mathrm{norm}}^{\max}$ increases, reaching the last extremum at $\eta = \eta_{02}$. The product $\alpha \cdot \eta_{02}$ is approximately equal to 0.60 for all α in the considered range $0.2 \le \alpha \le 0.3$. Furthermore, $\left(\varepsilon_{\mathrm{norm}}^{\max}(\alpha)\right)_{\eta=\eta_{02}}$ is approximately linear and can be characterized by $\left(\frac{\partial \varepsilon_{\mathrm{norm}}^{\max}}{\partial \alpha}\right)_{\eta=\eta_{02}} = 33$.

With further increasing of η, $\eta > \eta_{02}$, $\varepsilon_{\mathrm{norm}}^{\max}$ decreases for all α, indicating that the slope of the curve $\varepsilon_{\max}(\eta)$ occurring at the bottom is smaller than the slope of $\varepsilon_{\mathrm{lin}}(\eta)$. The curves $\varepsilon_{\mathrm{norm}}^{\max}$ converge, indicating no dependence on α, and they approach a constant, which indicates no dependence on η.

The above observations are further illustrated in Figure 12, where the remaining normalized strain (after the wave energy is completely radiated out of the building), ε_{norm}^{end}, is shown versus dimensionless frequency, η. For the smaller amplitudes, such as $\alpha \le 0.1$ in zone 1, the response is linear and the plot shows zero ordinates. After satisfying condition (4.4), the ordinates become nonzero. The largest strains for these amplitudes occur at the top.

For larger amplitudes ($\alpha = 0.2$ and $\alpha = 0.3$) permanent strain occurs in zone 1 also. For $\alpha = 0.2$ this strain is small, but with increasing α it rapidly increases with decreasing frequency, where this peak occurs. The maximum normalized strain, $\varepsilon_{norm}^{\max}(\alpha, \eta)$, in the first zone, Z_1, is shown in Fig. 13.

The large negative strain occurring in Z_2 at the very beginning of the pulse entering the building is not stable, and at the end of the analysis the permanent strain in this zone is converted to substantial positive permanent strain and negligible negative strain. In contrast, the strain in zone Z_3 remains close to its maximum value. With increasing α, the frequencies in the zones where the maxima of the normalized strains $\varepsilon_{norm}^{\max}(\eta)$ and $\varepsilon_{norm}^{end}(\eta)$ occur—η_{0i} (where i stands for the zone number)—decrease.

As can be seen from Fig. 11a and Fig. 12, the curves for $\varepsilon_{norm}^{\max}(\eta)$ and $\varepsilon_{norm}^{end}(\eta)$ experience local maxima for $\eta > 0.5$, indicating that for all amplitudes, for $0.5 < \eta < \eta_{0i}$ (i = 2, 3), the strain in the beam grows faster than the entry strain $\varepsilon_{lin} = \dfrac{v_{lin}(\eta)}{\beta_b}$. For $\eta > \eta_{0i}$ (i = 2, 3) the linear entry strain grows faster than the maximum strain in the building.

For small amplitudes of excitation, here illustrated by $\alpha = 0.01$, the wave energy in the shear beam is linear, and $\varepsilon_{\text{norm}}^{\max} = \varepsilon_{\max}\beta_{\text{b}} / \text{v}_{\text{entr}}^{\text{lin}}$ is equal to 2, essentially everywhere in the beam due to the doubling of amplitudes caused by reflection from the stress-free surface at x = H. An exception to this occurs near x = 0 and for $\eta = 0.45$, where $\varepsilon_{norm} = 2.5363$ (see Table 1 and Figs. 14a and 14b), due to reflection of the remaining energy back into the beam during the second complete passage (Gicev and Trifunac, 2006). For $\alpha = 0.01$, the beam response is linear everywhere, and $\mu = \varepsilon_{\max} / \varepsilon_y$ is less than 1 (see Fig 14b and Table 3).

In various parts of Figs. 15 through 22 we illustrate the dependence of normalized strain $\varepsilon_{\max} / \beta_{entr}^{lin}$ for $\gamma = 0.0, 0.1, 0.2, \text{and } 0.3$, and $\alpha = 0.05, 0.1, 0.2, \text{and } 0.3$ (in Figs. 15a, 16a, 17a, and 18a). Normalized strain $\varepsilon_{end}\beta_b / v_{entr}^{lin}$ is shown in Figures 15b, 16b, 17b, and 18b for the same ratios of γ and α. Figures 15c, 16c, 17c, and 18c show ductility, $\varepsilon_{\max} / \varepsilon_y$, again for the same set of α's and γ's. Figures 19 through 22 show the corresponding normalized strains (parts a and b) and ductilities (parts c) in groups of four, for γ = 0.0, 0.1, 0.2, and 0.3 in each figure, and for α = 0.05, 0.1, 0.2, and 0.3, in different figures.

In Fig. 15a, the strain normalized by $\varepsilon_{lin} = v_{entr}^{lin} / \beta_b$ along the building is plotted in the instance when the absolute maximum of the normalized strain occurs for a given frequency. In Fig. 15b, the normalized strain is plotted at the end of the analysis, and in Fig. 15c the strain normalized by ε_{yb} along the building is plotted in the instance when its maximum occurs. This is done for all frequencies considered in this work, with frequency increment $\Delta\eta = 0.01$ for $\eta \le 0.5$ and $\Delta\eta = 0.03$ for $\eta > 0.5$. The purpose of the smaller increment for low frequencies has been to represent with more detail the large, narrow peak in zone 1. The first of the four plots in these figures corresponds to amplitude $\alpha = 0.05$, the second to $\alpha = 0.1$, the third to $\alpha = 0.2$, and the fourth to $\alpha = 0.3$. In these three figures (Fig. 15a, b, and c), the model of the building material is elasto-plastic ($\gamma = 0$).

Comparing Figs. 15a and 15c, it can be seen that for $\alpha = 0.05$ and for larger amplitudes the ordinates are approximately equal, which shows that the normalization of the strain is approximately with respect to the same factor. Indeed, from Eq. (4.6),

Table 3. Extrema of ductility and their location in the three zones.

$$\mu = \left(\frac{\varepsilon}{\varepsilon_{yb}} \right)_{t=t(\varepsilon_{\max})}$$

Zone 1: $\eta < 0.5 \bigcup x \le 10m$

Zone 2: $0.5 \le \eta \le 5 \bigcup x \le 1m$

Zone 3: $0.5 \le \eta \le 5 \bigcup x > 1m$

$\gamma = \frac{\mu_2}{\mu_1}$	Fig. No.	Zone #	α	$\eta_{\max}$	$x_{\max}$ (m)	$\varepsilon_{n\max}$	$\eta_{\min}$	$x_{\min}$ (m)	$\varepsilon_{n\min}$
0.0	15c	1	0.01	0.46	0.	0.0522	/	/	/
			0.05	0.46	0.	0.2650	0.11	0.	-0.0266
			0.1	0.46	0.	0.5290	0.11	0.	-0.0532
			0.2	0.46	0.	1.1071	0.11	0.	-0.1064
			0.3	0.41	0.	16.1760	0.11	0.	-0.1596
		2	0.01	/	/	/	/	/	/
			0.05	5.00	0.	0.0384	4.49	0.05	-0.1941
			0.1	5.00	0.	3.1215	5.00	0.10	-0.9968
			0.2	1.70	0.	4.2582	5.00	0.	-24.1150
			0.3	1.07	0.	5.7485	5.00	0.	-41.9090
		3	0.01	5.00	9.24	0.4176	/	/	/
			0.05	5.00	9.34	3.1914	/	/	/
			0.1	3.11	9.04	5.5850	/	/	/
			0.2	1.70	8.27	6.6990	1.97	1.02	-1.0003
			0.3	1.07	7.21	6.6601	1.28	1.02	-1.0003
0.1	16c	1	0.01	0.46	0.	0.0522	/	/	/
			0.05	0.46	0.	0.2650	0.11	0.	-0.0266
			0.1	0.46	0.	0.5290	0.11	0.	-0.0532
			0.2	0.46	0.	1.1337	0.11	0.	-0.1064
			0.3	0.42	0.	2.9786	0.11	0.	-0.1596
		2	0.01	/	/	/	/	/	/
			0.05	5.00	0.	0.0906	4.49	0.05	-0.1364
			0.1	4.49	0.	2.9127	5.00	0.	-5.0058
			0.2	1.97	0.	2.5955	5.00	0.	-14.0210
			0.3	1.25	0.	2.4221	5.00	0.	-23.0440
		3	0.01	5.00	9.24	0.4176	/	/	/
			0.05	5.00	9.34	2.7452	/	/	/
			0.1	2.87	8.88	3.8031	/	/	/
			0.2	1.40	7.66	3.8031	/	/	/
			0.3	1.01	6.85	3.7553	1.25	1.02	-0.3344

Continued on the next page

Table 3. (continued)

$\gamma = \frac{\mu_2}{\mu_1}$	Fig. No.	Zone #	α	$\eta_{\max}$	$x_{\max}$ (m)	$\varepsilon_{n\max}$	$\eta_{\min}$	$x_{\min}$ (m)	$\varepsilon_{n\min}$
0.2	17c	1	0.01	0.46	0.	0.0522	/	/	/
			0.05	0.46	0.	0.2650	0.11	0.	-0.0266
			0.1	0.46	0.	0.5290	0.11	0.	-0.0532
			0.2	0.46	0.	1.1456	0.11	0.	-0.1064
			0.3	0.42	0.	2.4113	0.11	0.	-0.1596
		2	0.01	/	/	/	/	/	/
			0.05	5.00	0.	0.0778	4.49	0.	-0.0985
			0.1	4.37	0.	2.3630	5.00	0.	-4.1400
			0.2	5.00	0.	10.8300	4.49	0.	-9.7296
			0.3	5.00	0.	18.2630	3.83	0.	-13.8440
		3	0.01	5.00	9.24	0.4176	/	/	/
			0.05	5.00	9.34	2.6827	/	/	/
			0.1	2.57	8.63	3.0786	/	/	/
			0.2	1.40	7.51	3.1037	5.00	1.32	-1.0027
			0.3	0.92	6.24	3.0471	4.49	1.02	-2.2946
0.3	18c	1	0.01	0.46	0.	0.0522	/	/	/
			0.05	0.46	0.	0.2650	0.11	0.	-0.0266
			0.1	0.46	0.	0.5290	0.11	0.	-0.0532
			0.2	0.46	0.	1.1259	0.11	0.	-0.1064
			0.3	0.43	0.	2.1444	0.11	0.	-0.1596
		2	0.01	/	/	/	/	/	/
			0.05	5.00	0.	0.0887	4.49	0.	-0.0759
			0.1	5.00	0.	3.1530	4.37	0.91	-0.1512
			0.2	5.00	0.	9.1063	2.48	0.	-4.2276
			0.3	5.00	0.	15.0980	2.12	0.	-5.8805
		3	0.01	5.00	9.24	0.4176	/	/	/
			0.05	4.82	9.29	2.4364	/	/	/
			0.1	2.45	8.53	2.7250	5.00	1.52	-1.0017
			0.2	1.34	7.26	2.7541	5.00	1.02	-1.6819
			0.3	0.83	5.63	2.6561	5.00	1.02	-3.9705

$$\left(\frac{\nu_{lin}}{\beta_b}\right)_{\alpha=0.05} = \left(\pi\alpha\eta\varepsilon_{yb}k_t\right)_{\alpha=0.05} = 0.2244\eta\cdot\varepsilon_{yb} \ . \tag{4.11}$$

For $\eta_e = 4.46$, the factors of normalization are the same and the solutions in both plots are the same. For $\eta < \eta_e$, $\varepsilon_{lin} < \varepsilon_{yb}$, the ordinates in Fig. 15a are larger, while for $\eta > \eta_e$, $\varepsilon_{lin} > \varepsilon_{yb}$ the ordinates in Fig. 15c are larger. The same trends hold for other amplitudes of α. Because the entry velocity is linear in α, the frequencies with equal factors of normalization are $\eta_e = 2.23$

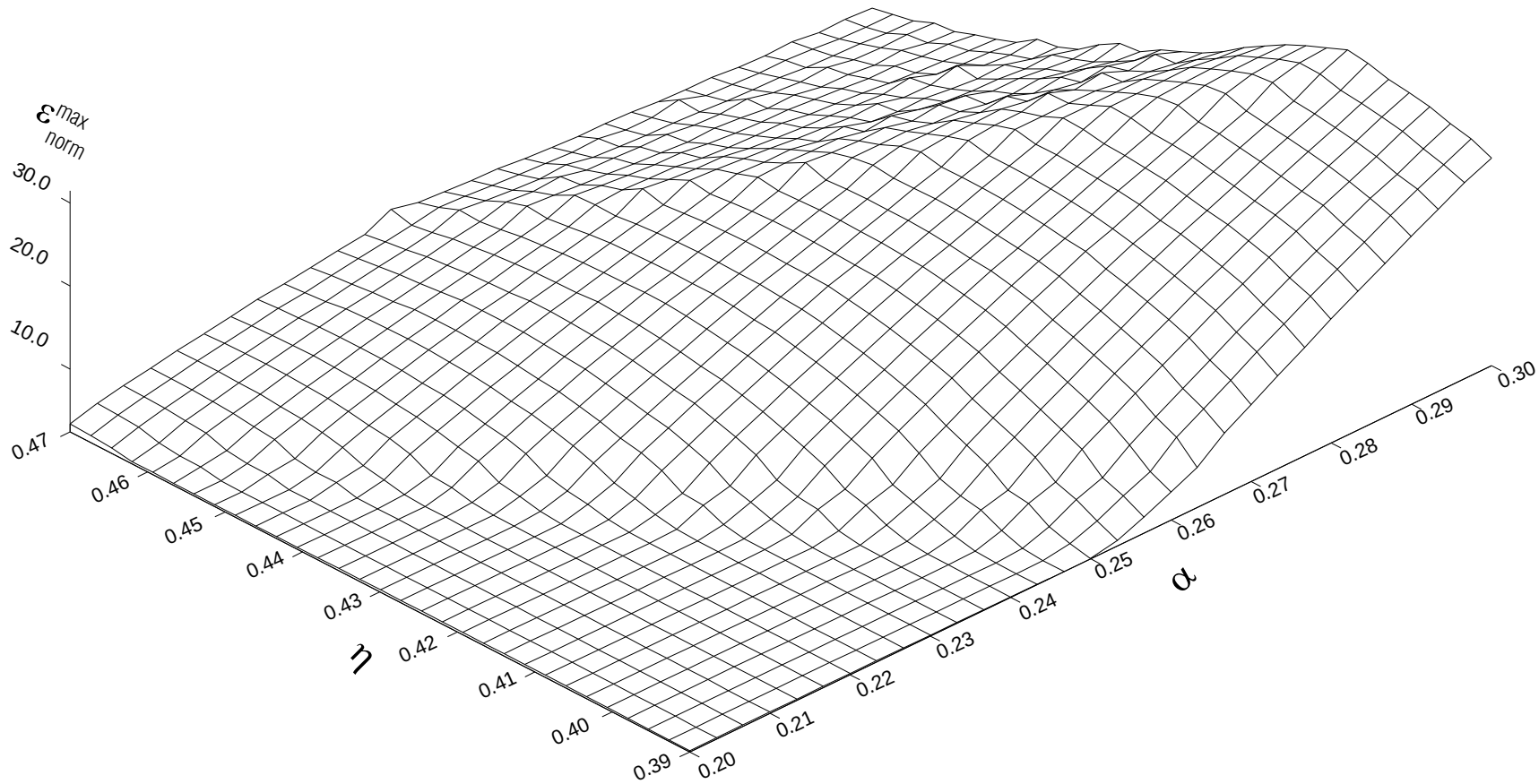

Fig. 13 The Maximum normalized strain in the first zone, Z1 as a function of the dimensionless amplitude η and the dimensionless frequency.

for $\alpha = 0.1$, $\eta_e = 1.115$ for $\alpha = 0.2$, and $\eta_e = 0.743$ for $\alpha = 0.3$. This means that the normalized strain ε_{norm}^{y} in the first zone is smaller than the normalized strain $\varepsilon_{norm}^{\max}$.

From Fig. 15a and Fig. 15b it can be seen that for $\alpha = 0.05$ and $\alpha = 0.1$ there is no substantial difference in the maximum strain in zones 2 and 3 when the maximum occurs at the end of the analysis. For $\alpha = 0.2$ and $\alpha = 0.3$, the initially large negative strain in Z_2 becomes a large, positive, permanent strain when the wave completely leaves the beam. In Fig. 15a, the length of the zone of negative strains at the bottom indicates the time when the maximum strain at the bottom occurs. For smaller η, this time is longer because the pulse is longer, so that the time needed for development of the maximum strain at the bottom is longer than that for larger η.

To get a better insight into the dependence of the strain on γ, see Fig. 23, where the propagation of the displacement along the dimensionless length of the beam, $\chi = \frac{\mathrm{x}}{\mathrm{H_b}}$, in dimensionless time, $\tau = \frac{\beta_\mathrm{b}\mathrm{t}}{2\mathrm{H_b}}$, is shown for the first two and a half passages of the wave on the path bottom-top-bottom of the beam. The dimensionless amplitude is $\alpha = 0.3$ in all plots. In Fig. 23a, the dimensionless frequency is $\eta = 3$, and in Fig. 23b the dimensionless frequency is $\eta = 0.41$. In both figures, the top plots are for elasto-plastic material, $\gamma = 0.0$, and the bottom plots are for material with $\gamma = 0.3$. Comparing the top and bottom plots, it is obvious that the increasing γ reduces the strain.

Everything discussed so far has been related for the elasto-plastic model $(\gamma = 0)$. The normalized strains for $\gamma = \frac{\mu_1}{\mu_0} = 0.1$ are shown in the set of figures 16a, 16b, and 16c. If we compare Fig. 16a with Fig. 15a, it can be seen that the plots are similar with smaller ordinates in Fig. 16a. The large peak in the first zone for $\alpha = 0.3$ is significantly reduced. The amplitudes are smaller, but the zones with permanent strain are wider. Because the modulus $\mu_1 = \gamma\mu_0 > 0$, the permanent strain now propagates with velocity $\beta_{b1} = \sqrt{\gamma} \cdot \beta_b$.

For longer pulses (Fig. 23b), this observation is not so obvious. The permanent strain occurs in the beginning of the second passage of the wave along the beam. Here it can be noticed that for the elasto-plastic material the permanent strain at the bottom is large, while for the material with $\gamma = 0.3$ this permanent strain is not even noticeable and it appears as if the beam is in linear state.

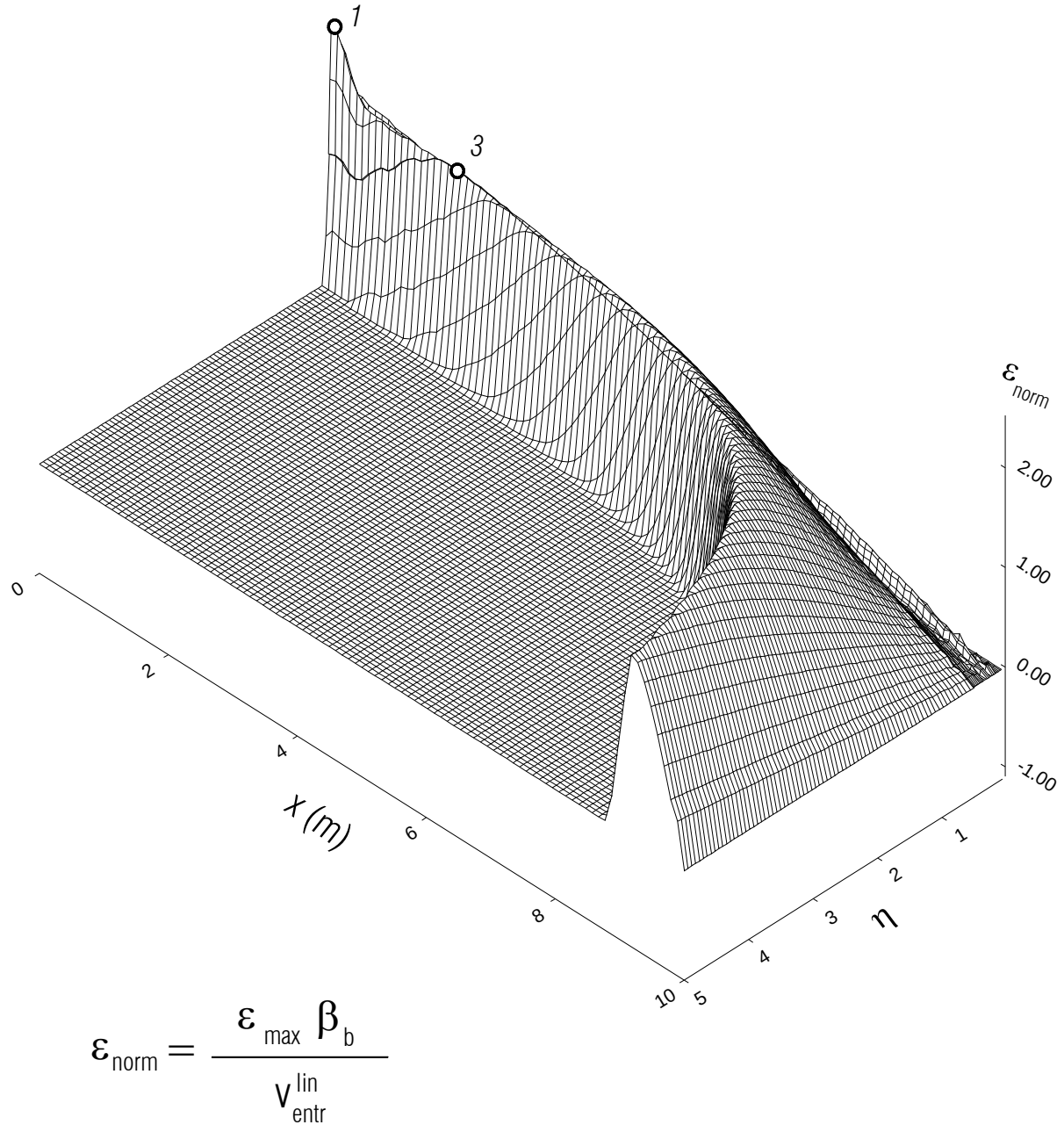

$$\varepsilon_{norm} = \frac{\varepsilon_{max}\,\beta_b}{V_{entr}^{lin}}$$

Fig. 14a Normalized strain along the beam, when its maximum occurs, versus dimensionless frequency, and for dimensionless amplitude.

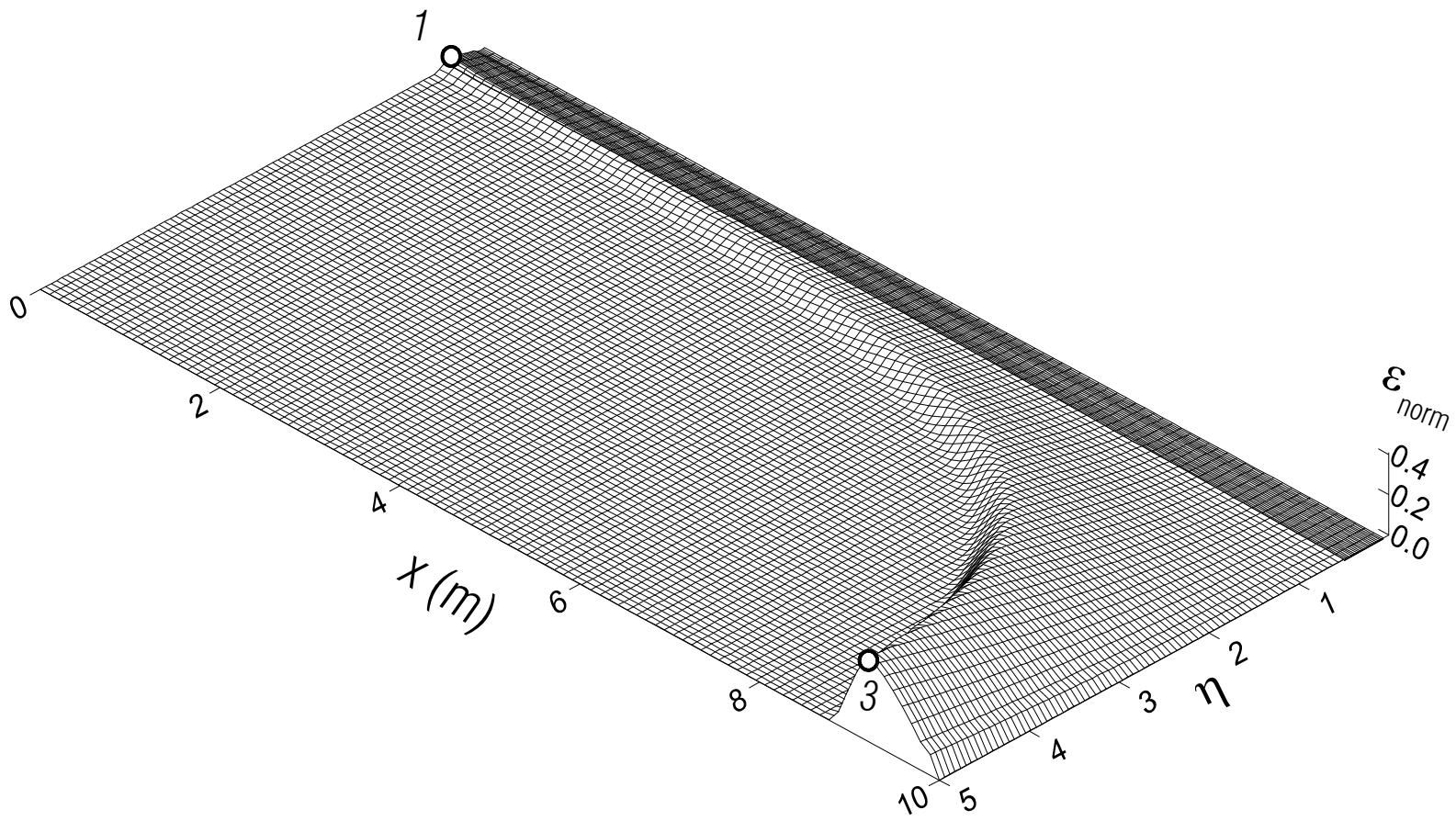

$$\varepsilon_{norm} = \frac{\varepsilon_{max}}{\varepsilon_y}$$

Fig. 14b Ductility along the beam, when its maximum occurs, versus dimensionless frequency, and for dimensionless amplitude.

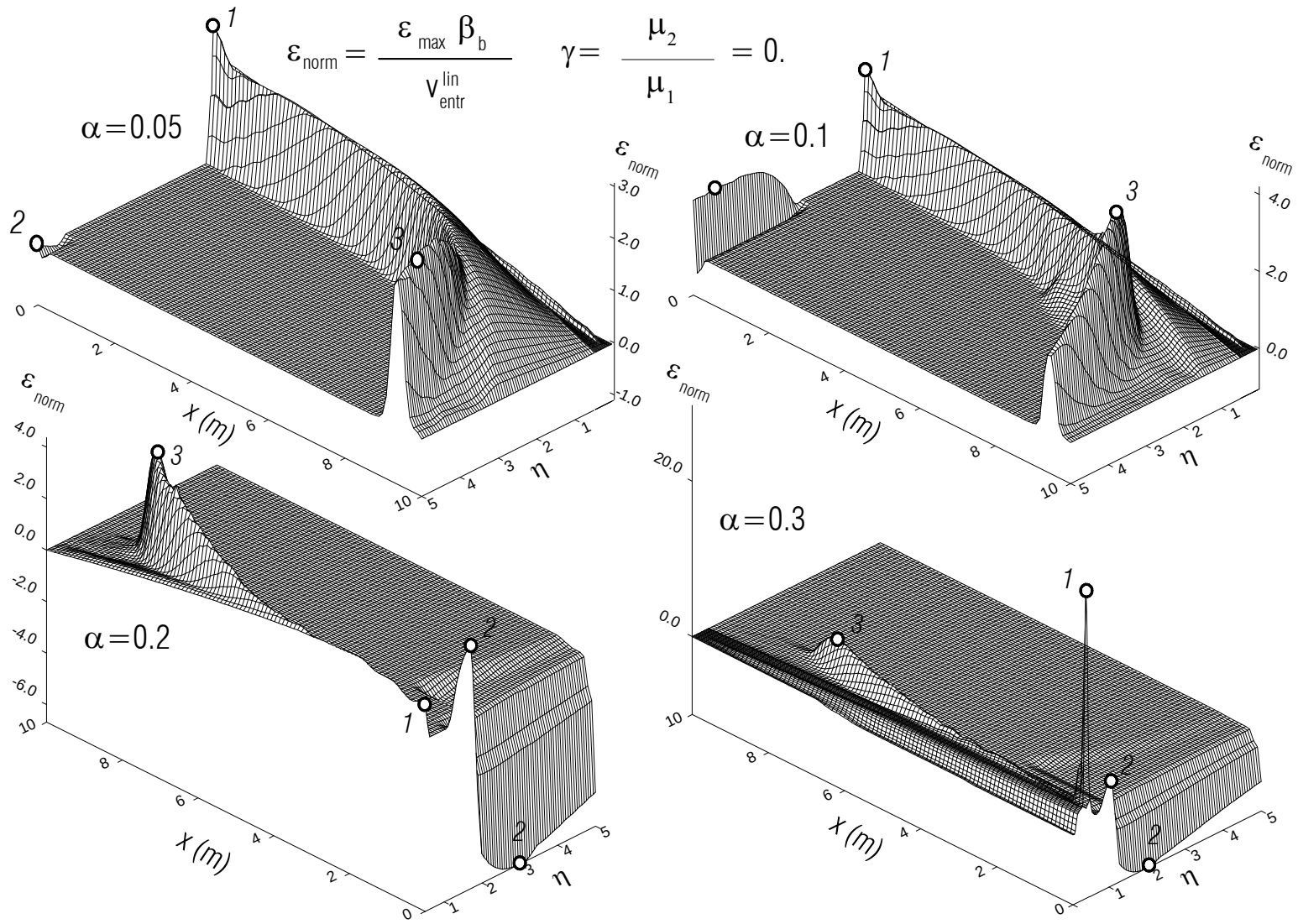

Fig. 15a Normalized strains along the beam, when its maximum occurs, vs. dimensionless frequency, for $\gamma = 0$, and for four dimensionless amplitudes.

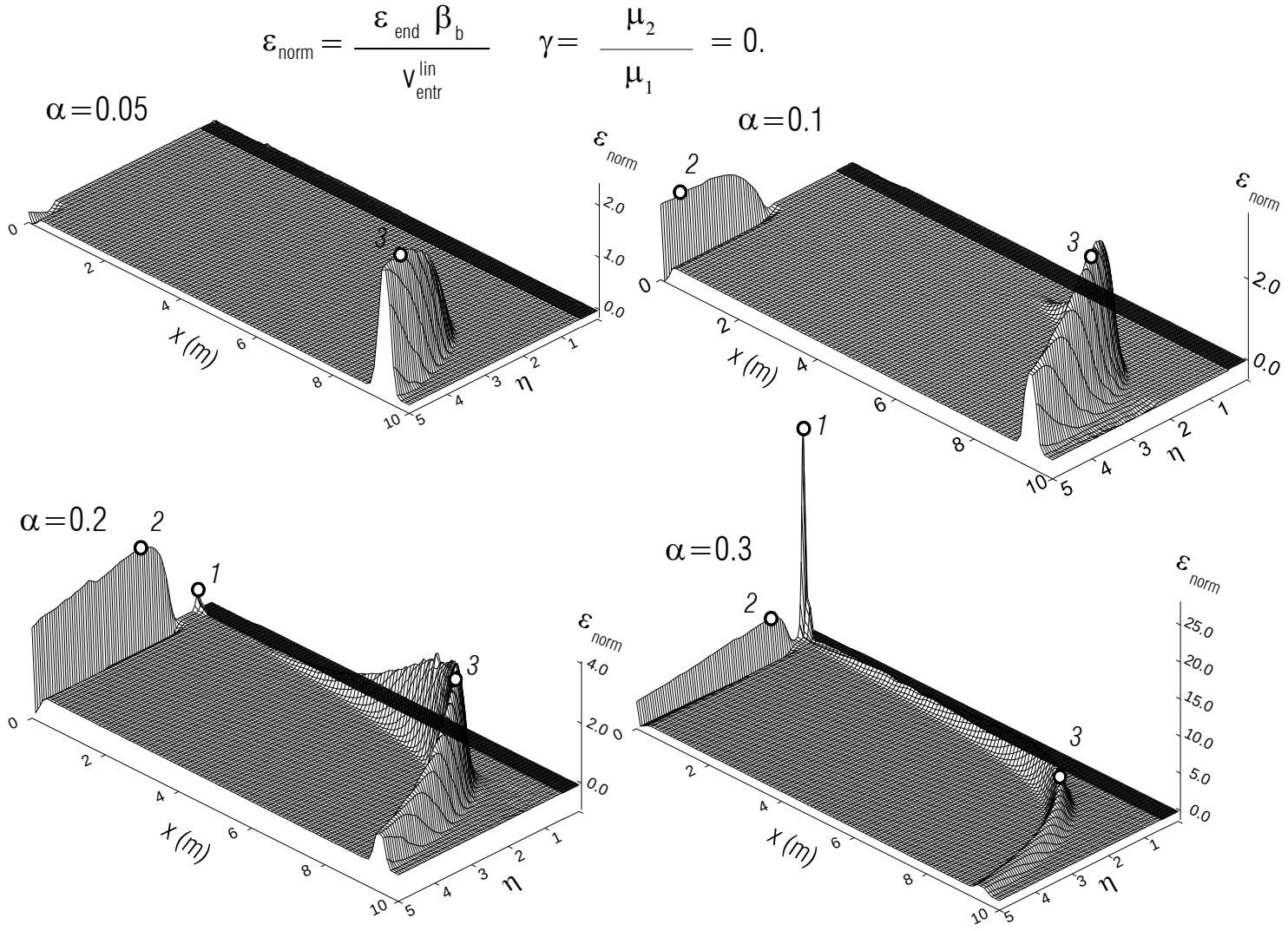

Fig. 15b Normalized strains along the beam at the end of the analysis vs. dimensionless frequency, for elastoplastic material $\gamma = 0.1$, and for four dimensionless amplitudes.

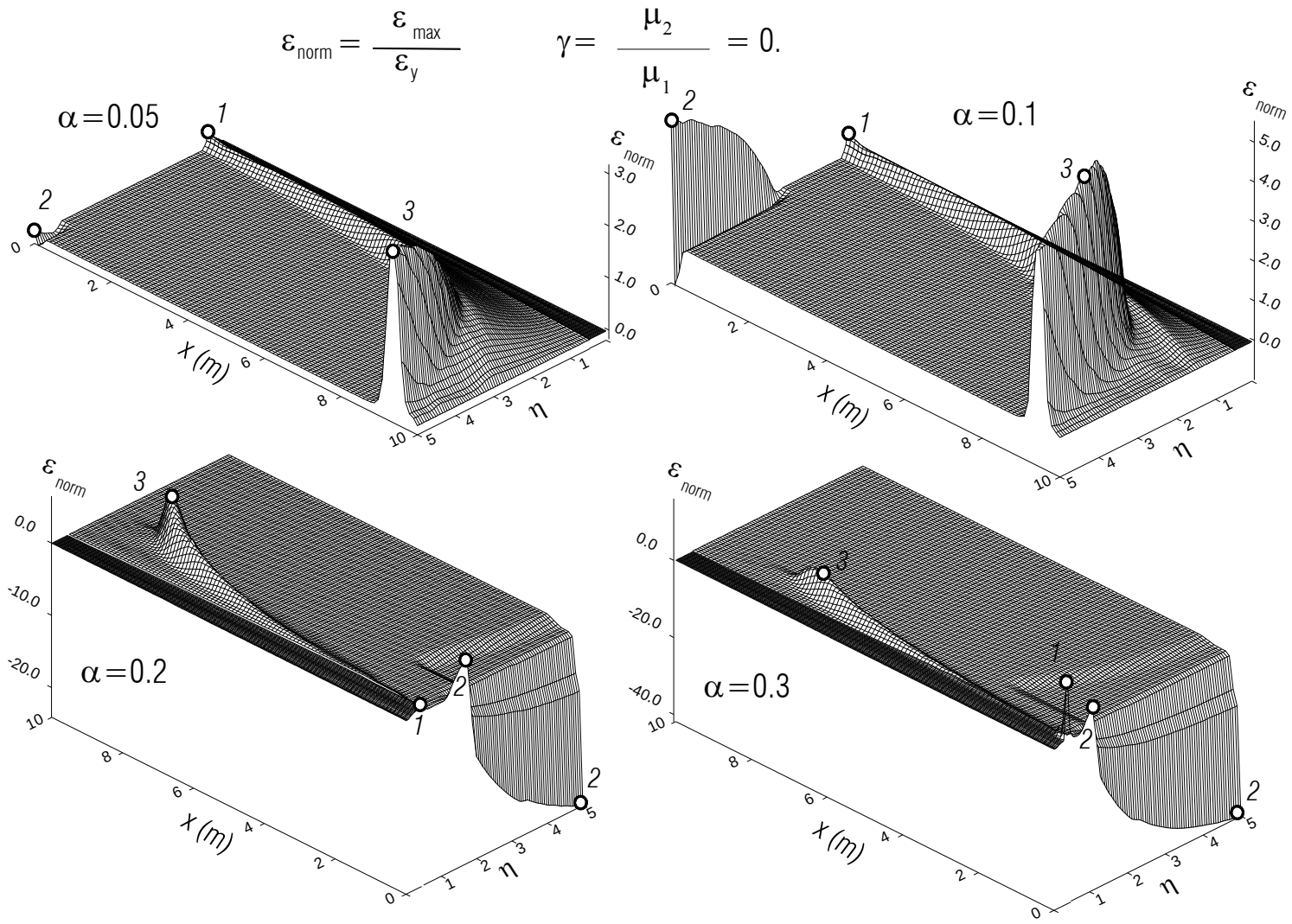

Fig. 15c Ductility along the beam when its maximum occurs, vs. dimensionless frequency, for elastoplastic material $\gamma = 0.$, and for four dimensionless amplitudes.

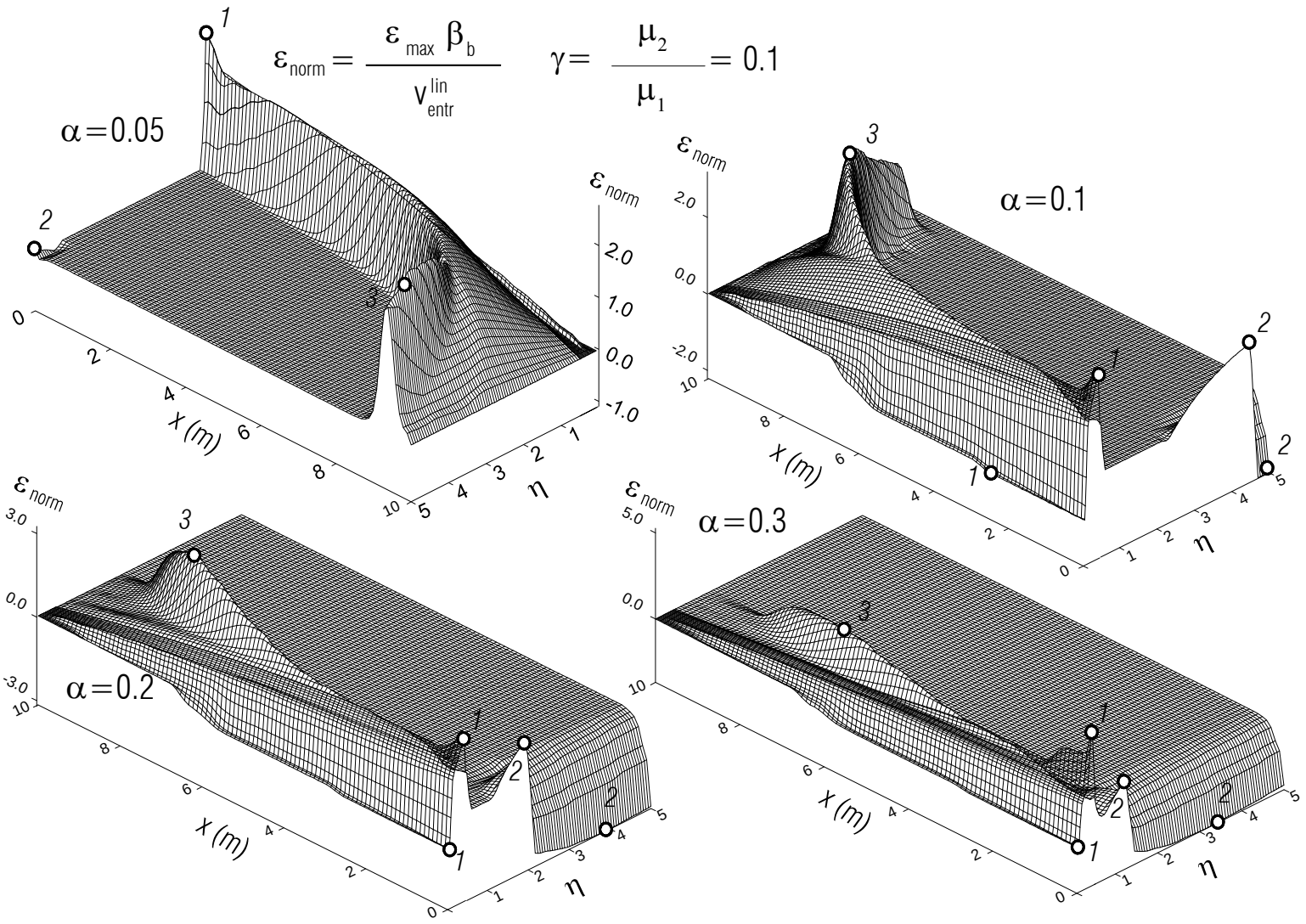

Fig. 16a. Normalized strains along the beam when its maximum occurs, vs. dimensionless frequency, for $\gamma = 0.1$, and four dimensionless amplitudes.

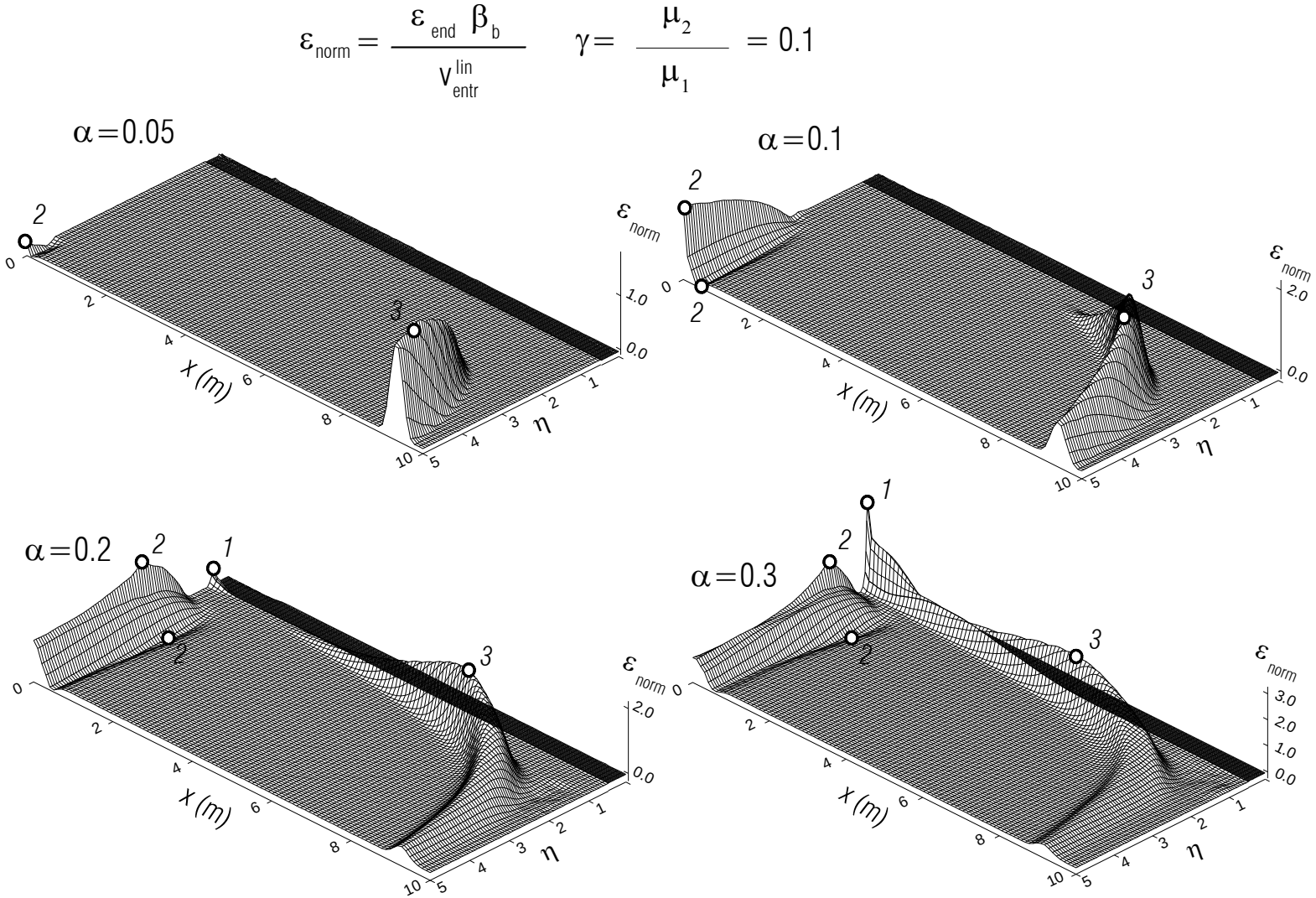

Fig. 16b Normalized strains along the beam when its maximum occurs, vs. dimensionless frequency, for $\gamma = 0.1$, and for four dimensionless amplitudes.

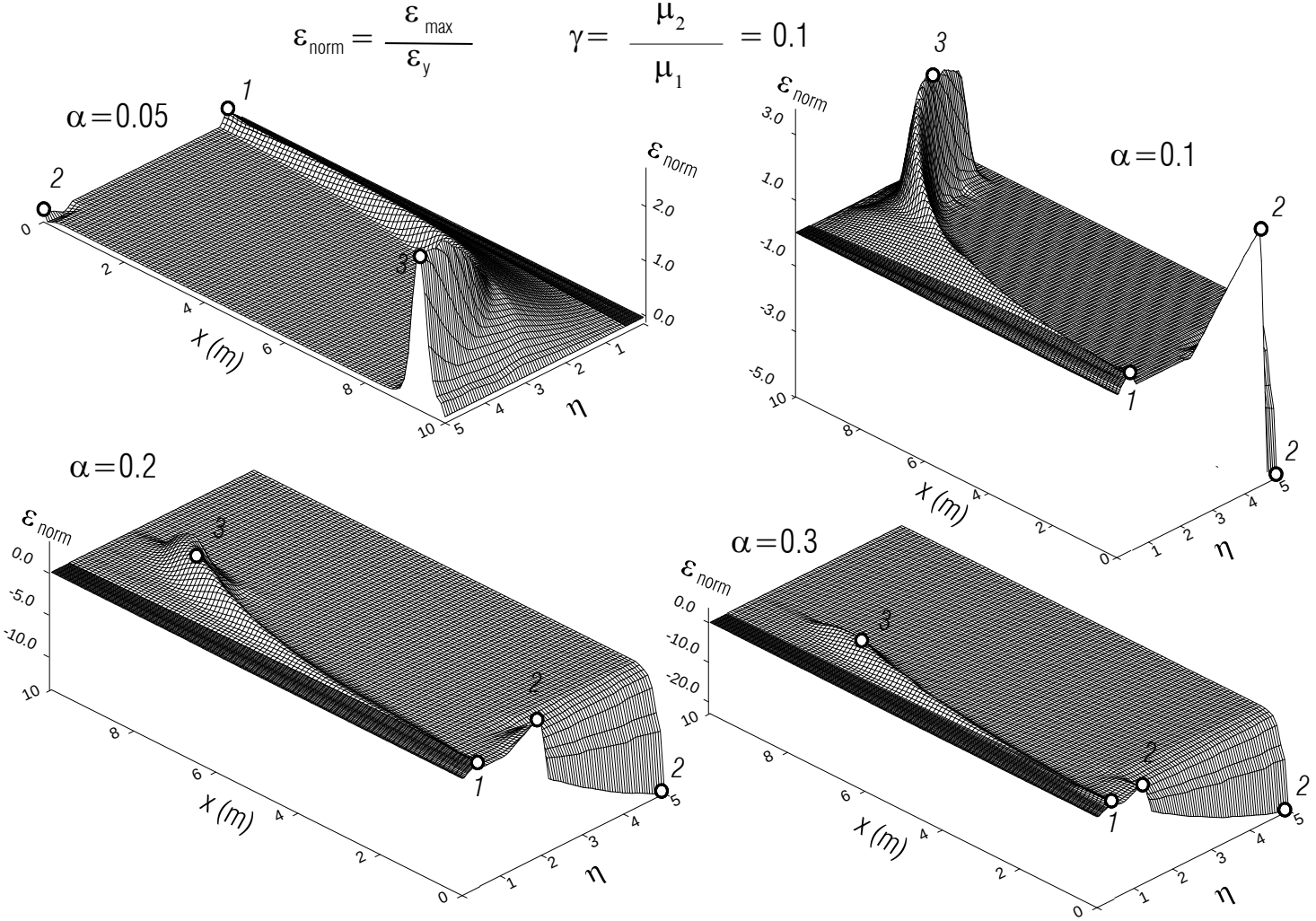

Fig 16c Ductility along the beam, when its maximum occurs, vs. dimensionless frequency, for $\gamma = 0.1$, and for four dimensionless amplitudes.

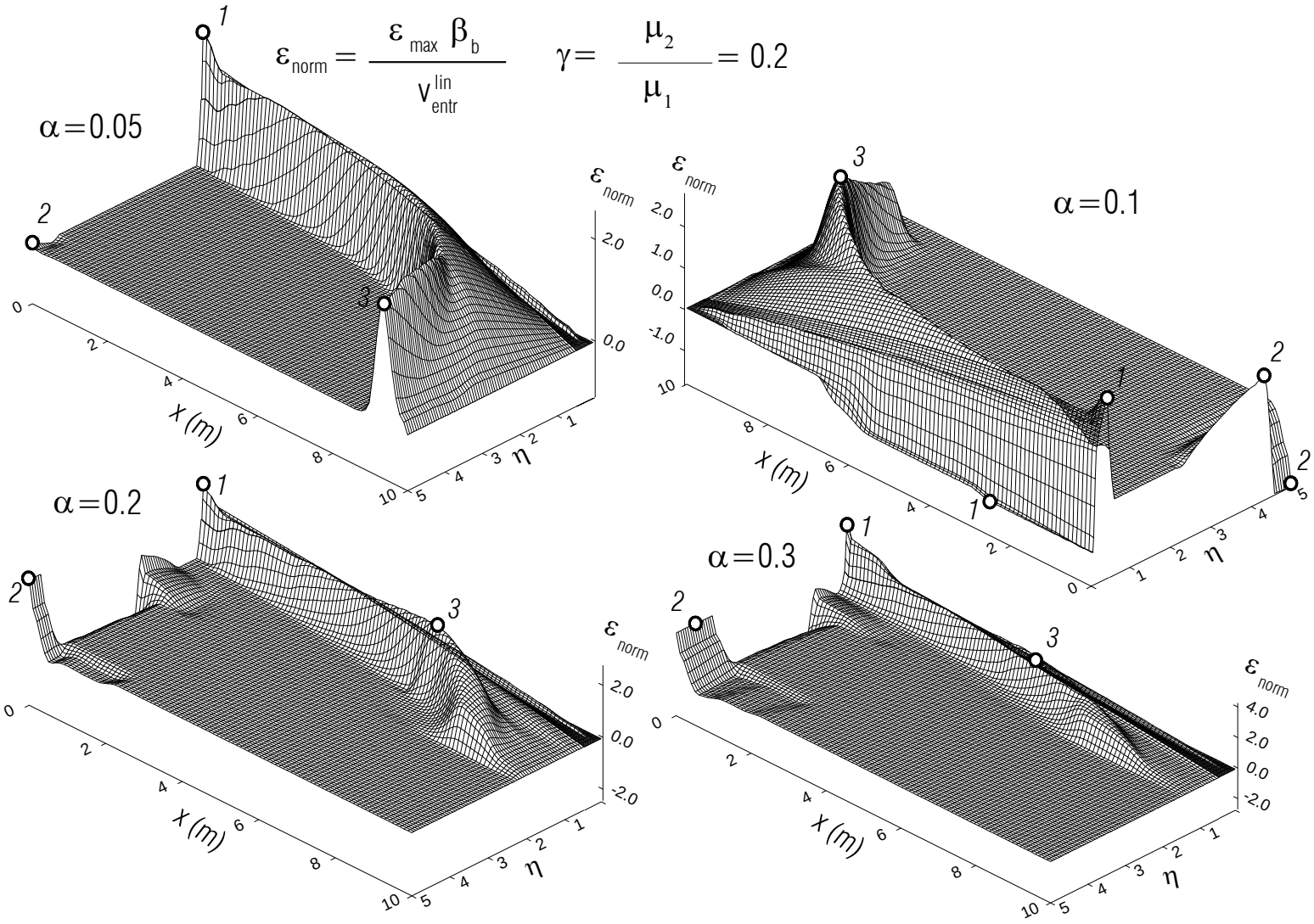

Fig. 17a Normalized strains along the beam, when its maximum occurs, vs. dimensionless frequency, for $\gamma = 0.2$, and for four dimensionless amplitudes.

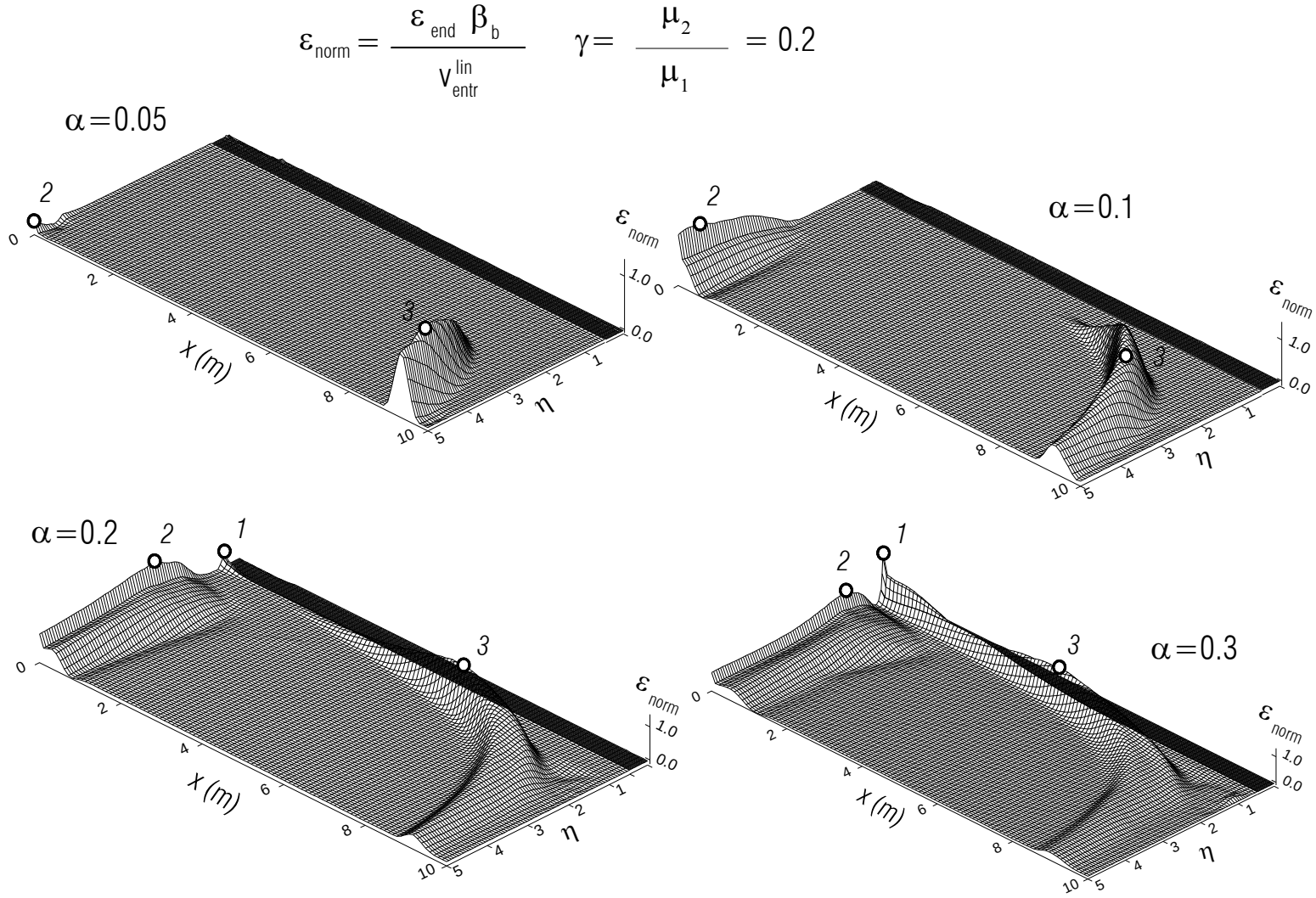

Fig. 17b Normalized strains along the beam, at the end of the analysis, vs. dimensionless frequency, for $\gamma = 0.2$, and for four dimensionless amplitudes.

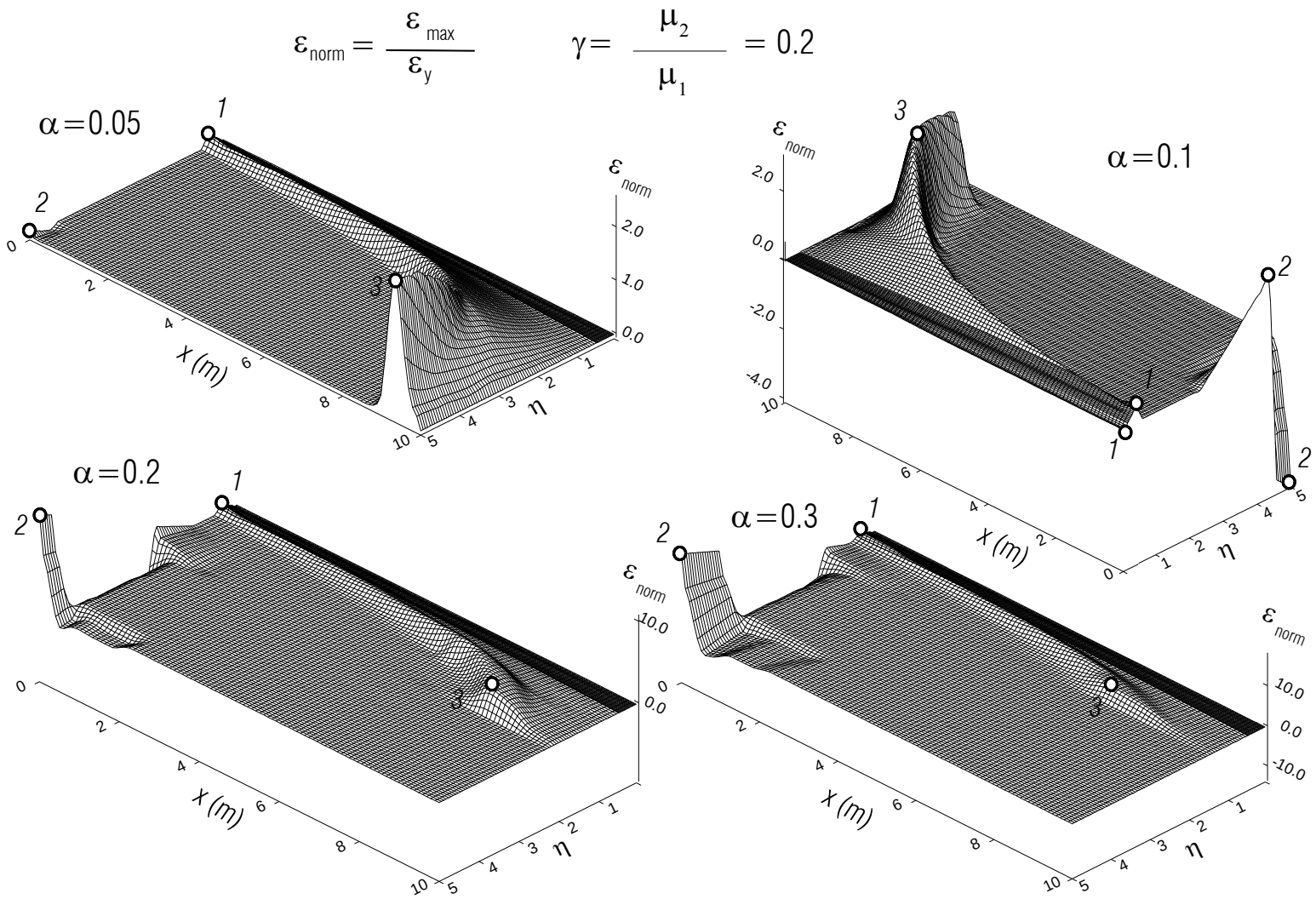

Fig. 17c Ductility along the beam, when its maximum occurs, vs. dimensionless frequency, for $\gamma = 0.2$, and for four dimensionless amplitudes.

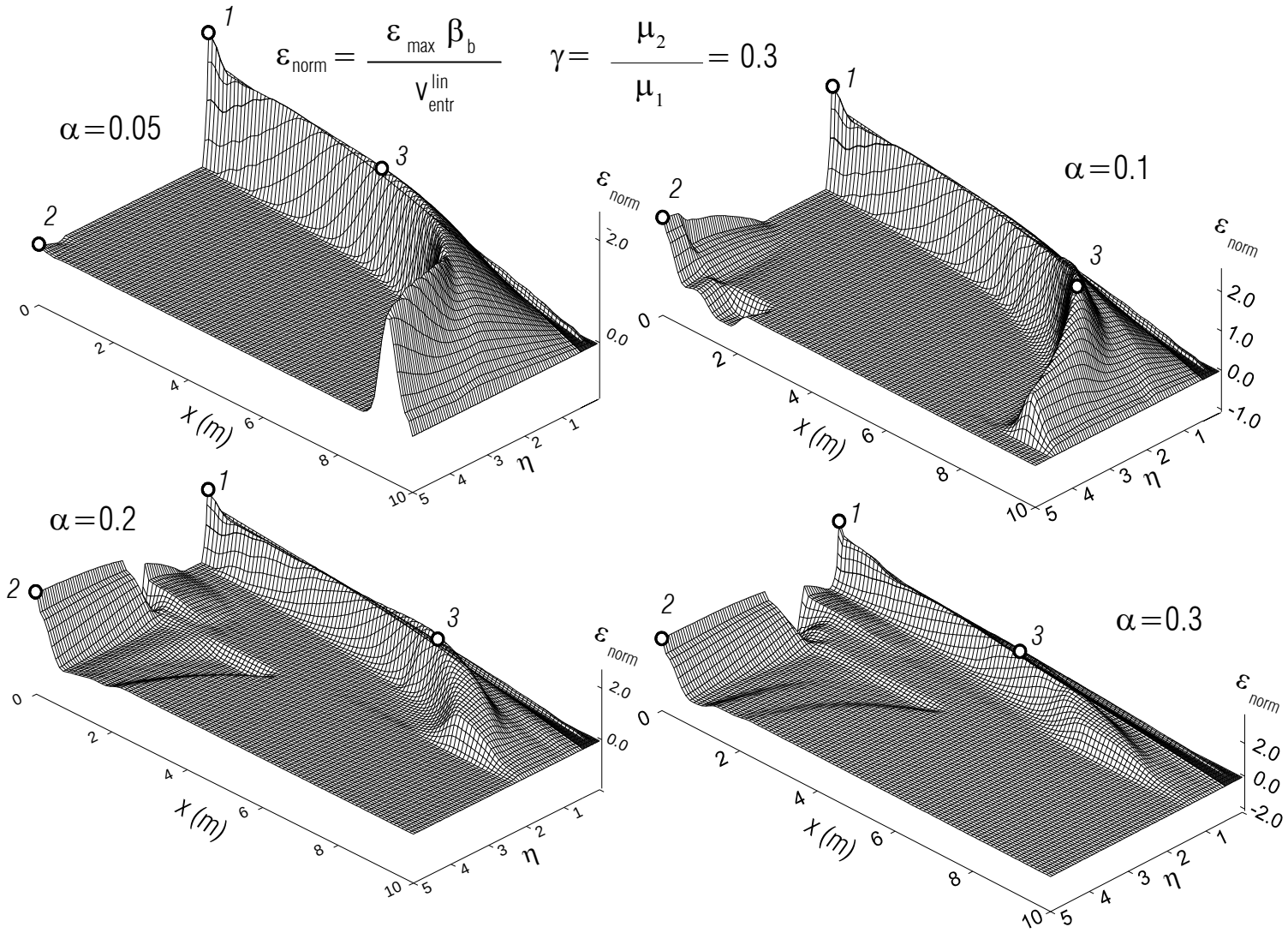

Fig. 18a Normalized strains along the beam, when its maximum occurs, vs. dimensionless frequency, for $\gamma = 0.3$, and for four dimensionless amplitudes.

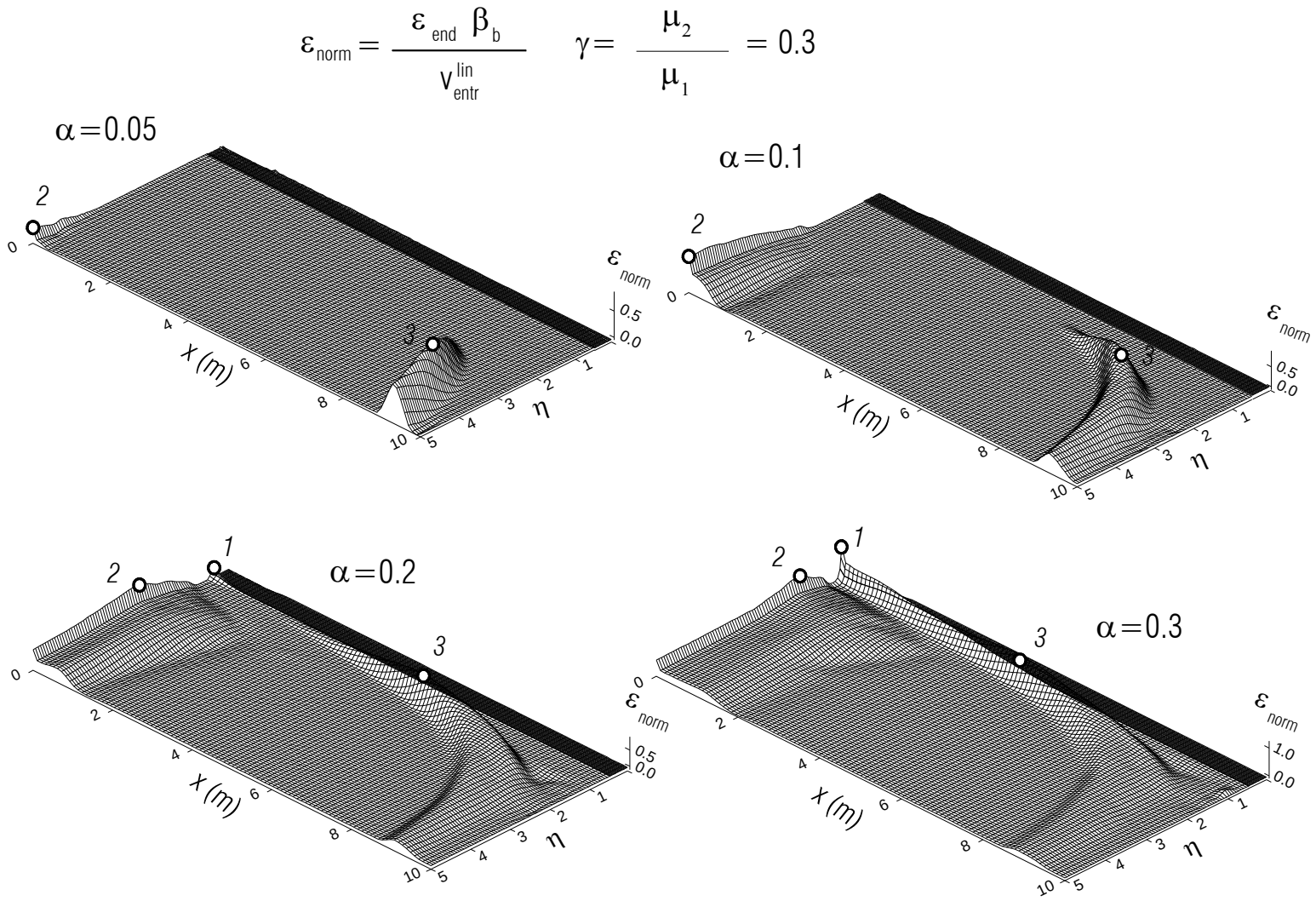

Fig. 18b Normalized strains along the beam, at the end of the analysis, vs. dimensionless frequency, for $\gamma = 0.3$, and for four dimensionless amplitudes.

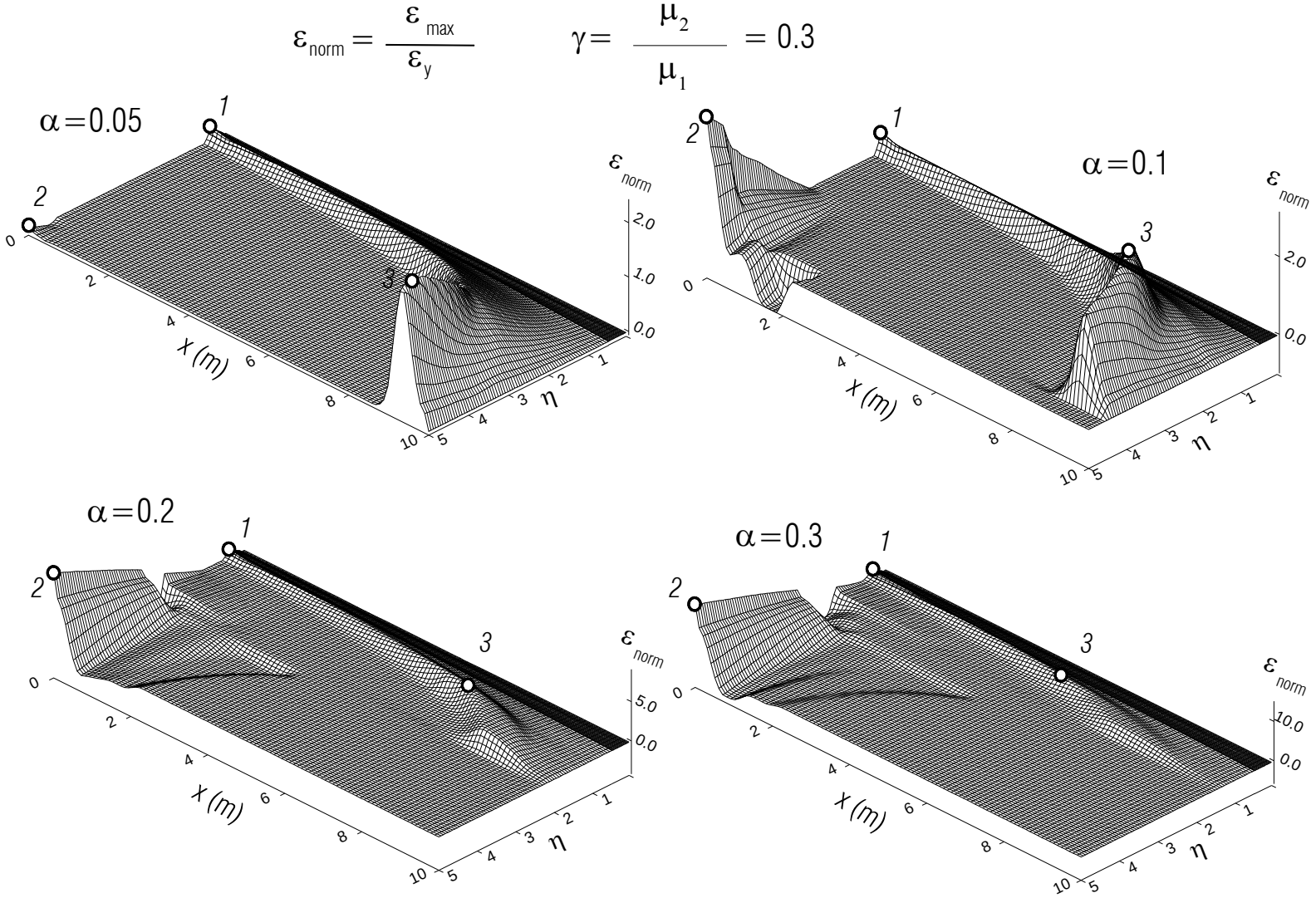

Fig. 18c Ductility along the beam, when its maximum occurs, vs. dimensionless frequency, for $\gamma = 0.3$, and for four dimensionless amplitudes.

Because for elasto-plastic material $\gamma = 0$, the permanent strain does not propagate and is accumulated in narrow zones of the beam, and the value of the strain at the point changes only when the pulse occupies the point. When $\gamma > 0$, with propagation of the permanent strain there is no accumulation of large strains at a certain point with each passage of the wave through that point. It can be noticed in the Figs. 16a, 17a, and 18a that as γ increases the ordinates decrease and the zones of the permanent strain elongate.

For $\alpha = 0.1$ and for large frequencies, the maximum normalized strain is negative in the very beginning. For $\gamma = 0.2$ and $\gamma = 0.3$, and for the largest amplitudes considered here, zone Z_2 consists of positive strains for smaller frequencies, negative strains for intermediate frequencies, and positive strains again for large frequencies. Similar trends can be seen for the normalized strains at the end of the analysis, with the difference that the strains in zone 2 are all positive.

In Fig. 23a, the maximum strain occurs at the beginning of the wave entering the beam. For elasto-plastic material, this strain is high. After reflecting from the top, almost the whole energy of the input wave is captured and spent for developing permanent strain in narrow zones, and only elastic strain continues to propagate along the beam. For the material with $\gamma = 0.3$, with the development of permanent strain at the top, this strain does not remain at the point but rather propagates with velocity β_{b1}, which causes a substantial amount of energy to continue to propagate along the beam.

For longer pulses (Fig. 23b), this observation is not so obvious. The permanent strain occurs in the beginning of the second passage of the wave along the beam. Here it can be noticed that for the elasto-plastic material the permanent strain at the bottom is large, while for the material with $\gamma = 0.3$ this permanent strain is not even noticeable and it appears as if the beam is in linear state.

Using Tables 1, 2, and 3 in Fig. 24a, b, c the normalized strains versus dimensionless amplitude α, are shown for the four values of $\gamma = 0.0, 0.1, 0.2, \text{and } 0.3$ in the three zones Z_1, Z_2, and Z_3, respectively, using a semi-logarithmic scale. From condition (4.5), the first nonlinear strain in zone 1 occurs for:

$$\alpha_1 > \frac{0.09174}{\eta_{\max}} = \frac{0.09174}{0.5} = 0.1835 \quad . \tag{4.12}$$

As can be noticed, in zone 1 (Fig. 24a), while the strain is linear ($\alpha \le \alpha_1$) there is no dependence on γ and all of the curves coincide. The normalized maximum strain, $\varepsilon_{\text{norm}}^{\max}$ (see

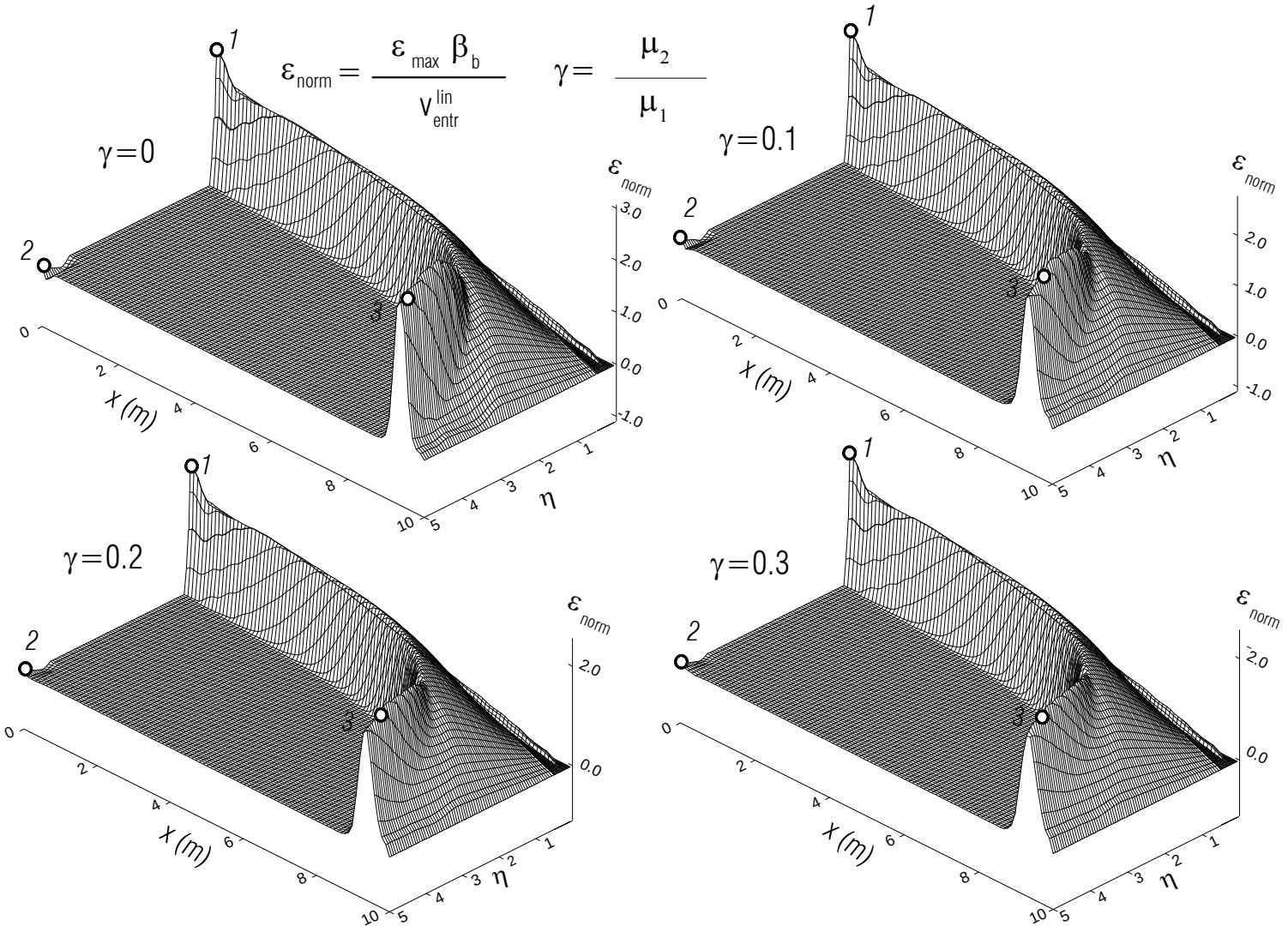

Fig. 19a Normalized strains along the beam, when its maximum occurs, vs. dimensionless frequency, and for dimensionless amplitude α = 0.05.

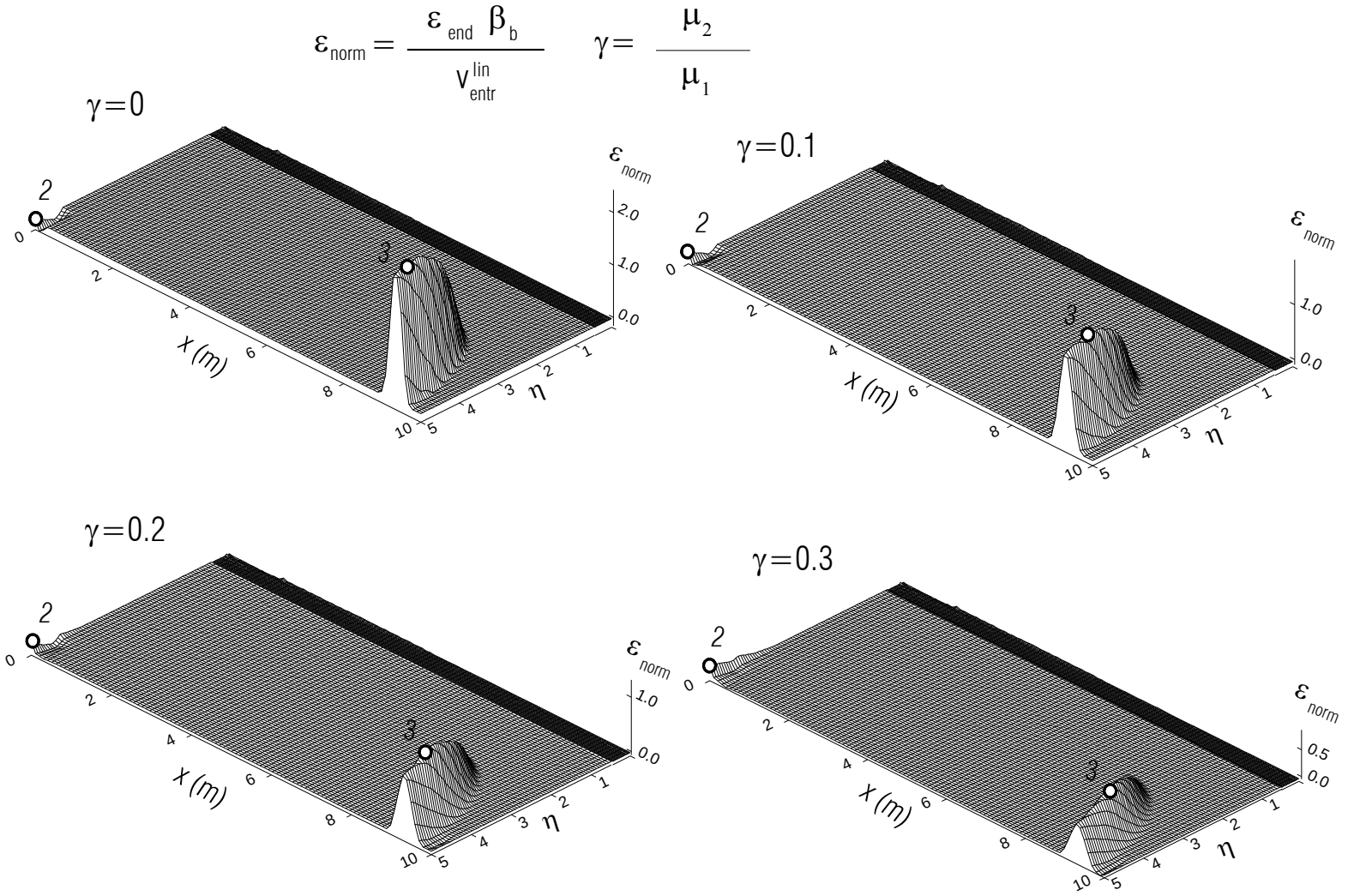

Fig. 19b Normalized strains along the beam, at the end of the analysis, vs. dimensionless frequency, and for dimensionless amplitude α = 0.05.

$$\varepsilon_{norm} = \frac{\varepsilon_{max}}{\varepsilon_y} \qquad \gamma = \frac{\mu_2}{\mu_1}$$

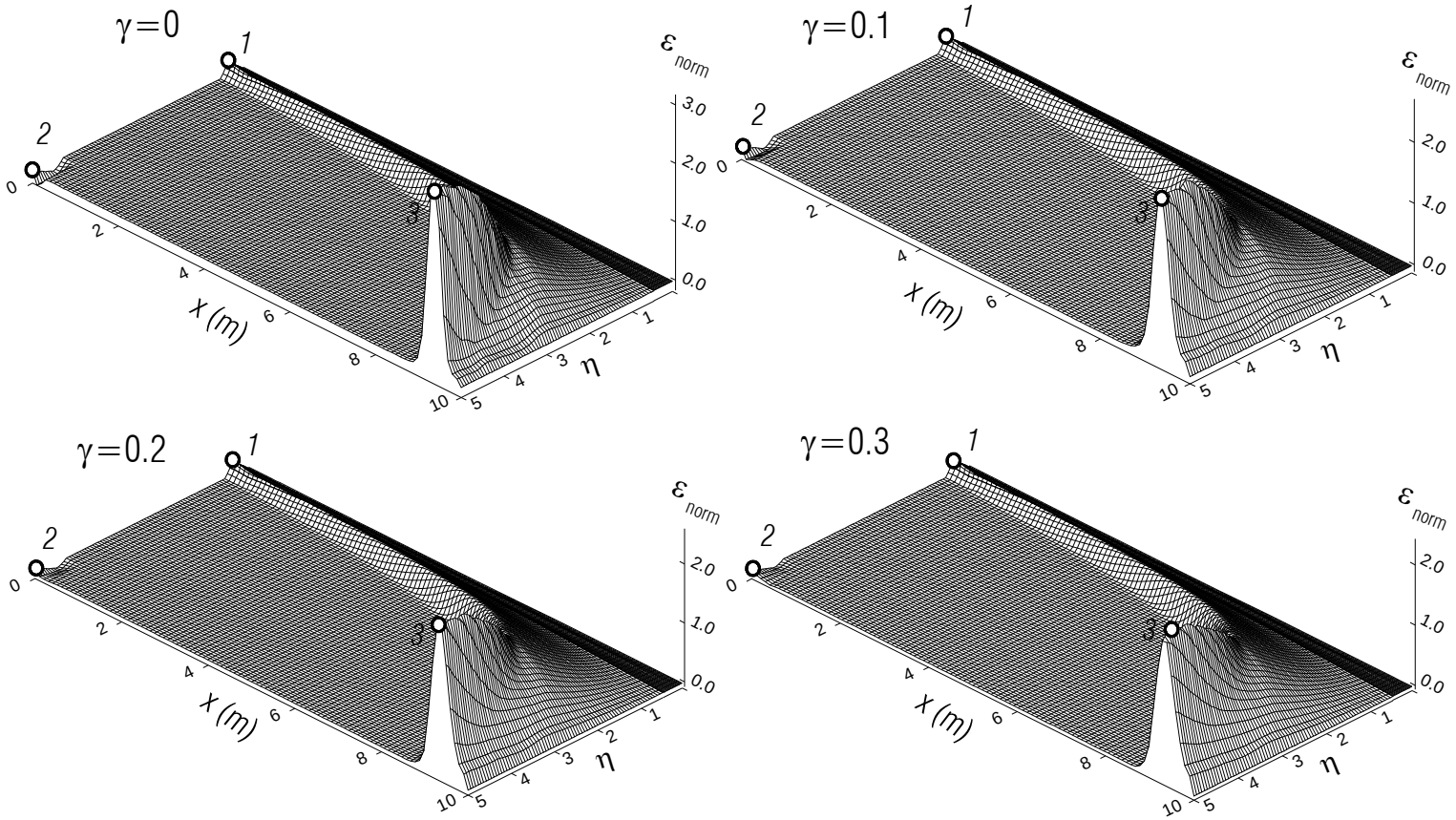

Fig. 19c Normalized strain along the beam, when its maximum occurs, vs. dimensionless frequency, and for dimensionless amplitude α = 0.05.

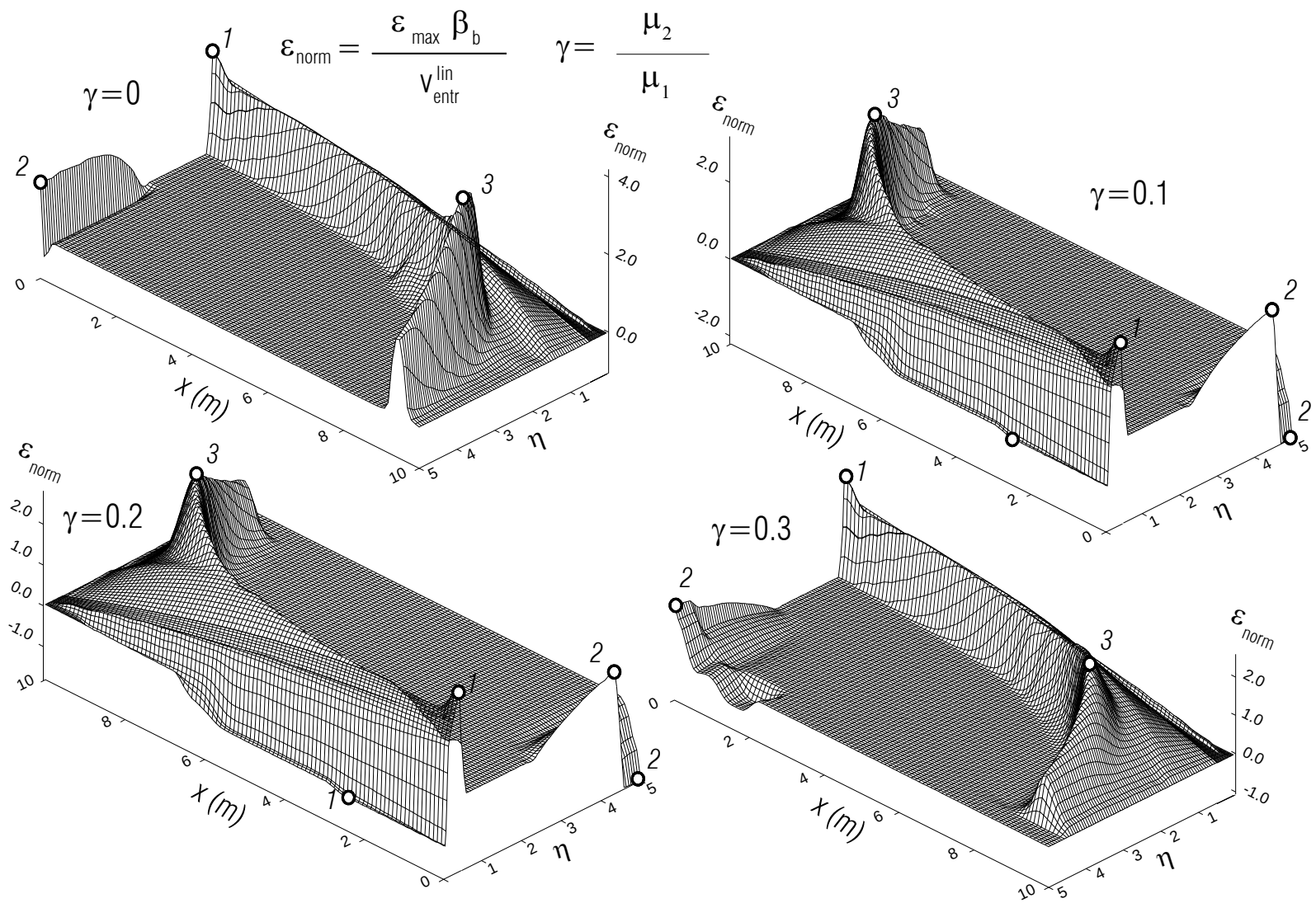

Fig. 20a Normalized strains along the beam, when its maximum occurs, vs. dimensionless frequency, and for dimensionless amplitude $\alpha = 0.1$.

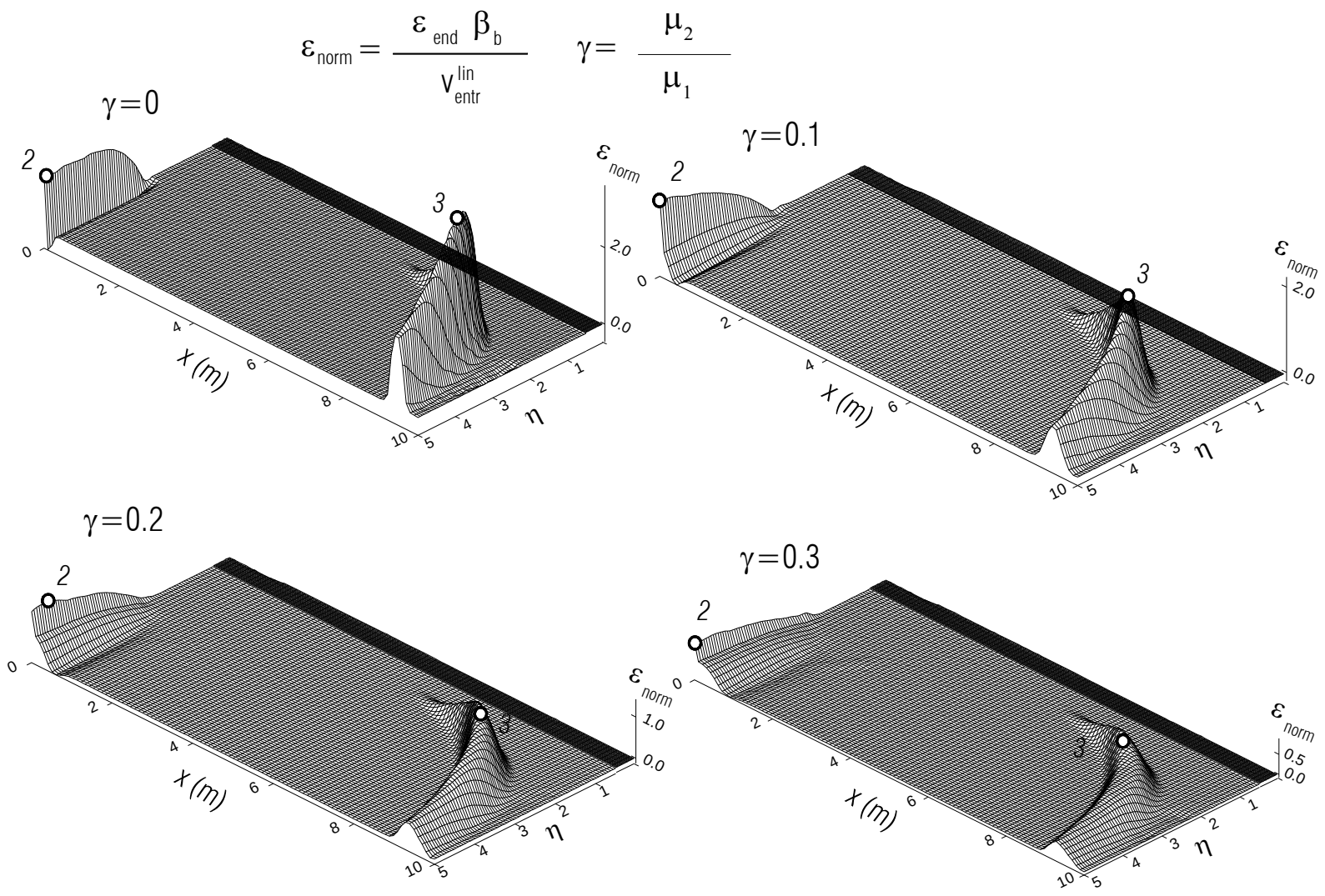

Fig. 20b Normalized strains along the beam, vs. dimensionless frequency, and for dimensionless amplitude α = 0.1.

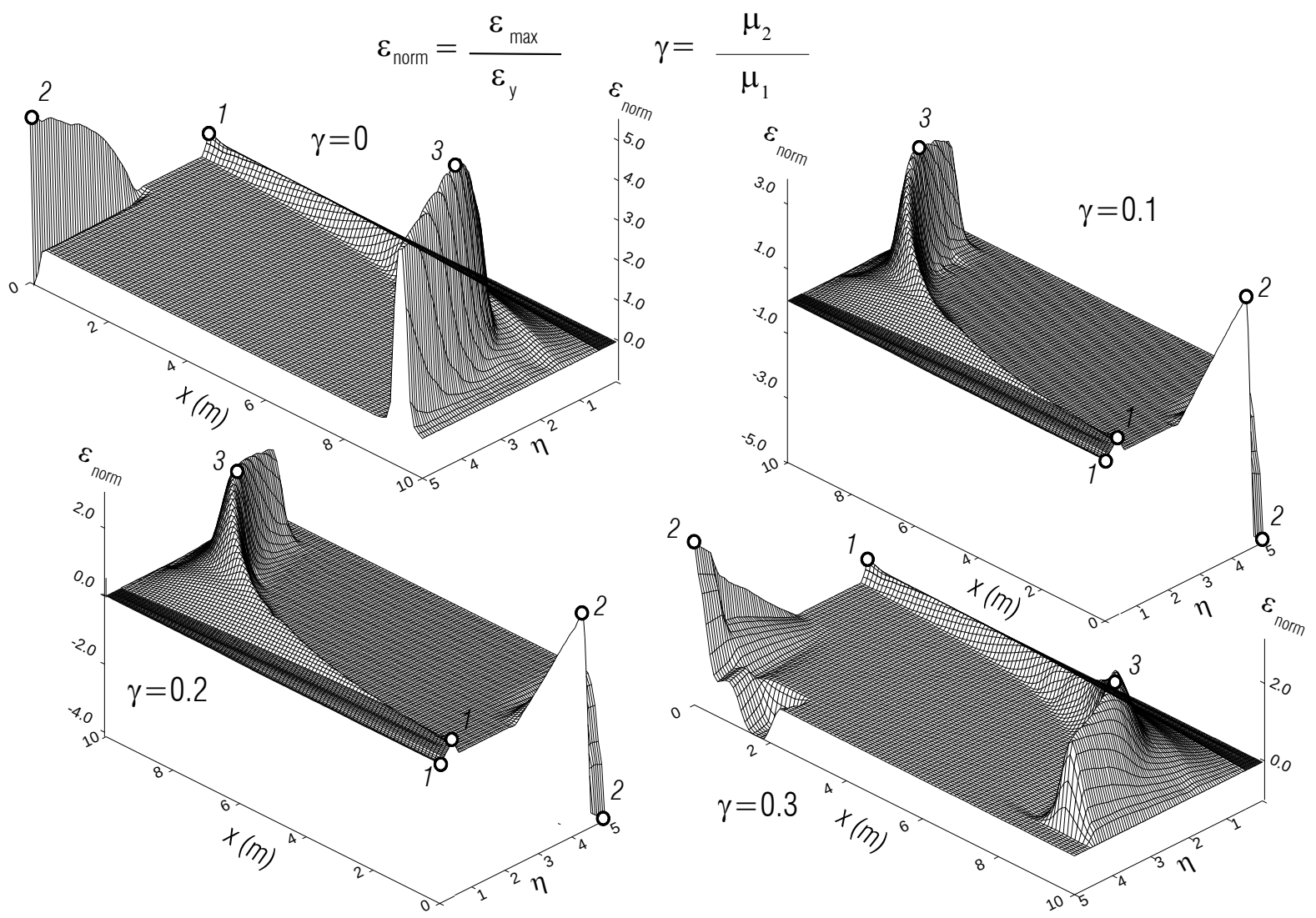

Fig. 20c Normalized strain along the beam, when its maximum occurs, vs. dimensionless frequency, and for dimensionless amplitude $\alpha = 0.1$.

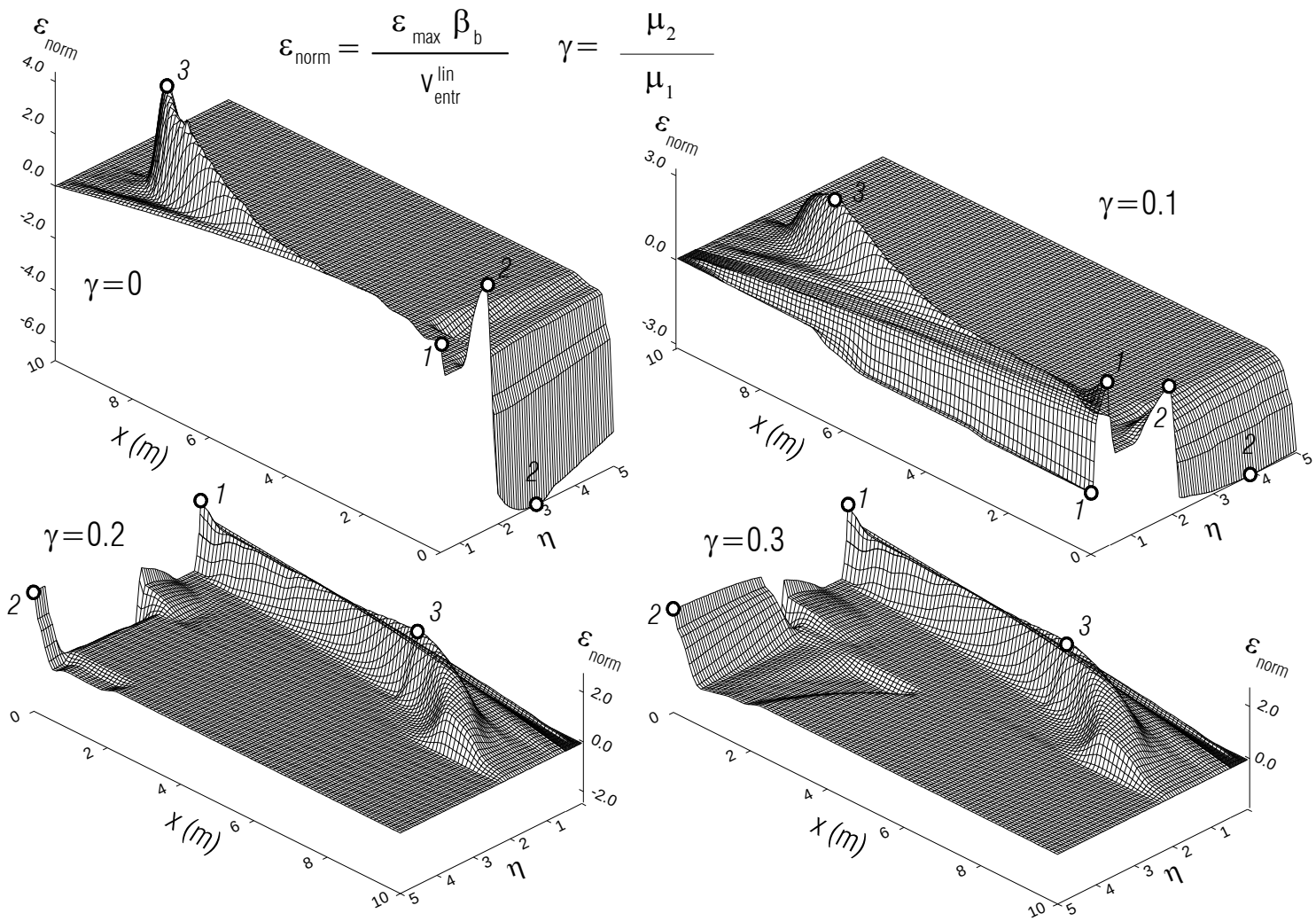

Fig. 21a Normalized strains along the beam, when its maximum occurs, vs. dimensionless frequency, and for dimensionless amplitude α = 0.2.

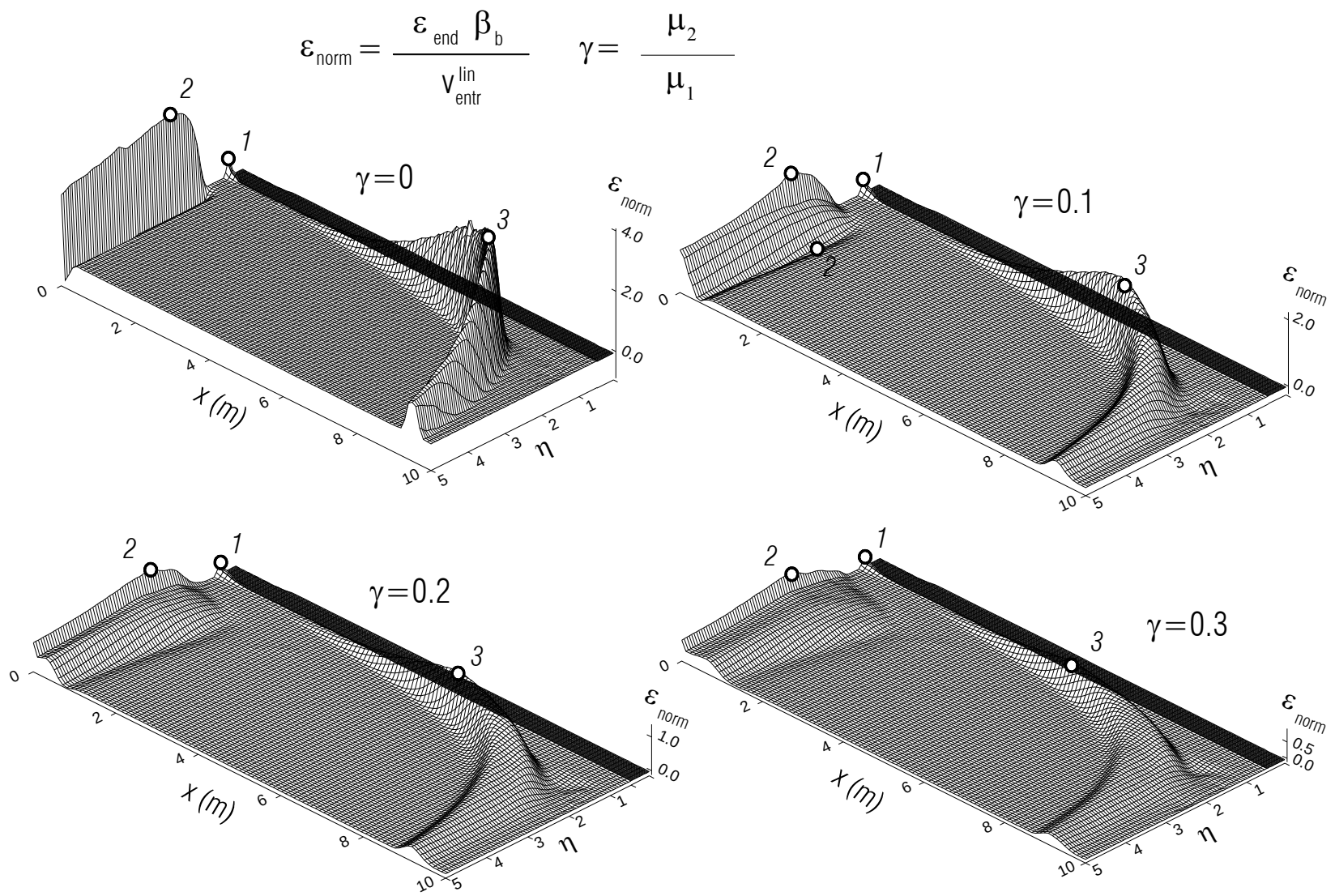

Fig. 21b Normalized strains along the beam, at the end of the analysis, vs. dimensionless frequency, and for dimensionless amplitude α = 0.2.

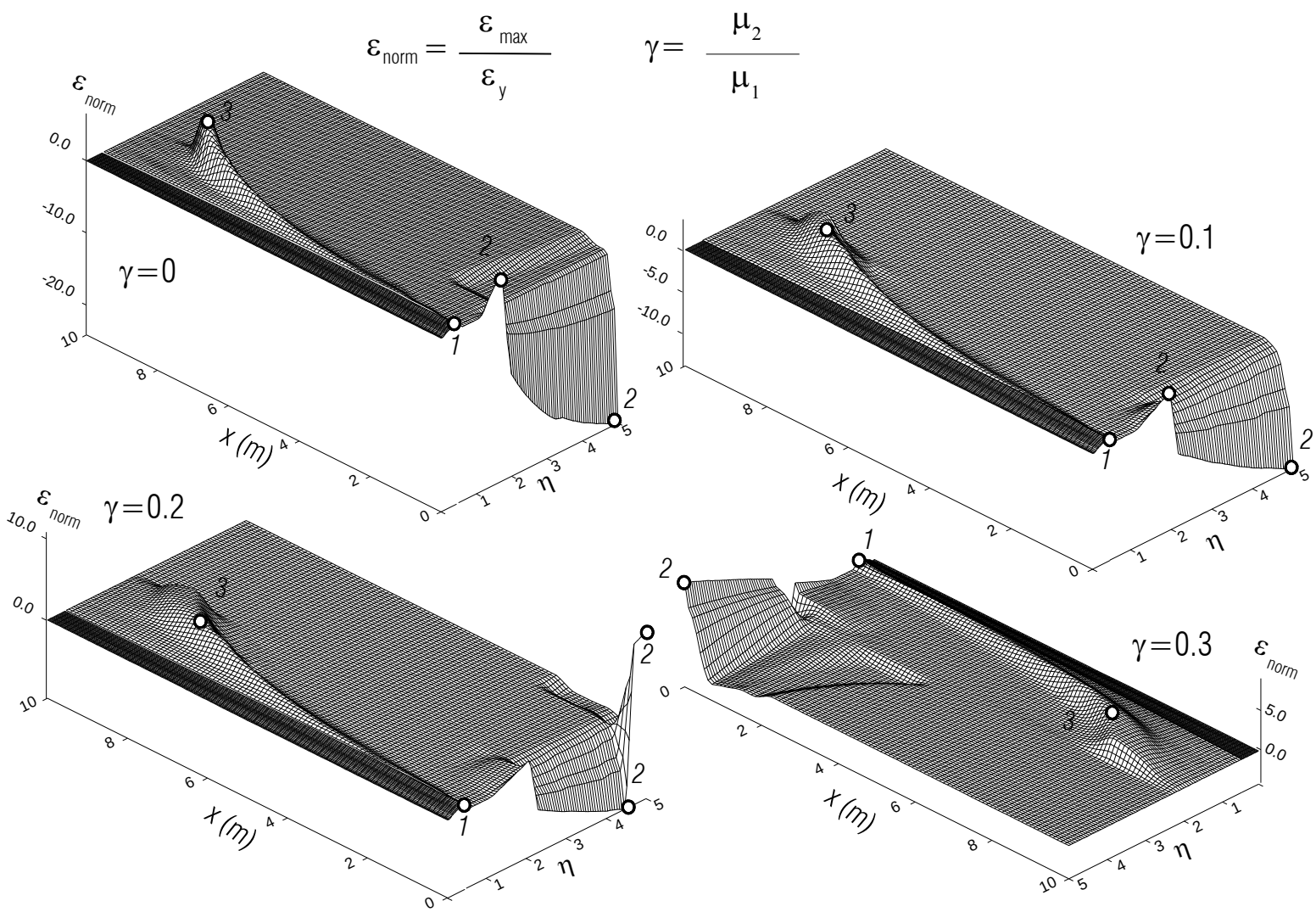

Fig. 21c Normalized strain along the beam, when its maximum occurs, vs. dimensionless frequency, and for dimensionless amplitude α = 0.2.

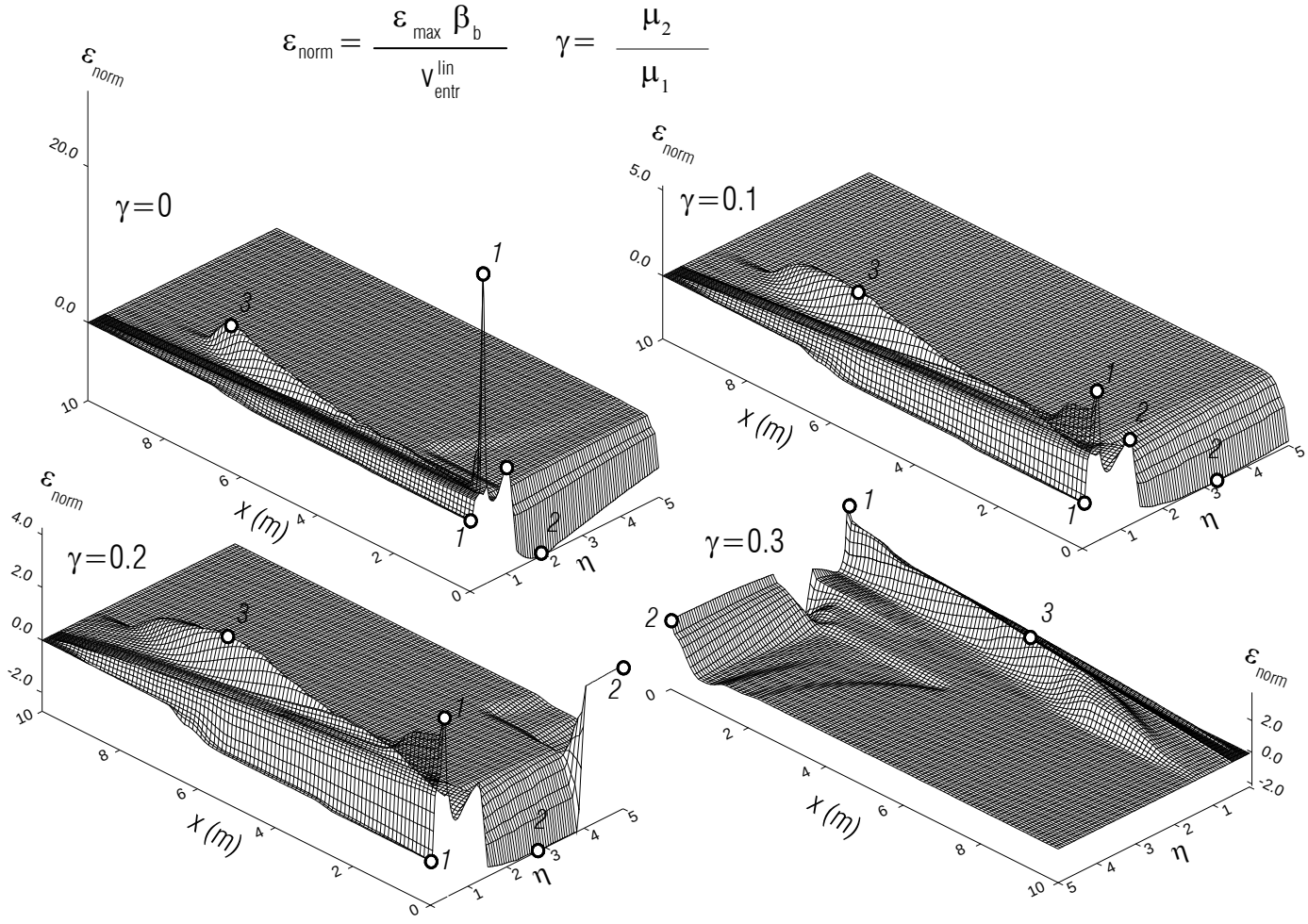

Fig. 22a Normalized strain along the beam, when its maximum occurs, vs. dimensionless frequency, and for dimensionless amplitude α = 0.3.

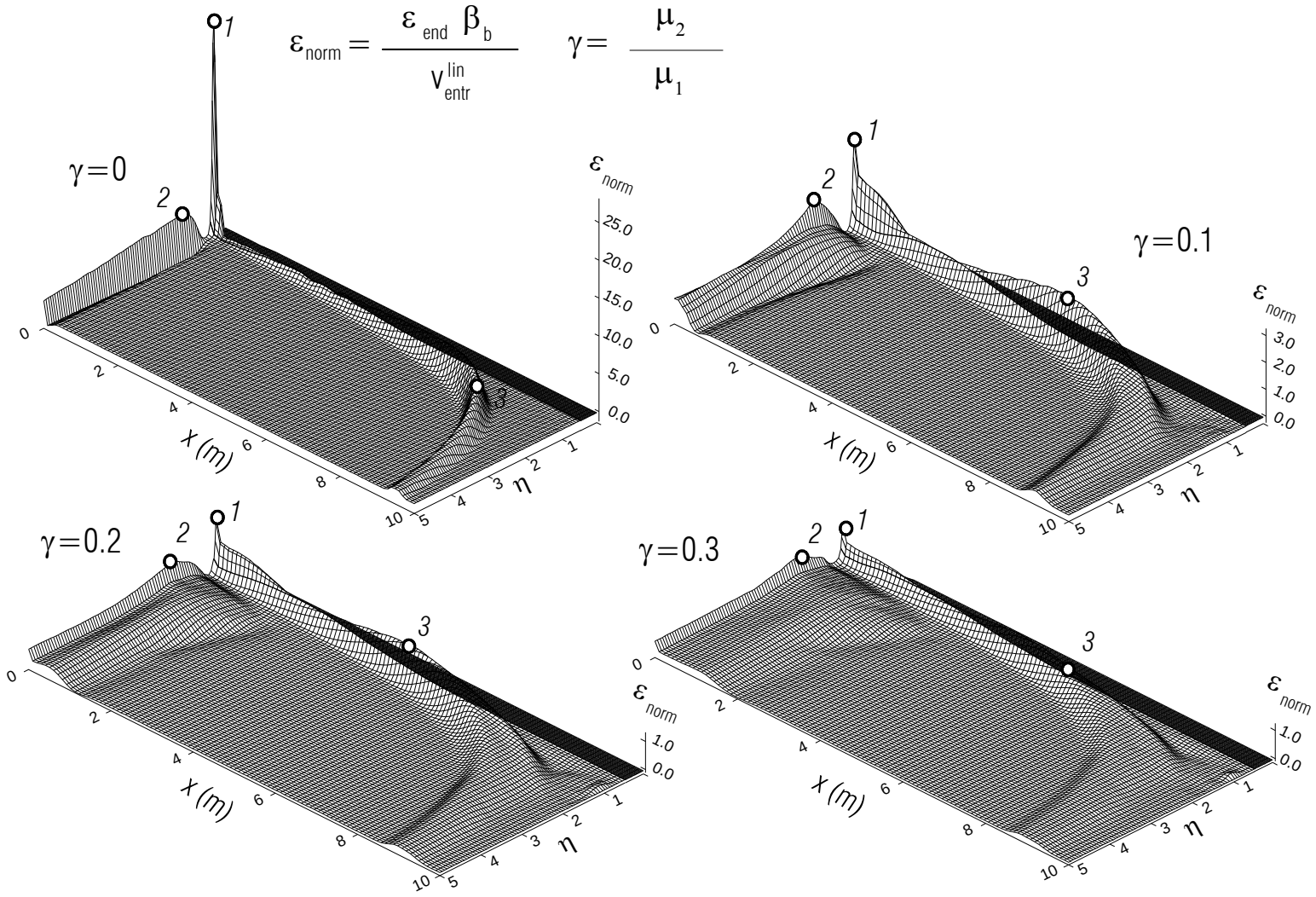

Fig. 22b Normalized strain along the beam, at the end of analysis, vs. dimensionless frequency, and for dimensionless amplitude $\alpha = 0.3$.

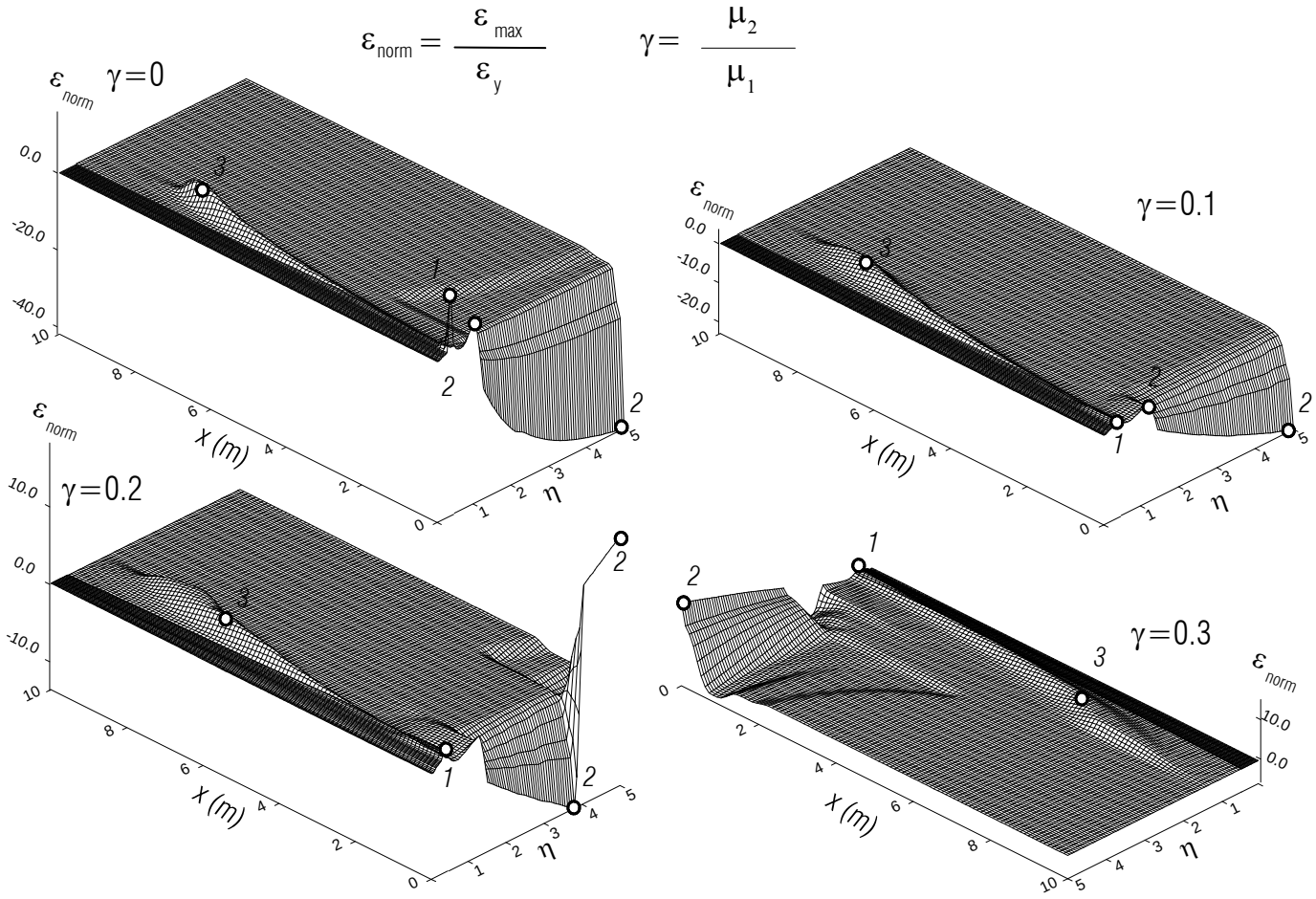

Fig. 22c Normalized strain along the beam, when its maximum occurs, vs. dimensionless frequency, and for dimensionless amplitude $\alpha = 0.3$

Eq. 4.7), is constant, and its value is about $\frac{17}{7}$, corresponding with the effect of the summation of the three strains at the beginning of the second passage. Because the response is linear, in this interval $\varepsilon_{\text{norm}}^{\max}$ shows only the effect of the interference on amplification of the linear entry strain.

The normalized strain, $\varepsilon_{\text{norm}}^{\text{end}}$, in this interval is zero, showing that the strains are reversible and the resistance capacity of the beam for some future excitation is not diminished. The normalized strain, $\varepsilon_{norm}^{y} = \varepsilon_{\max} / \varepsilon_{yb}$, approaches zero as α approaches zero. With increasing α, beyond α_1, the response at the bottom becomes nonlinear at the beginning of the second passage and the curves for different γ separate, and the normalized strains increase with decreasing γ, being the largest for elasto-plastic material, $\gamma = 0$.

The normalized strain $\varepsilon_{\text{norm}}^{\max}$ reaches its maximum value of 29.74 at $\alpha = 0.3$ for elasto-plastic material. In this case, the effect of the nonlinearity of the building response dominates over the effect of constructive interference of the three strains at the bottom. The remaining normalized permanent strain at the end, after the wave exits the beam completely, $\varepsilon_{\text{norm}}^{\text{end}}$, is 28.17 for the elasto-plastic material, while the normalized strain, $\varepsilon_{\text{norm}}^{\text{y}}$, is 16.18, indicating that the beam will probably fail at $\alpha = 0.3$.

In Fig. 24b, the normalized strains versus α in zone 2 are shown, again using the semi-logarithmic scale. It can be seen that for small amplitudes, $\alpha \le 0.05$, all of the curves converge to zero (see also Fig. 19a, b, c). For $\alpha = 0.05$, there is an appearance of some negligible permanent strain at high frequencies, $\eta \ge 4.5$. As α increases, all normalized strains increase.

For α larger than 0.1, the dependence of all of the normalized strains on α for elasto-plastic material, $\gamma = 0$, in this scale resemble a logarithmic function, which means that the normalized strains for elasto-plastic material are linear functions of α.

For materials with $\gamma \neq 0$, the normalized strains $\varepsilon_{\text{norm}}^{\text{end}}$ are independent of α, while the normalized strains $\varepsilon_{\text{norm}}^{\max}$ and $\varepsilon_{\text{norm}}^{\text{y}}$ are approximately linear, with the slope $\frac{\partial \varepsilon_{\text{norm}}^{\max}}{\partial \alpha}$ smaller than the slope $\frac{\partial \varepsilon_{\text{norm}}^{\text{y}}}{\partial \alpha}$.

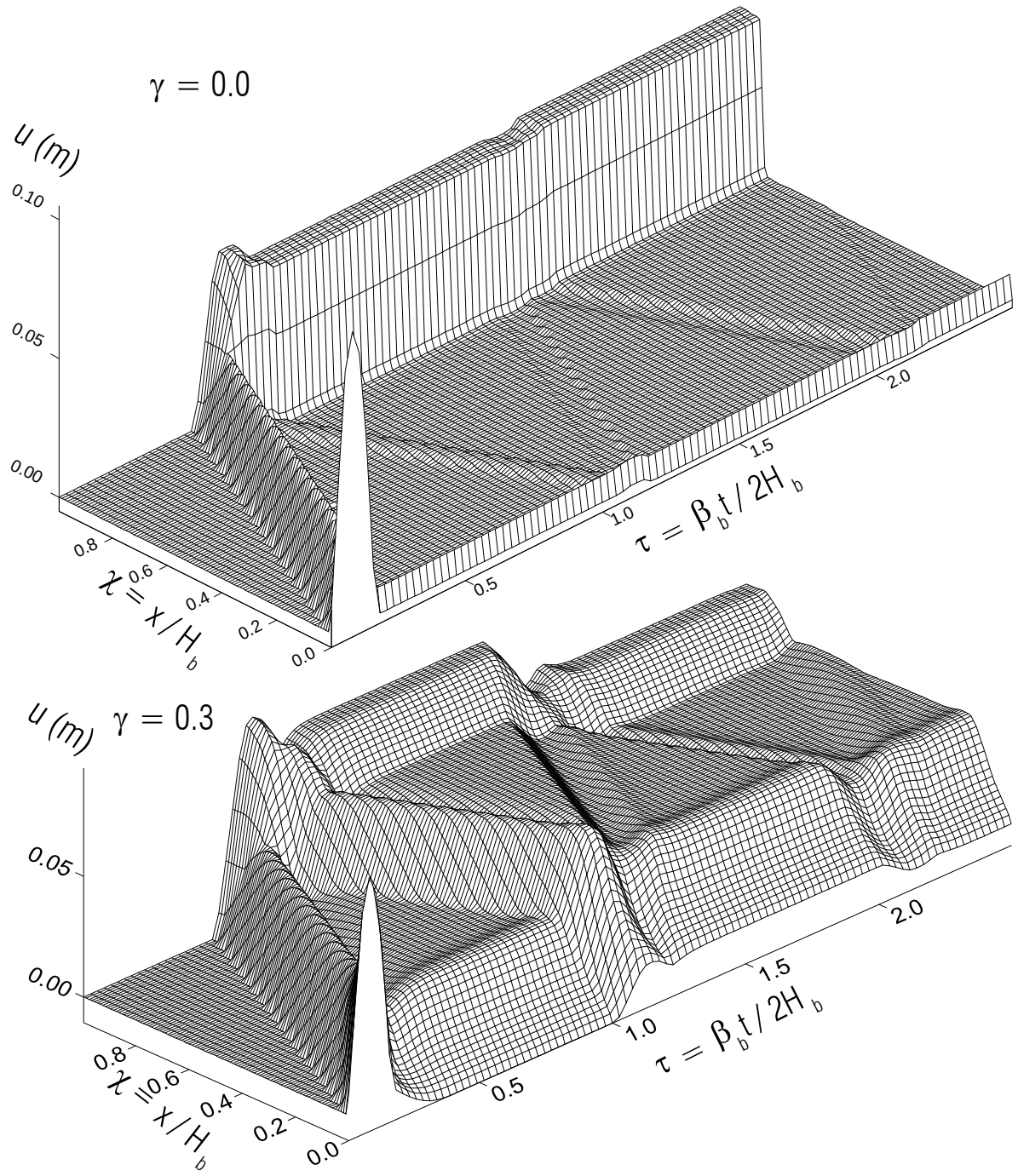

Fig. 23a Plot of the displacements along the normalized length of the beam χ, vs. normalized time τ, for dimensionless amplitude $\alpha = 0.3$, $\eta = 3$, and for $\gamma = 0$, and $\gamma = 0.3$.

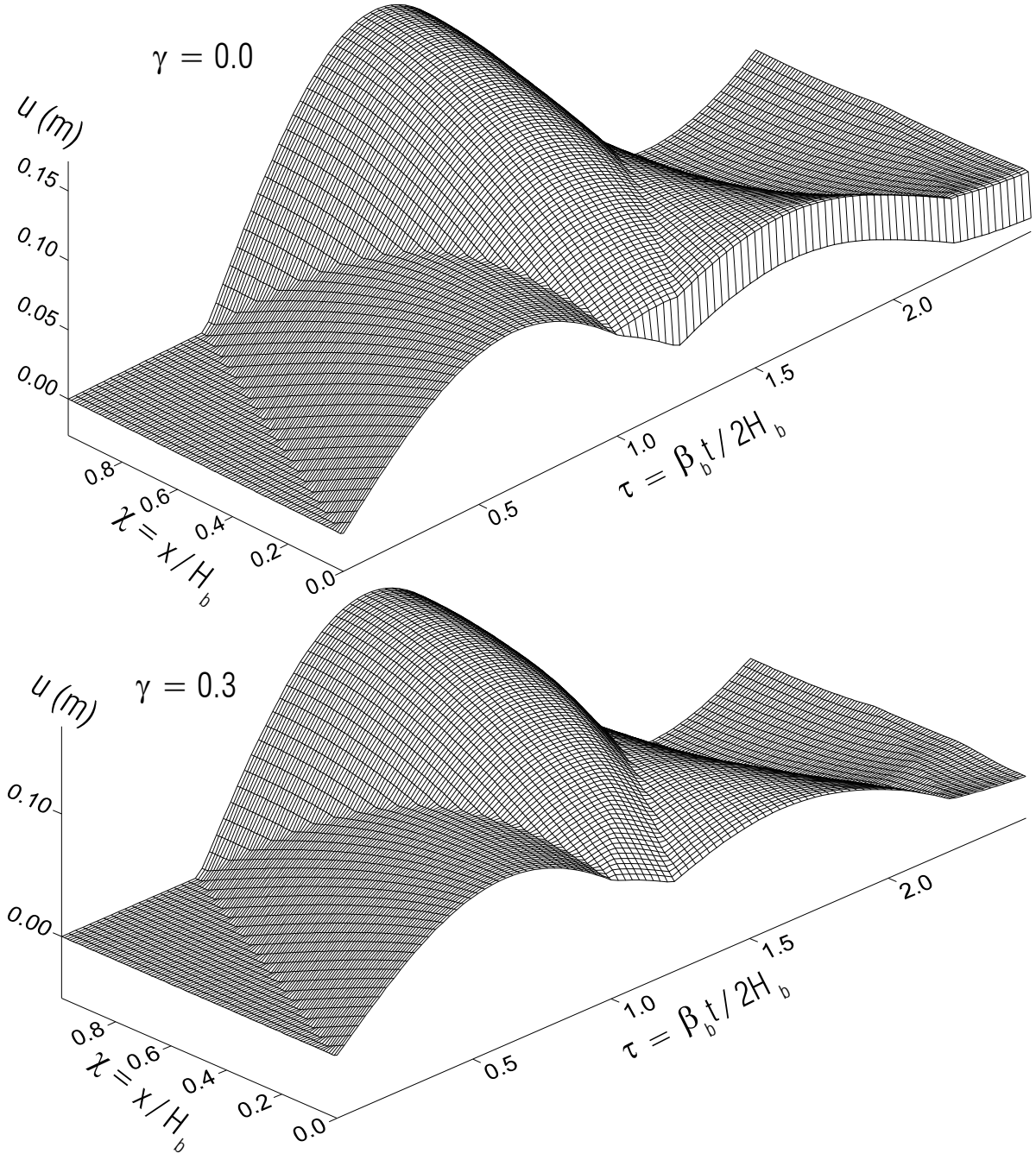

Fig. 23b Plot of the displacements along the normalized length of the beam χ , vs. normalized time τ , for dimensionless amplitude $\alpha = 0.3$, dimensionless frequency $\eta = 0.41$, and for $\gamma = 0$, and $\gamma = 0.3$.

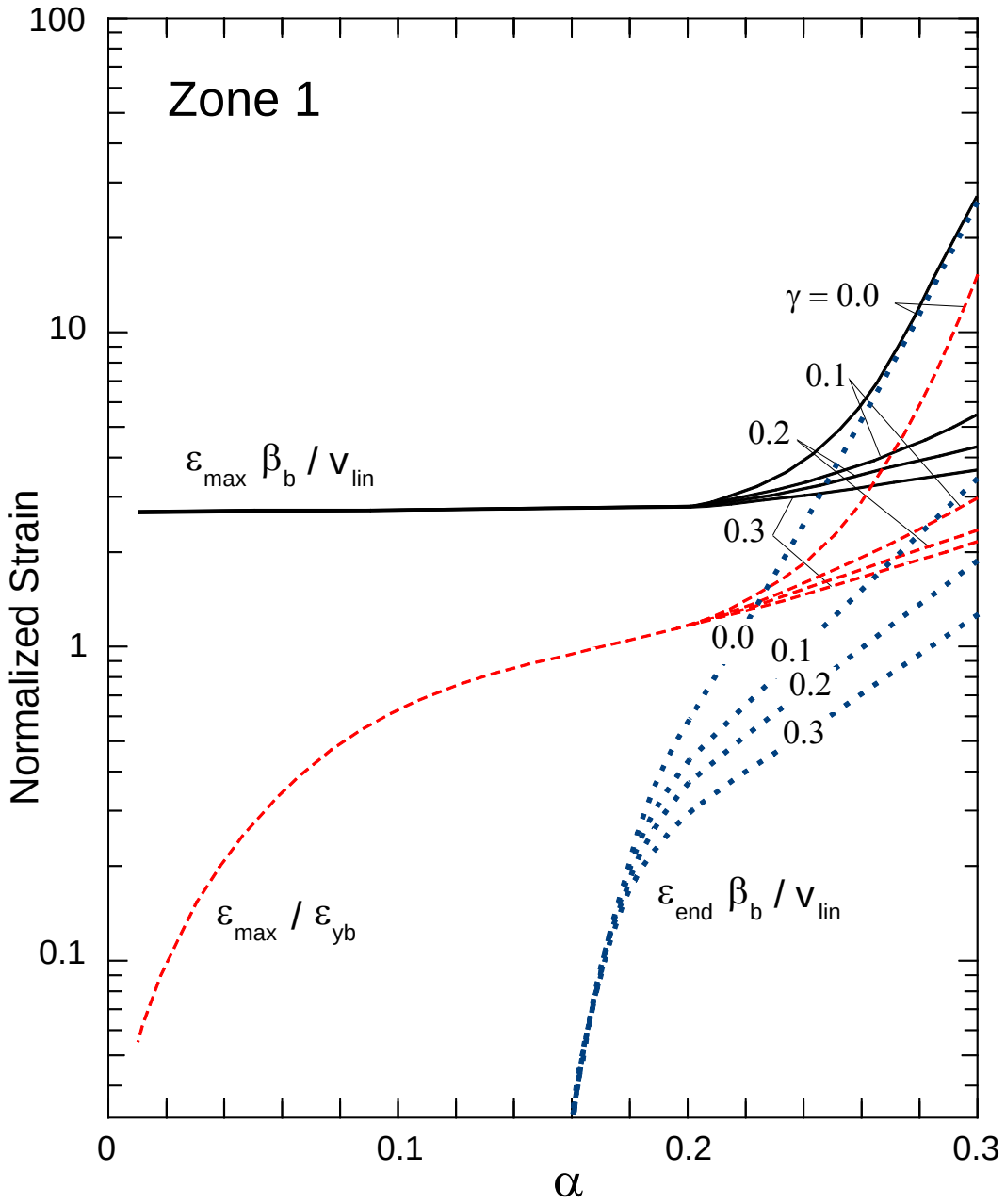

Fig. 24a Dependence of the normalized strains on the dimensionless amplitude, α, in the zone 1 for four different γ = 0.0, 0.1, 0.2, and 0.3.

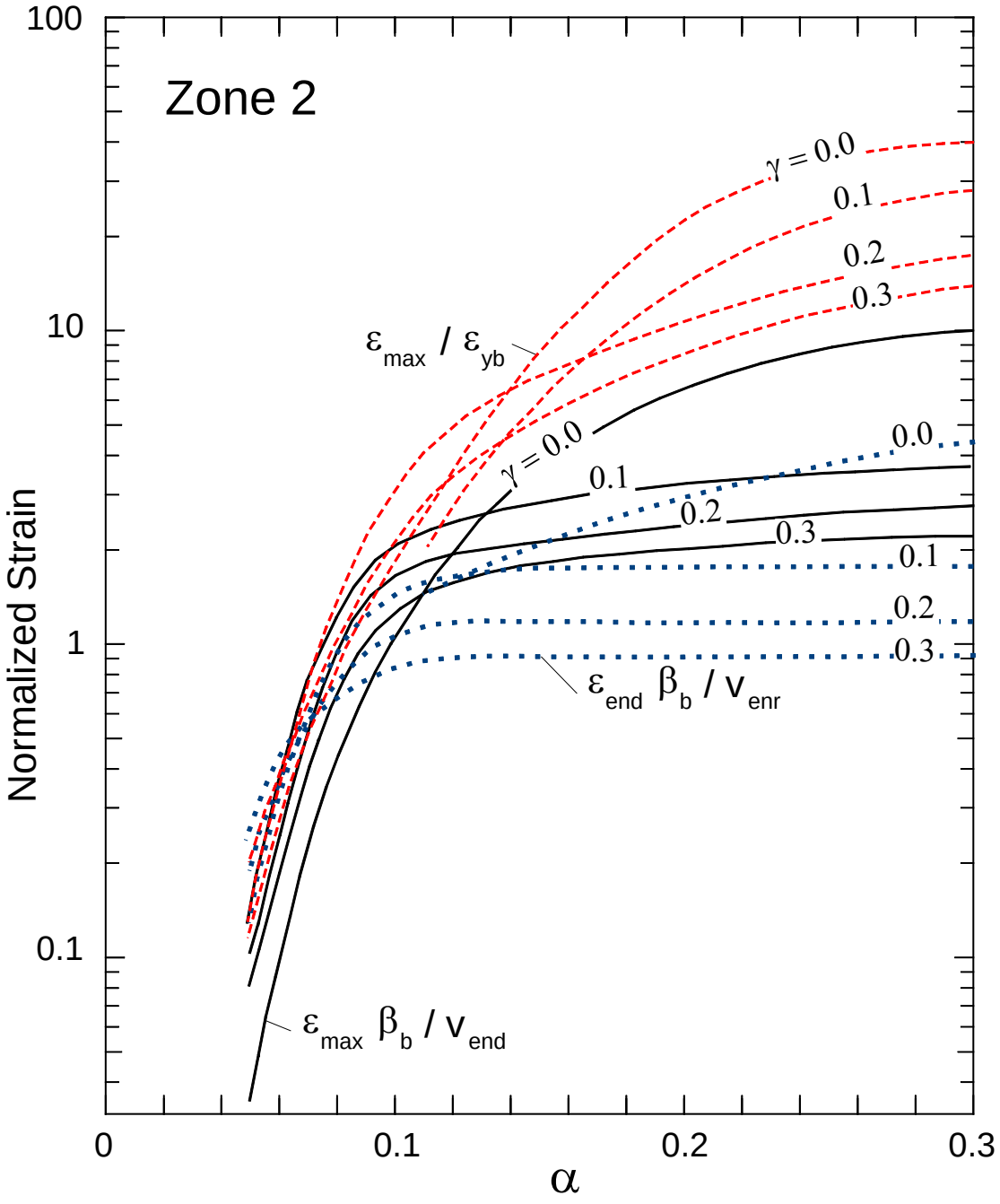

Fig. 24b Dependence of the normalized strains on the dimensionless amplitude, α, in the zone 2 for four different γ = 0.0, 0.1, 0.2, and 0.3.

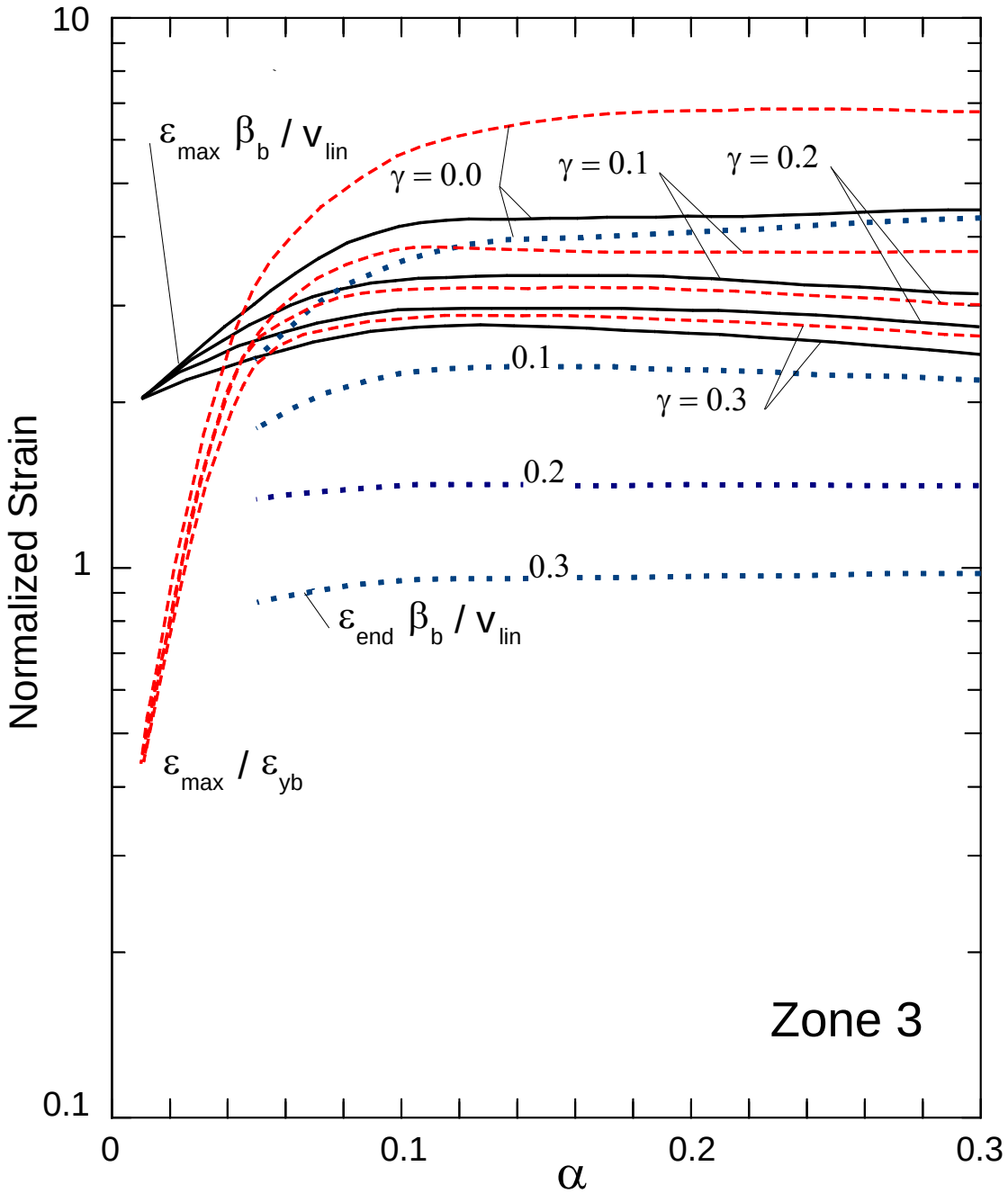

Fig. 24c Dependence of the normalized strains on the dimensionless amplitude, α , in the zone 3 for four different γ = 0.0, 0.1, 0.2, and 0.3.

In Fig. 24c, the normalized strains versus α in zone 3 are shown using a semi-logarithmic scale. For any γ, the normalized strains $\varepsilon_{\text{norm}}^{\max}$ and $\varepsilon_{\text{norm}}^{\text{y}}$ approach 2 and 0, respectively, as α approaches 0. The normalized strain $\varepsilon_{\text{norm}}^{\text{end}}$ depends only on γ and is independent of α. The lowest amplitude, when it occurs, can be found from condition (4.4) at the highest considered η as $\alpha_{\min} > \dfrac{0.1114}{5} = 0.02228$. For $\alpha \le \alpha_{\min}$, $\varepsilon_{\text{norm}}^{\text{end}} = 0$.

5. SUMMARY AND CONCLUSIONS

In this report, we described the consequences of earthquake energy flow into a structure, with the objectives of providing some understanding of the resulting response and making this useful for the design of structures experiencing transient excitation. Starting with a linear strong-motion pulse in the soil and ending with nonlinear waves propagating through a structure, we attempted to identify the extreme transient and permanent rotations occurring during various stages of seismic energy flow. For the wave energy to become a viable design tool, it is necessary to understand and to quantify empirically all stages of this flow, as well as to show that it provides more realistic and spatially more informative results than the currently accepted design methods. One of the principal weaknesses of the classical Biot's response spectrum method is its dependence upon the peak response amplitude alone, without explicit consideration of the duration of strong shaking and of the rate of arrival of the incident strong-motion energy.

We examined some elementary aspects of transient waves propagating in a structure, and we illustrated the relationships between the amplitude of peak velocity of the wave entering the structure, v_{lin}, and transient and permanent rotations (drifts) associated with the resulting response. The presented analysis is qualitative as it describes the response of a simple shear beam with constant material properties only. Nevertheless, it shows that consideration of the response in terms of propagating nonlinear waves can provide invaluable details on where inter-story drifts may occur and how large they can be. In terms of the more detailed models of actual structures (or layers of soft soil near the ground surface), the approach we presented can offer major improvements and can represent an excellent starting point for use in earthquake-resistant design. While our results can provide direct data for initiating the displacement-based design, the power of the incident waves—that is, the time rate of the incoming seismic wave energy—must also be considered if damage to structures is to be controlled or eliminated.

6. REFERENCES

1. Biot, M.A. (1942). Analytical and experimental methods in engineering seismology, *ASCE, Transactions*, **108**, 365-408.

2. Dablain, M.A. (1986). The application of high order differencing to the shear wave equation, Geophysics, 51(1), 54-66.

3. Fajfar, P. and Krawinkler, H. (Eds.) (1992). Nonlinear Seismic Analysis and Design of Reinforced Concrete Buildings, Elsevier Applied Science, London, New York.

4. Fajfar, P., and Krawinkler, H. (Eds.) (1997). Seismic design methodologies for the next generation of codes, Proc. International Workshop on Seismic Design Methodologies for the Next Generation of Codes. Bled Slovenia, June 24-27, 1997. Balkema, Rotterdam.

5. Fajfar, P. (1998). Trends in seismic design and performance evaluation approaches, Proc. Eleventh European Conf. on Earthquake Eng., September 6-11, 1998. Paris, France, Invited Lectures, 237-249.

6. Fujino, Y., and Hakuno, M. Characteristics of elasto-plastic ground motion during an earthquake. Bull. Earthquake Res. Institute, Tokyo Univ., 1978; 53, 359-378.

7. Gicev, V. and Trifunac, M.D. (2006). Permanent deformations and strains in a shear building excited by a strong motion pulse, Soil Dynamics and Earthquake Engineering, (in press).

8. Kanai, K. (1965). Some problems of seismic vibration of structures, Proc. Third World Conf. On Earthquake Eng., New Zealand, Vol. II, 260-275.

9. Lax, P.D., and Wendroff, B. Difference schemes for hyperbolic equations with high order of accuracy. Comm. on Pure and Applied Mathematics 1964; XVII, 381-398.

10. Lee, V.W., Trifunac, M.D., and Feng, C.C. (1982). Effects of foundation size on fourier spectrum amplitudes of earthquake accelerations recorded in buildings, Soil Dynam. and Earthquake Eng., 1(2), 52-58.

11. Moslem, K., and Trifunac, M.D. (1987). Spectral amplitudes of strong earthquake accelerations recorded in buildings, Soil Dynam. and Earthquake Eng., 6(2), 100-107.

12. Safak, E. (1998). New approach to analyzing soil-building systems, Soil Dynam. and Earthquake Eng, 17, 509-517.

13. Sezawa, K., and Kanai, K. (1935). Decay in the seismic vibration of a simple or tall structure by dissipation of their energy into the ground, Bull. Earth. Res. Inst., XIII, Part 3, 681-697.

14. Sezawa, K,, and Kanai, K. (1936). Improved theory of energy dissipation in seismic vibrations on a structure, Bull. Earth. Res. Inst., XIV, Part 2, 164-168.

15. Todorovska, M.I., and Lee, V.W. (1989). Seismic waves in buildings with shear walls or central core, J. Engrg. Mech., ASCE, 115(12), 2669-2686.

16. Todorovska, M.I., and Trifunac, M.D. (1989). Antiplane earthquake waves in long structures, J. of Engrg. Mech., ASCE, 115(12), 2687-2708.

17. Todorovska, M.I., and Trifunac, M.D. (1990a). A note on the propagation of earthquake waves in buildings with soft first floor, J. of Engrg. Mech., ASCE, 116(4), 892-900.

18. Todorovska, M.I., and Trifunac, M.D. (1990b). A note on excitation of long structures by ground waves, J. of Engrg Mech., ASCE, 116(4), 952-964.

19. Todorovska, M.I., and Trifunac, M.D. (1990c). Analytical model for in-plane building-foundation-soil interaction: Incident p-, sv- and rayleight waves, Dept. of Civil Engrg, Report No. 90-01, Univ. of Southern California, Los Angeles.

20. Todorovska, M.I., and Trifunac, M.D. (1991). Radiation damping during two-dimensional building-soil interaction, Dept. of Civil Eng., Rep. No. 91-01, Univ. of Southern California, Los Angeles, California.

21. Todorovska, M.I., and Trifunac, M.D. (1992). The system damping, the system frequency and the system response peak amplitudes during in-plane building-soil interaction, Earthquake Eng. and Struct. Dynam., 21(2), 127-144.

22. Todorovska, M.I., and Trifunac, M.D. (1993). The effects of wave passage on the response of base-isolated buildings on rigid embedded foundations, Dept of Civil Eng., Report No. CE 93-10, Univ. of Southern California, Los Angeles.

23. Todorovska, M.I., and Trifunac, M.D. (1997a). Distribution of pseudo spectral velocity during the Northridge, California, earthquake of 17 January 1994, Soil Dynam. and Earthquake Eng., 16(3), 173-192.

24. Todorovska, M.I., and Trifunac, M.D. (1997b). Amplitudes, polarity and times of peaks of strong ground motion during the 1994 Northridge, California earthquake, Soil Dynam. and Earthquake Eng., 16(4), 235-258.

25. Todorovska, M.I., Trifunac, M.D., and Lee, V.W. (1988). Investigation of earthquake response of long buildings, Dept of Civil Engrg, Report No. CE 88-02, Univ. of Southern California, Los Angeles.

26. Todorovska, M.I., Ivanović, S.S., and Trifunac, M.D. (2001a). Wave propagation in a seven-story reinforced concrete building, Part I: Theoretical models, Soil Dynam. and Earthquake Eng., 21(3), 211-223.

27. Todorovska, M.I., Ivanović, S.S., and Trifunac, M.D. (2001b). Wave propagation in a seven-story reinforced concrete building, Part II: Observed wave numbers, Soil Dynam. and Earthquake Eng., 21(3), 211-223.

28. Todorovska, M.I., Hayir, A., and Trifunac, M.D. (2001c). Antiplane response of a dike on flexible embedded foundation to incident SH-waves, Soil Dynam. and Earthquake Eng. 21 (7), 593–601.

29. Trifunac, M.D. (1972a). Stress estimates for San Fernando, California earthquake of February 9, 1971: Main event and thirteen aftershocks, Bull Seism. Soc. Amer., 62, 721-750.

30. Trifunac, M.D. (1972b). Tectonic stress and source mechanism of the Imperial Valley, California earthquake of 1940, Bull. Seism. Soc. Amer., 62, 1283-1302.

31. Trifunac, M.D. (1972c). Interaction of a shear wall with the soil for incident plane SH-waves, Bull. Seism. Soc. Amer., 62(1), 63-83.

32. Trifunac, M.D. (1998). Stresses and intermediate frequencies of strong motion acceleration, Geofizika, 14, 1-27.

33. Trifunac, M.D. (2006). Effects of torsional and rocking excitations on the response of structures, In Earthquake Source Asymmetry, Structural Media and Rotation Effects, R. Teisseyre, M. Takeo, and E. Majewski (Eds.) Springer, Heidelberg, Germany.

34. Trifunac, M.D. and Hudson, D.E. (1971). Analysis of the Pacoima Dam accelerogram, San Fernando, California, earthquake of 1971, Bull. Seism. Soc. Amer., 61, 1393-1411.

35. Trifunac, M.D., Todorovska, M.I., and Lee, V.W. (1998). The Rinaldi strong motion accelerogram of the Northridge, California, earthquake of 17 January 1994, Earthquake Spectra, 14(1), 225-239.

36. Trifunac, M.D., Ivanovic, S.S., and Todorovska, M.I. (2003). Wave propagation in a seven-story reinforced concrete building, III: Damage detection via changes in wave numbers, Soil Dynamics. and Earthquake Eng., 23(1), 65-75.